NAVAL POSTGRADUATE SCHOOL
MONTEREY, CALIFORNIA

THESIS

A COMPARITIVE STUDY INTO THE COKING RESISTIVITY OF SWIRLPLATES WITH VARIOUS SURFACE FINISHES

by

Stephen Frederick Williamson

June, 1996

Thesis Advisor: Jeff Perkins

Approved for public release; distribution is unlimited.

19961008 186

DTIC QUALITY INSPECTED 1

REPORT DOCUMENTATION PAGE

Form Approved OMB No. 0704-0188

Public reporting burden for this collection of information is estimated to average 1 hour per response, including the time for reviewing instruction, searching existing data sources, gathering and maintaining the data needed, and completing and reviewing the collection of information. Send comments regarding this burden estimate or any other aspect of this collection of information, including suggestions for reducing this burden, to Washington Headquarters Services, Directorate for Information Operations and Reports, 1215 Jefferson Davis Highway, Suite 1204, Arlington, VA 22202-4302, and to the Office of Management and Budget, Paperwork Reduction Project (0704-0188) Washington DC 20503.

1. AGENCY USE ONLY *(Leave blank)*	2. REPORT DATE	3. REPORT TYPE AND DATES COVERED
	June 1996	Master's Thesis

4. A COMPARITIVE STUDY INTO THE COKING RESISTIVITY OF SWIRLPLATES WITH VARIOUS SURFACE FINISHES	5. FUNDING NUMBERS
6. AUTHOR(S) Stephen F. Williamson	
7. PERFORMING ORGANIZATION NAME(S) AND ADDRESS(ES) Naval Postgraduate School Monterey CA 93943-5000	8. PERFORMING ORGANIZATION REPORT NUMBER
9. SPONSORING/MONITORING AGENCY NAME(S) AND ADDRESS(ES) NAVAIR	10.SPONSORING/MONITORING AGENCY REPORT NUMBER
11. SUPPLEMENTARY NOTES The views expressed in this thesis are those of the author and do not reflect the official policy or position of the Department of Defense or the U.S. Government.	
12a. DISTRIBUTION/AVAILABILITY STATEMENT Approved for public release; distribution is unlimited.	12b. DISTRIBUTION CODE

13. ABSTRACT *(maximum 200 words)*

Gas turbine nozzle swirlplates used in the T56-A-427 engines of the E-2C Hawkeye aircraft were tested for their resistivity to fuel deposit formation, or 'coking'. The coking occurred after the engines were shut down due to the fuel trapped in the line and temperature ranges present at the nozzle tip. As the coke built up, the holes in the swirlplate clogged and the aircraft required intensive servicing. The search for alternative solutions led to the possibility of using swirlplates that had been polished or coated in an attempt to reduce the coking rates. Several swirlplate's surface finishes were investigated.

14. SUBJECT TERMS Gas Turbine Nozzle Fuel Deposits			15. NUMBER OF PAGES 141
			16. PRICE CODE
17. SECURITY CLASSIFICATION OF REPORT Unclassified	18. SECURITY CLASSIFICATION OF THIS PAGE Unclassified	19. SECURITY CLASSIFICATION OF ABSTRACT Unclassified	20. LIMITATION OF ABSTRACT UL

NSN 7540-01-280-5500

Standard Form 298 (Rev. 2-89)
Prescribed by ANSI Std. 239-18 298-102

Approved for public release; distribution is unlimited.

A COMPARITIVE STUDY INTO THE COKING RESISTIVITY OF SWIRLPLATES WITH VARIOUS SURFACE FINISHES

Stephen Frederick Williamson
Lieutenant, United States Navy
B.A., University of Maryland, 1988

Submitted in partial fulfillment
of the requirements for the degree of

MASTER OF SCIENCE IN MECHANICAL ENGINEERING

from the

NAVAL POSTGRADUATE SCHOOL
June 1996

Author: _____
Stephen F. Williamson

Approved by: _____
Jeff Perkins, Thesis Advisor

_____
Terry R. McNelley, Chairman
Department of Mechanical Engineering

ABSTRACT

Gas turbine nozzle swirlplates used in the T56-A-427 engines of the E-2C Hawkeye aircraft were tested for their resistivity to fuel deposit formations, or 'coking'. The coking occured after the engines were shut down due to the fuel trapped in the line and temperature ranges present at the nozzle tip. As the coke built up, the holes in the swirl plates clogged and the aircraft required intensive servicing. The search for alternative solutions led to the possibility of using swirl plates that had been polished or coated in an attempt to reduce the coking rates. Several swirlplates with various surface finishes and coatings were investigated.

TABLE OF CONTENTS

I. INTRODUCTION 1

A. GENERAL 1

B. DEPOSIT MECHANISMS 2

C. NOZZLES AND SWIRLPLATES 3

D. BACKGROUND 6

E. OBJECTIVES 7

F. TEMPERATURE PROFILE DETERMINATION 7

G. WEIGHT AND FLOW MEASUREMENTS 10

II. EXPERIMENTAL PROCEDURE 13

A. EXPERIMENTAL SET-UP 13

B. EXPERIMENT CYCLE AND DATA FLOW 16

C. DATA INTERPRETATION 19

III. RESULTS 23

A. GENERAL 23

B. WEIGHT MEASUREMENTS 23
1. A vs. A' 24
2. A vs. B. 27
3. A vs. A' 29
4. B vs. B-md. 31
5. B vs. A-md. 33
6. A vs. A-sil. 35
7. B vs. A-sil. 37
8. B vs. B 39

C. OPTICAL MICROSCOPY 41
1. A01 vs. A'01, Figures 18 - 23 41
2. B17 vs. B-md20, Figures 24 - 33. 41
3. B10 vs. A-md25, Figures 34 - 45 41
4. A28 vs. A-sil23, Figures 46 - 59 41

5. B12 vs. A-sil24, Figures 60 - 67 41
6. B13 vs. B14, Figures 68 - 75 41

D. SCANNING ELECTRON MICROSCOPE PHOTO ANALYSIS 74
1. Typical hole and edge photos, Figures 76 - 80. 74
2. A01 vs. A'01, Figures 81 - 90 74
3. B17 vs. B-md20, Figures 91 - 94. 74
4. B10 vs. A-md25, Figures 95 - 103 74
5. A28 vs. A-sil23, Figures 104 - 111. 74
6. B12 vs. A-sil24, Figures 112 - 123. 74
7. B13 vs. B14, Figures 124 -131. 74

E. HOLE CLOSURE AND FLOW MEASUREMENTS 106
1. A01 and A'01 107
2. B17 and B-md20. 109
3. A-md25 and B19. 111
4. 28 and A-sil23. 113
5. A-sil24 and B12. 115
6. B13 and B14. 117

IV. CONCLUSIONS AND RECOMMENDATIONS 119

A. CONCLUSIONS 119
1. A type swirlplates. 119
2. A' type swirlplates. 119
3. Amorphous Diamond Coating. 119
4. Silicon Coating. 120
5. Dupont Plates. 120

B. RECOMMENDATIONS 121

LIST OF REFERENCES 123

INITIAL DISTRIBUTION LIST 125

LIST OF FIGURES

1: Schematic of Dual Entry Fuel Nozzle. 3
2: Side-view of nozzle head and schematic of swirlplate. 4
3: Schematic of the swirlplate hole numbering system 5
4: Temperature-Time profile 9
5: Photographs of the experimental and flow set-ups for the Nozzle Project. 15
6: Temperature-Time profile for one 30 minute cycle. 17
7: Temperature-Time profile for multiple cycles. 18
8: Schematic of the flow measurement experiment set-up. 20
9: Pressure transducer calibration curve. 21
10: Weight increase versus number of cycles completed by A22 and A'27. 26
11: Weight increase versus number of cycles completed by A27 and B18. 28
12: Weight increase versus number of cycles completed by A01 and A'01. 30
13: Weight increase versus number of cycles completed by B17 and B-md20. 32
14: Weight increase versus number of cycles completed by B10 and A-md25. 34
15: Weight increase versus number of cycles completed by A28 and A-sil23. 36
16: Weight increase versus number of cycles completed by B12 and A-sil24. 38
17: Weight increase versus number of cycles completed by B13 and B14. 40
18: Optical photo of A01, 12 o'clock, zero cycles. 42
19: Optical photo of A'01, 12 o'clock, zero cycles. 42
20: Optical photo of A01, 12 o'clock, 150 cycles. 43
21: Optical photo of A'01, 12 o'clock, 150 cycles. 43
22: Optical photo of A01, 6 o'clock, 150 cycles. 44
23: Optical photo of A'01, 6 o'clock, 150 cycles. 44
24: Optical photo of B17, 12 o'clock, zero cycles. 45
25: Optical photo of B-md20, 12 o'clock, zero cycles. 45
26: Optical photo of B17, 12 o'clock, 90 cycles. 46
27: Optical photo of B-md20, 12 o'clock, 60 cycles. 46
28: Optical photo of B17, 6 o'clock, 90 cycles. 47
29: Optical photo of B-md20, 6 o'clock, 60 cycles. 47
30: Optical photo of B17, 12 o'clock, 150 cycles. 48
31: Optical photo of B-md20, 12 o'clock, 150 cycles. 48
32: Optical photo of B17, 6 o'clock, 150 cycles. 49
33: Optical photo of B-md20, 6 o'clock, 150 cycles. 49
34: Optical photo of B10, 12 o'clock, zero cycles. 51
35: Optical photo of A-md25, 12 o'clock, zero cycles. 51
36: Optical photo of B10, 12 o'clock, 60 cycles. 52
37: Optical photo of A-md25, 12 o'clock, 60 cycles. 52
38: Optical photo of B10, 6 o'clock, 60 cycles. 53
39: Optical photo of A-md25, 6 o'clock, 60 cycles. 53
40: Optical photo of B10, 12 o'clock, 150 cycles. 54
41: Optical photo of A-md25, 12 o'clock, 150 cycles. 54
42: Optical photo of B10, 6 o'clock, 150 cycles. 55

43: Optical photo of A-md25, 6 o'clock, 150 cycles. 55
44: Optical photo of A-md25, 2 o'clock, 150 cycles. 56
45: Optical photo of A-md25, 10 o'clock, 150 cycles. 56
46: Optical photo of A28, 12 o'clock, zero cycles 57
47: Optical photo of A-sil23, 12 o'clock, zero cycles. 57
48: Optical photo of A28, 12 o'clock, 60 cycles. 58
49: Optical photo of A-sil23, 12 o'clock, 60 cycles. 58
50: Optical photo of A28, 6 o'clock, 60 cycles. 59
51: Optical photo of A-sil23, 6 o'clock, 60 cycles. 59
52: Optical photo of A28, 12 o'clock, 150 cycles. 60
53: Optical photo of A-sil23, 12 o'clock, 150 cycles. 60
54: Optical photo of A28, 6 o'clock, 150 cycles. 61
55: Optical photo of A-sil23, 6 o'clock, 150 cycles. 61
56: Optical photo of A28, 1 o'clock, 150 cycles. 62
57: Optical photo of A-sil23, 2 o'clock, 150 cycles. 62
58: Optical photo of A28, 10 o'clock, 150 cycles. 63
59: Optical photo of A-sil23, 3 o'clock, 150 cycles. 63
60: Optical photo of B12, 12 o'clock, zero cycles. 65
61: Optical photo of A-sil24, 12 o'clock, zero cycles. 65
62: Optical photo of B12, 12 o'clock, 90 cycles 66
63: Optical photo of A-sil24, 12 o'clock, 90 cycles. 66
64: Optical photo of B12, 12 o'clock, 150 cycles 67
65: Optical photo of A-sil24, 1 o'clock, 150 cycles. 67
66: Optical photo of B12, 6 o'clock, 150 cycles 68
67: Optical photo of A-sil24, 6 o'clock, 150 cycles. 68
68: Optical photo of B13, 12 o'clock, 60 cycles 70
69: Optical photo of B14, 12 o'clock, 60 cycles 70
70: Optical photo of B13, 6 o'clock, 60 cycles 71
71: Optical photo of B14, 6 o'clock, 60 cycles 71
72: Optical photo of B13, 12 o'clock, 150 cycles 72
73: Optical photo of B14, 12 o'clock, 150 cycles 72
74: Optical photo of B13, 6 o'clock, 150 cycles 73
75: Optical photo of B14, 6 o'clock, 150 cycles 73
76: SEM photo of typical A swirl plate, magnification 133X. 75
77: SEM photo of typical B swirl plate, magnification 130X. 75
78: SEM photo of typical A' swirl plate, magnification 130X. 76
79: SEM photo of typical A swirl plate hole, magnification 273X. 77
80: SEM photo of typical B swirl plate hole, magnification 549X. 77
81: SEM photo of typical A01, 12 o'clock, zero cycles, magnification 132X. 78
82: SEM photo of typical A'01, 12 o'clock, zero cycles, magnification 130X. 78
83: SEM photo of A01, 12 o'clock, 60 cycles, mag. 133X. 79
84: SEM photo of A'01, 12 o'clock, 60 cycles, mag. 130X. 79
85: SEM photo of A01, 6 o'clock, 60 cycles, mag. 133X. 80
86: SEM photo of A'01, 6 o'clock, 60 cycles, mag. 133X. 80
87: SEM photo of A01, 12 o'clock, 150 cycles, mag. 130X. 81

88: SEM photo of A'01, 12 o'clock, 150 cycles, mag. 130X. 81
89: SEM photo of A01, 6 o'clock, 150 cycles, mag. 130X. 82
90: SEM photo of A'01, 6 o'clock, 150 cycles, mag. 130X. 82
91: SEM photo of B17, 12 o'clock, zero cycles, mag. 130X. 84
92: SEM photo of B-md20, 12 o'clock, zero cycles, mag. 130X. 84
93: SEM photo of B17, 9 o'clock, 150 cycles, mag. 130X. 85
94: SEM photo of B-md20, 9 o'clock, 150 cycles, mag. 133X. 85
95: SEM photo of A-md25, 12 o'clock, 60 cycles, mag. 128X. 86
96: SEM photo of A-md25, 6 o'clock, 60 cycles, mag. 128X. 86
97: SEM photo of B10, 12 o'clock, 120 cycles, mag. 133X. 87
98: SEM photo of A-md25, 12 o'clock, 120 cycles, mag. 133X. 87
99: SEM photo of B10, 6 o'clock, 120 cycles, mag. 133X. 88
100: SEM photo of A-md25, 6 o'clock, 120 cycles, mag. 133X. 88
101: SEM photo of B10, 12 o'clock, 150 cycles, mag. 133X. 89
102: SEM photo of A-md25, 2 o'clock, 150 cycles, mag. 133X. 89
103: SEM photo of A-md25, 6 o'clock, 150 cycles, mag. 133X. 90
104: SEM photo of A28, 12 o'clock, 60 cycles, mag. 128X. 91
105: SEM photo of A-sil23, 12 o'clock, 60 cycles, mag. 121X. 91
106: SEM photo of A28, 5 o'clock, 60 cycles, mag. 124X. 92
107: SEM photo of A-sil23, 6 o'clock, 60 cycles, mag. 121X. 92
108: SEM photo of A28, 12 o'clock, 150 cycles, mag. 128X. 93
109: SEM photo of A-sil23, 12 o'clock, 150 cycles, mag. 128X. 93
110: SEM photo of A28, 4 o'clock, 150 cycles, mag. 128X. 94
111: SEM photo of A-sil23, 4 o'clock, 150 cycles, mag. 128X. 94
112: SEM photo of B12, 12 o'clock, zero cycles, mag. 130X. 95
113: SEM photo of A-sil24, 12 o'clock, zero cycles, mag. 133X. 95
114: SEM photo of B12, 12 o'clock, 90 cycles, mag. 124X. 96
115: SEM photo of A-sil24, 12 o'clock, 90 cycles, mag. 124X. 96
116: SEM photo of B12, 6 o'clock, 90 cycles, mag. 124X. 97
117: SEM photo of A-sil24, 6 o'clock, 90 cycles, mag. 124X. 97
118: SEM photo of B12, 12 o'clock, 150 cycles, mag. 119X. 98
119: SEM photo of A-sil24, 12 o'clock, 150 cycles, mag. 119X. 98
120: SEM photo of B12, 6 o'clock, 150 cycles, mag. 119X. 99
121: SEM photo of A-sil24, 6 o'clock, 150 cycles, mag. 119X. 99
122: SEM photo of A-sil24, 1 o'clock, 150 cycles, mag. 119X. 100
123: SEM photo of A-sil24, 2 o'clock, 150 cycles, mag. 119X. 100
124: SEM photo of B13, 12 o'clock, 60 cycles, mag. 119X. 102
125: SEM photo of B14, 12 o'clock, 60 cycles, mag. 119X. 102
126: SEM photo of B13, 6 o'clock, 60 cycles, mag. 119X. 103
127: SEM photo of B14, 6 o'clock, 60 cycles, mag. 119X. 103
128: SEM photo of B13, 12 o'clock, 150 cycles, mag. 133X. 104
129: SEM photo of B14, 12 o'clock, 150 cycles, mag. 133X. 104
130: SEM photo of B13, 6 o'clock, 150 cycles, mag. 133X. 105
131: SEM photo of B14, 6 o'clock, 150 cycles, mag. 133X. 105
132: Linear flow relationship for B17 swirlplate. 106

133: Average Percent Hole Closure of A01 and A'01 versus Cycles Completed. 108
134: Average Percent Hole Closure of B17 and B-md20 versus Cycles Completed. 110
135: Average Percent Hole Closure of A-md25 and B10 versus Cycles Completed. 112
136: Average Percent Hole Closure of A28 and A-sil23 versus Cycles Completed. 114
137: Average Percent Hole Closure of A-sil24 and B12 versus Cycles Completed. 116
138: Average Percent Hole Closure of B13 and B14 versus Cycles Completed. 118

LIST OF TABLES

1: Pressure transducer calibration data....21
2: Nomenclature for Swirlplates....24
3: Weight measurements of A22 from initial test of old test rig....25
4: Weight measurements of A'27 from initial test of old test rig....25
5: Weight measurements of A27 from initial tests with new test rig....27
6: Weight measurements of B18 from initial tests with new test rig....27
7: Weight measurements of A01....29
8: Weight measurements of A'01....29
9: Weight measurements of B17....31
10: Weight measurements of B-md20....31
11: Weight measurements of B10....33
12: Weight measurements of A-md25....33
13: Weight measurements of A28....35
14: Weight measurements of A-sil23....35
15: Weight measurements of B12....37
16: Weight measurements of A-sil24....37
17: Weight measurements of B13....39
18: Weight measurements of B14....39
19: Flow Rate in Standard Liters per Minute for A01....107
20: Flow Rate in Standard Liters per Minute for A'01....107
21: Flow Rate in Standard Liters per Minute for B17....109
22: Flow Rate in Standard Liters per Minute for B-md20....109
23: Flow Rate in Standard Liters per Minute for A-md25....111
24: Flow Rate in Standard Liters per Minute for B10....111
25: Flow Rate in Standard Liters per Minute for A28....113
26: Flow Rate in Standard Liters per Minute for A-sil23....113
27: Flow Rate in Standard Liters per Minute for A-sil24....115
28: Flow Rate in Standard Liters per Minute for B12....115
29: Flow Rate in Standard Liters per Minute for B13....117
30: Flow Rate in Standard Liters per Minute for B14....117

I. INTRODUCTION

A. GENERAL

The objective of this research was to further investigate the coking problem currently experienced in the turbine engines of the Navy E-2C (Hawkeye). The Allison Engine Company's T56-A-427 turbine engines, installed on the E-2C, have experienced severe coking problems on the swirlplates of the engine's nozzles due to the breakdown of the JP-5 fuel, thus reducing the effective operation of the aircraft by limiting the number of flight hours before mandatory maintenance. The E-2C is the navy's premiere early warning aircraft and is used extensively on deployed aircraft carriers. Due to safety considerations, the plane's engines are placed in High Speed Ground Idle (HSGI) upon landing on the aircraft carrrier and then immediately shut down. The temperature within the nozzle then rises to 350-400°F and stays in this range for 30-50 minutes [Ref. 1]. With temperatures above 320F, coking can occur at accelerated rates due to thermal soak back, causing significant hole blockage. A study conducted by Allison indicates that at least one swirlplate will become blocked in 30% of the engines operated after 200 hours, at least one swirlplate will be blocked in 45% of the engines after 400 hours and at least one swirlplate will be blocked in 88% of the engines operated after 800 hours [Ref. 2]. Initial studies by NAVAIR have shown that the nozzles are in need of maintenance after only 10% of the expected limit set by the US Navy at a range of 3000 hours [Ref. 1,3]. While reasons for the formation of the deposits have yet to be fully understood, the problem of finding a way of reducing the coking is of major concern.

B. DEPOSIT MECHANISMS

Many theories have been developed on the possible mechanisms involved in the coking process. While some scientists maintain that the mechanisms are caused by purely physical factors, others maintain that chemical factors are the main impetus behind the reactions. It is generally believed that deposits are produced by free-radical autoxidation of hydrocarbon molecules, involving hydroperoxide formation and decomposition, and are condensed in a stepwise manner [Ref. 4,5].

Extensive work regarding the possible contributing factors was completed by W. T. Reid, who postulated that both physical and chemical factors take part in the formation and accumulation of deposits [Ref. 6]. His research states that at least four physical processes are involved in the accumulation of deposits: (1) molecular diffusion, in which tiny particles move with velocities approaching that of gas molecules; (2) Brownian motion, in which somewhat larger particles behave as discrete pieces of matter during the "random-walk" motion imparted by collision with gas molecules; (3) turbulent diffusion, in which larger particles entering a boundary layer are propelled through a laminar sublayer by velocities imparted by the turbulent gas layer between the laminar sublayer and the bulk gas stream; and (4) inertial impacting, in which still larger particles receive sufficient kinetic energy from the main gas stream for the particles to penetrate a boundary layer or a turbulent region, or to follow a different path from the propelling gas stream.

The chemical factors include: (1) sintering, in which particles coalesce with the surface at elevated temperatures; and (2) chemical reactions such as autoxidation (at

temperatures below 500F) or pyrolysis (at temperatures above 900F) [Ref. 7]. Factors that are considered to be an inherent part of the formation of coking deposits are (1) the local temperature of the gas stream and the metal; (2) the wall material; (3) velocity of gas stream; and (4) exposure time [Ref. 5,6].

C. NOZZLES AND SWIRLPLATES

The E-2C Hawkeye is powered by two Allison T56-A-427 gas turbine engines and fueled by JP-5 jet fuel. The turbines have Dual Entry Fuel Nozzles (or double orifice nozzles). The advantage of using a double orifice nozzle is that they provide good fuel atomization and proper spray pattern at all rates of fuel delivery and airflow without the necessity of utilizing abnormally high fuel pressures [Ref. 8]. Schematics of the dual entry fuel nozzle can be seen in Figure 1.

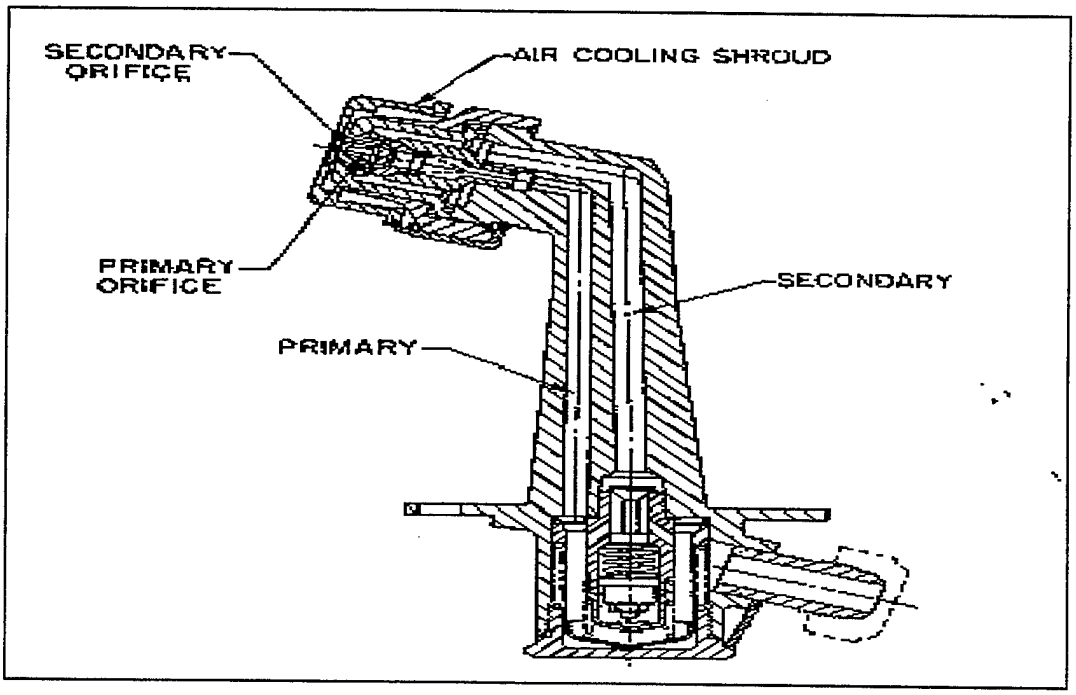

Figure 1: Schematic of Dual Entry Fuel Nozzle (from [9]).

A modification to the duplex nozzle is the dual orifice nozzle. It was developed to double the flow range of the duplex nozzle and to maintain a practically constant spray cone angle throughout the operating range. This nozzle features two concentric orifices and swirl chambers. The inner swirl chamber provides for primary flow and the outer swirl chamber allows for secondary flow. Since the secondary pressure is low, the atomization of the secondary fuel is assisted by the energy of the fully developed primary spray [Ref. 9]. Each of the nozzles contains a swirlplate that is used to provide the proper angle and flow for the fuel atomization. The swirlplate has 12 holes each of approximately 0.0165 inches in diameter. The swirlplate and nozzle sideview are shown in Figure 2. The major concern is the deposition of coke on the swirlplate itself and not so much of a concern is the coking of the external pilot body.

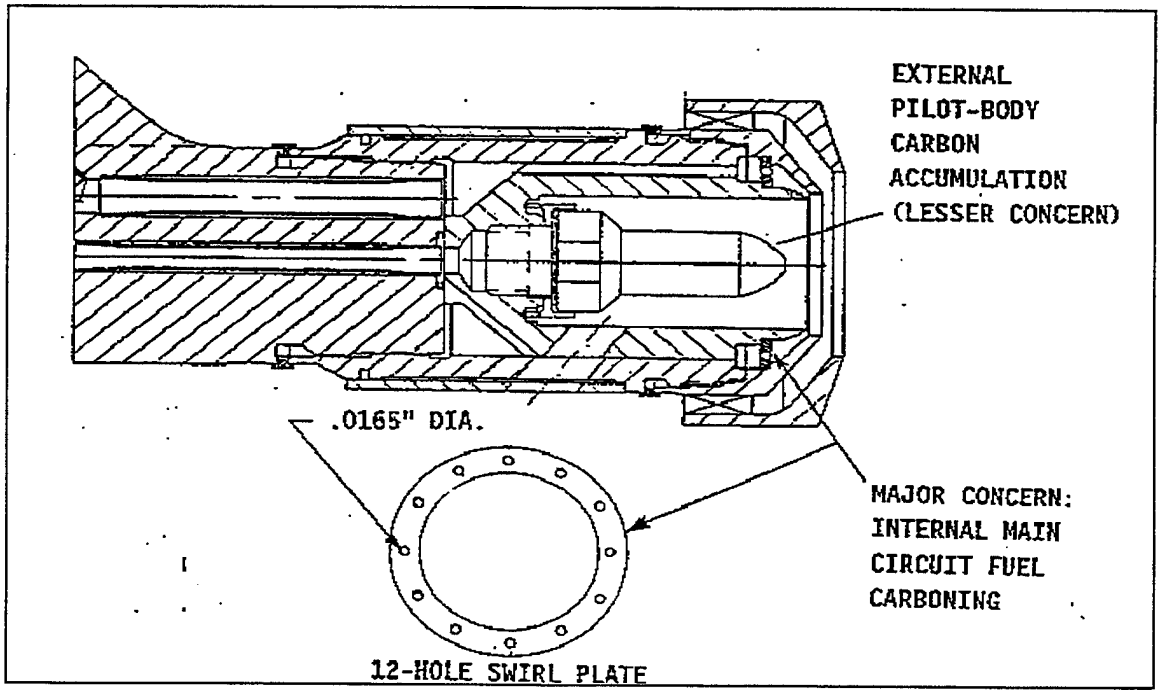

Figure 2: Side-view of nozzle head and schematic of swirlplate (from [10]).

The swirlplate's 12 holes are drilled at an angle in order to give the fuel/air mixture a swirling effect as it exits to ensure proper combustibility. It is seated in the internal main circuit of the nozzle assembly. During shutdown of the aircraft, the pressure falls below 125 psi, which is the opening pressure for the main valve. A small amount of fuel is then trapped in the fuel line and it is mainly this fuel that leads to the formation of coke deposits on the swirlplate [Ref. 1].

Each of the swirlplate's 12 holes has been labeled with reference to the positions of numerals on a clock. Each plate has a mark on it to indicate which hole is the 12 o'clock position. This hole is always placed top dead center in order to determine if there is any preferential coking related to the hole positions. All optical and SEM photos reference hole position in accordance with this system. Figure 3 shows the swirlplate hole nomenclature.

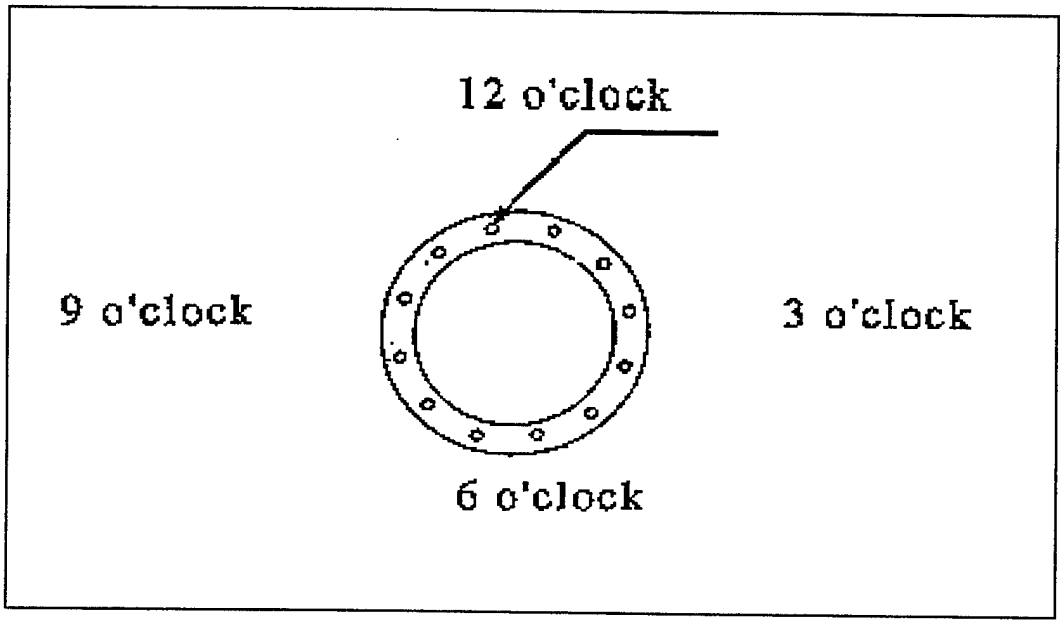

Figure 3: Schematic of the swirlplate hole numbering system (after [11]).

D. BACKGROUND

The exact mechanisms for coking are a great concern but the immediate concern is a possible solution to the problem with the engines of the E-2C. Several potential solutions that have been previously researched are as follows:

1. A purge system that would use low pressure air to force out trapped fuel before it reached the swirlplates [Ref. 12]. Although testing of this system was found to significantly decrease the coking rates, the idea was rejected by the NAVY because of the high cost to maintain the system, the added weight to the aircraft which would affect the performance of the plane and the time that would be required to install the system [Ref. 3, 12].

2. Using a shutdown procedure known as Low Speed Ground Idle(LSGI) [Ref. 1]. This interim solution is currently in use as it does reduce the coking rate by not allowing the temperature to reach the optimum range for coking and did not cost anything to implement. However, it poses a potential safety problem as the aircraft must maintain moving rotors while they are moved about the aircraft carrier's deck.

3. A further possible solution is to use different types of swirlplates. Currently, the swirlplates are made by Parker Co. and are manufactured from Type 347 stainless steel. Previous work by Prof. Roy Crooks [Ref. 1] and Vassiloyanakopoulos [Ref. 13] indicate that a possible solution to the coking problem lie in an improvement in the finish of the swirlplate being used. Vassiloyanakopoulos' work in the redesign of a testing method for this problem led to preliminary results that indicated that surface finish could significantly affect coking formation. His work verified that the test rig did work to expectations and that the surface finish of the swirlplates seemed to have an effect. This conclusion seems to be a valid one since both Allison Engine Co. and General Electric have been working on this coking problem by altering the surface finishes of the swirlplates [Ref. 1, 10, 14].

The solution that the Navy has temporarily accepted not only involves adopting the LSGI option but also using Allison Engine Co.'s swirlplates after they have been surface polished to a 30 micron finish.

E. OBJECTIVES

The objectives of this investigation are as follows:

1. To compare the Allison Engine Co.'s original production swirlplates with the replacement swirlplates currently in use to verify that they do, in fact, offer greater resistance to the formation of coke deposits.

2. To test additional swirlplates with various surface finishes in order to determine if a better alternative is available and to gain insight into the effect of surface finishes on coking rates.

3. To provide comparative data to NAVAIR concerning the coking rates of the various swirlplates in order to assist in determining a viable replacement swirlplate.

4. To perform microscopy on the swirlplates to verify the data extracted by weight and flow measurements.

The objectives listed above will provide an initial assessment of the possible usefulness of swirlplates with various surface finishes. The data collected could offer some insight into the factors affecting coking but is intended to solely determine the swirlplate that provides the best coking resistance.

F. TEMPERATURE PROFILE DETERMINATION

Laboratory tests on JP-5 have determined that coke formation occurs at temperatures greater than 300F when the fuel was exposed to air. While the fuel is flowing through the nozzle, during normal engine operation, only dissolved oxygen is available for coke formation [Ref. 15]. However, during engine shut down when soak back occurs as the fuel is trapped in the line, severe coking can occur at the nozzle tip.

Temperatures within the nozzle just seconds after shutdown are in the range of 350-400F and remein in this range for 30 to 50 minutes. This temperature range is the baseline for which testing was accomplished. Initial testing of the fuel coking problem of the T56-A-427 gas turbine engines was conducted by Allison Engine Co.[Ref. 1]. In these tests, Allison Engine Co. simplified the test procedure by setting their tests at a constant temperature of 400F. Although initial apparatus at the Naval Postgraduate School could accomplish the entire range using an oven driven by computer software, it was decided that NPS should adopt the constant temperature plan to facilitate the comparison of data with that of Allison Engine Co.

Subsequent work done by Vassiloyanakopoulos [Ref. 13] used the actual temperature profile provided by NAVAIR [Ref. 16]. This profile can be seen in Figure 4. It is this profile that will be used in the present work.

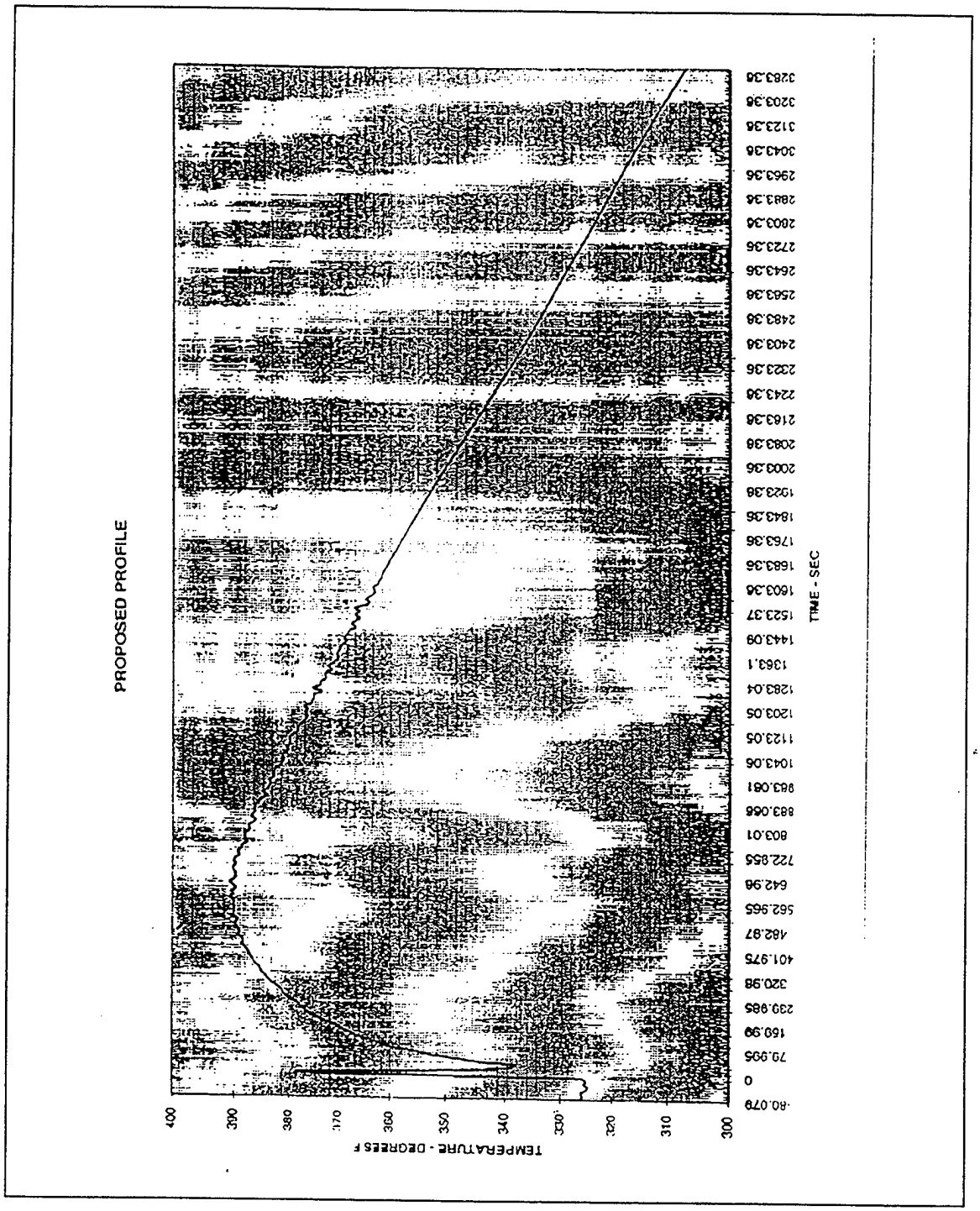

Figure 4: Temperature-Time profile (from [16]).

G. WEIGHT AND FLOW MEASUREMENTS

Measuring the weight of each swirlplate after every cycle gives an indication of the amount of fuel deposits on each swirlplate. However, it can only determine the total deposition on the swirlplate and not the location of the deposits. The location of the coking is important as coking on the broad surfaces of the plate is of no consequence since it does not restrict the flow by blocking the holes. By knowing that the fuel is depositing in the holes, a measure of hole closure can be performed and a quantitative result can be obtained as to the degree of blockage. Therefore, along with a weight measurement, a flow indication must be made. If we pass a gas through the nozzle and thus the swirlplate and measure various parameters such as pressure and temperature, we use a given model to determine the percent hole closure. For these flow measurements, the model adopted was the isentropic flow model.

Although isentropic flow can never be reached for flow with real gases, it can be used as a model as it is the closest flow model to the real situation. Since we are passing gas through a nozzle, and the distance that the gas travels is very short, we can neglect frictional effects as well as heat transfer [Ref. 17]. Using the same model that was used in previous experiments by Vassiloyanakopoulos [Ref. 13], the following model will be used for flow measurements:

For the gas mass flow rate equation $\dot{m} = \rho S v$ **(1)**

- $\dot{m}$: mass flow rate of gas
- ρ: density of gas
- S: surface area of holes
- v: velocity of gas stream

Using ideal gas flow model $\rho = \frac{P}{RT}$ **(2)**

P: gage pressure of gas
R: universal gas constant
T: temperature

From equations (1) and (2) along with the equation **(3)** for the speed of sound $a = \sqrt{\gamma RT}$

we get $\frac{\dot{m}}{S} = P(\frac{v}{a}) \times \sqrt{\frac{\gamma}{RT}}$ **(4)** , note also that $\gamma = \frac{C_P}{C_V}$ **(5)**

We then specify the temperatures and pressures measured at a particular point and we get the following for stagnation temperature and pressure:

$$T_o = T[1 + \frac{\gamma - 1}{2} M^2] \qquad \textbf{(6)}$$

$$P_o = P[1 + \frac{\gamma - 1}{2} M^{2\frac{\gamma}{\gamma - 1}}] \qquad \textbf{(7)}$$

Putting equations (6) and (7) together with equation (4) results in the following:

$$\frac{\dot{m}}{S} = \frac{P_o}{\sqrt{T_o}} \sqrt{\frac{\gamma}{R}} [1 + \frac{\gamma - 1}{2} M^{2\frac{\gamma + 1}{2(\gamma - 1)}}] \qquad \textbf{(8)}$$

For continuity of work previously accomplished by Vassiloyanakopoulos [Ref. C], we will assume that we have sonic flow through the holes and thus M=1. We can therefore use the equations above and manipulate them to solve for S, hole surface area, after each run. In this manner, we can determine the percent hole closure from run to run. We will denote the percent hole closure again for continuity purposes as:

$$\phi_2 = \frac{S_2 - S_1}{S_2} \times 100 \qquad \textbf{(9)}$$

II. EXPERIMENTAL PROCEDURE

A. EXPERIMENTAL SET-UP

The procedure and set-up to be used in this investigation are a direct result of the work that Vassiloyanakopoulos [Ref. 13] accomplished in his design of a testing apparatus and method. Vassiloyanakopoulos indicated that the need for a new design arose from safety factors concerning the amount of fuel present as well as the need to have a furnace that was more user friendly. His work produced the following experimental equipment in an effective test set-up:

1. A box furnace instead of an oven to allow for better temp-time profile control (220V Ney Co. series II model 2-525).
2. Two Zippette fuel pumps activated by relays to trigger fuel into regulators.
3. Two 3-way control values with Whitey regulators to control flow from Zippettes.
4. Two dual entry fuel nozzles.
5. A computer that used a LABTECH NOTEBOOK software package [Ref. 18] to control the cycles of the experiment.

The software allowed the programmer the flexibility of several different programming options. The options that pertain to the experiment are listed below:

1. Control over the length of cycle. Length was chosen at 30 minutes to allow for maximum number of cycles to increase number of experiments.
2. Control of temperature set-points to allow the user to select maximum and minimum temperatures.
3. Control over the duration of the climb and fall of the cycle. This allows for a given slope to be accomplished.

4. Control over total number of cycles to allow user to leave set-up and have the program run its course.

While the computer runs the experiment it is the coupling of it with the furnace that allow for maximum control and safety. The furnace also has an internal programming capability that allows the user to select the maximum temperature as well as the maximum rate to achieve these temperatures. The furnace is set at a point above the desired maximum temperature of the cycle. This allows a safety mechanism to be used. In the event that the temperature exceeds the desired and reaches the furnaces internal maximum set-point, the furnace will not allow the controlling program to raise the temperature any higher thus providing an over-temp safety mechanism. The new system design also uses no more than 100 milliliters of fuel per run which reduces the risk of fire. Also, the entire furnace and fuel system is enclosed in a fume hood.

While the system is operating, the software program provides the following data on screen:

1. A graphical display of the temperature time profile of each swirlplate.
2. The total number of cycles elapsed.
3. The total time elapsed.
4. The current temperature of each swirlplate as well as the ambient air temperature. This is accomplished using thermocouples attached to the relays.

Additionally, the temperature values of the thermocouples are saved to a file for later use. A schematic of the entire set-up can be seen in Figure 5.

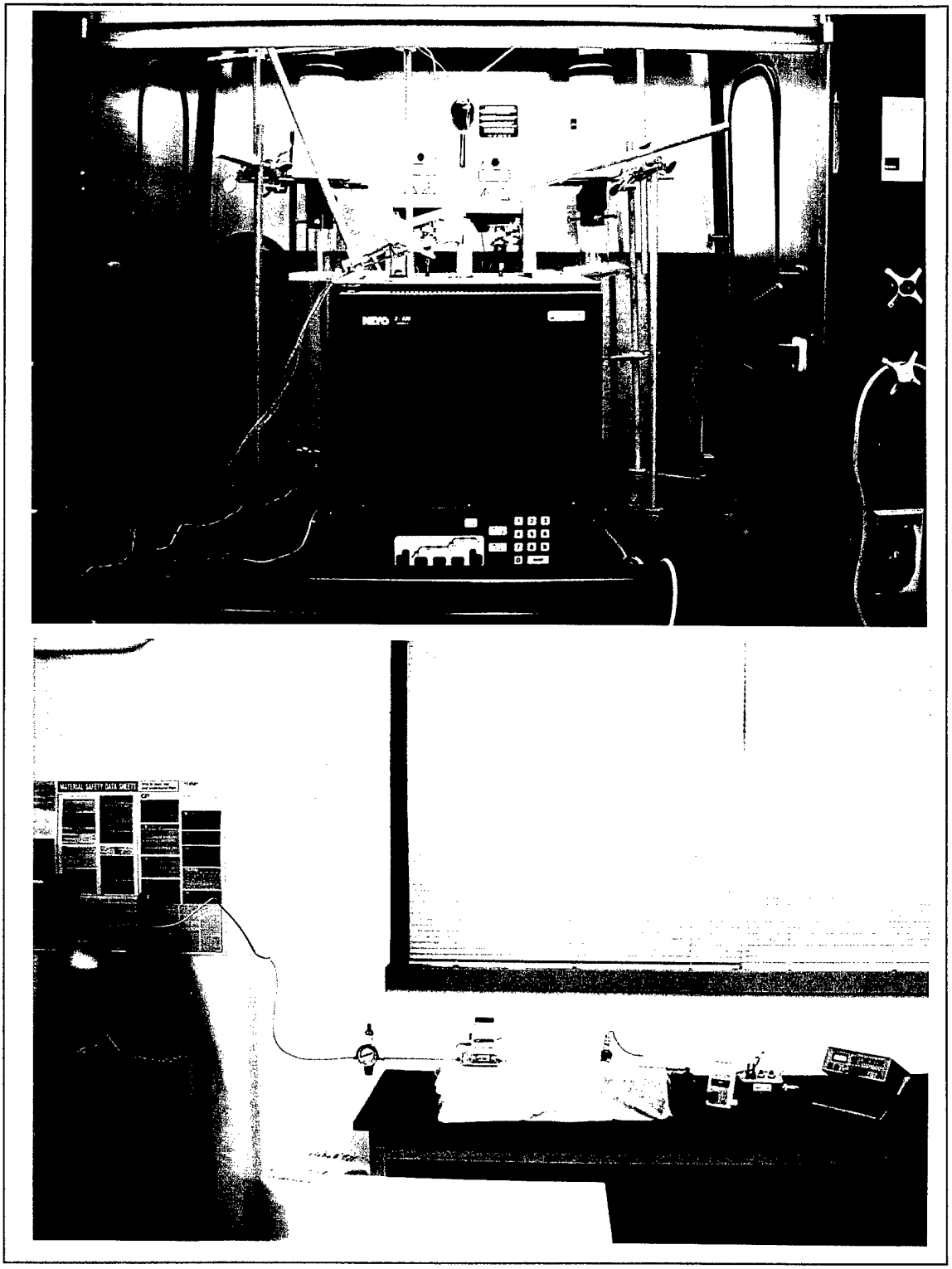

Figure 5: Photographs of the experimental and flow set-ups for the Nozzle Project.

B. EXPERIMENT CYCLE AND DATA FLOW

The experiment is started by turning the oven on and choosing the run icon on the software program. When the control program is started, the following actions account for one complete cycle:

1. The Zippettes are tripped and draw fuel into their inlets creating a positive pressure at the inlet to the three way valve due to the gravity fed fuel from the Zippette.

2. The three way valve cycles and allows fuel into the nozzle.

3. The valve closes.

4. The temperature of the swirlplates is increased by the increasing temperature of the furnace controlled by the program. The temperature follows the profile of Figure 3 for 30 minutes. The maximum temperature reached is approximately 380 F.

5. The temperature is decreased following the temperature profile to the start point of 350 F.

6. The cycle is repeated.

The furnace holds two dual entry fuel nozzles which allows for swirlplates to be tested against one another in the same environment, thus reducing the potential errors involved with separate tests. Data could be accumulated at twice the rate of a single test run. The temperature values for the two thermocouples are sent to a data file and can be used to verify the temperature-time profile. An example of a single cycle can be seen in Figure 6. The data file stores the entire run so that the temperature at any particular time can be chosen. Figure 7 shows the output from a data file plotted for multiple cycles.

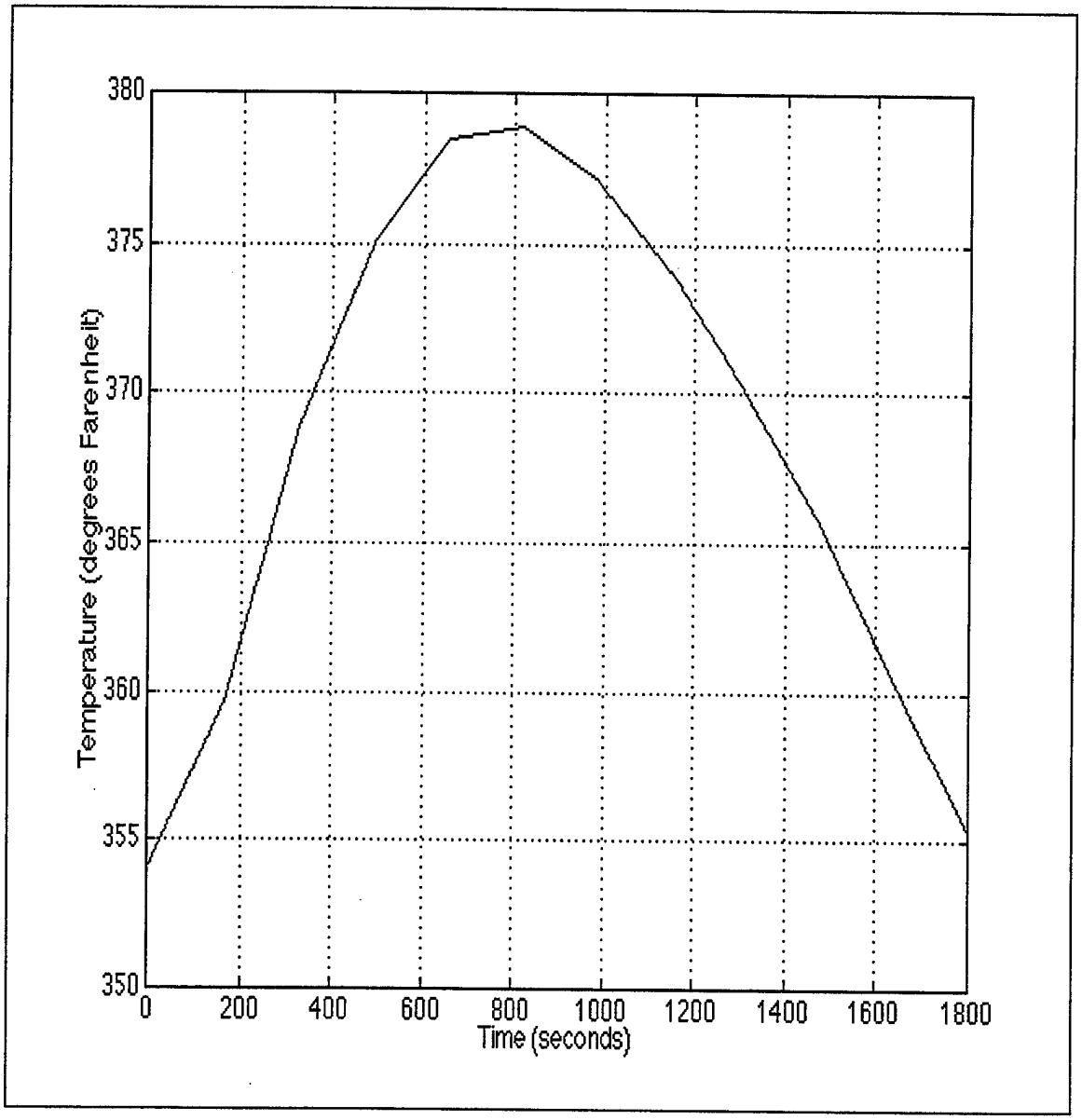

Figure 6: Temperature-Time profile for one 30 minute cycle.

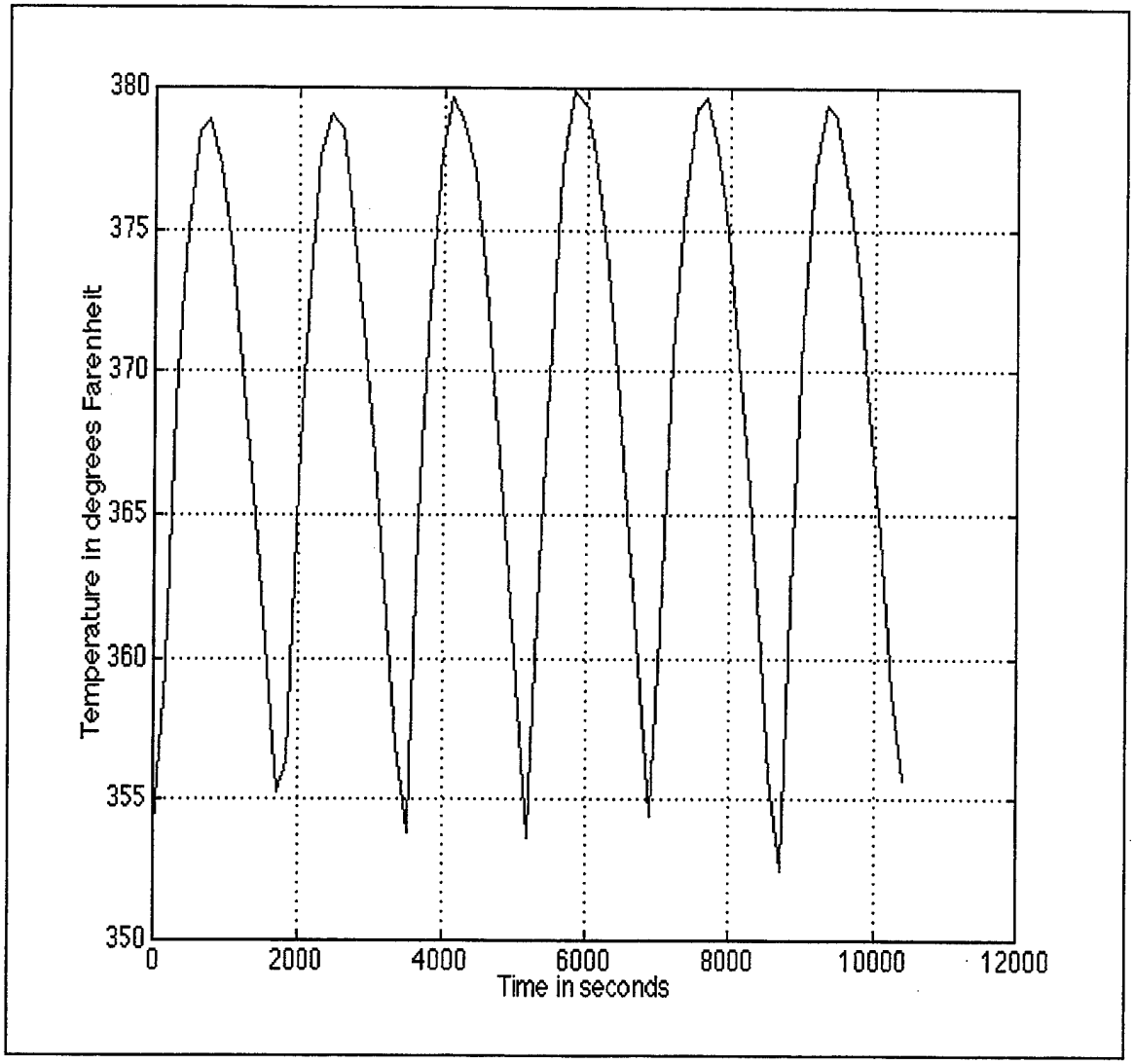

Figure 7: Temperature-Time profile for multiple cycles.

The program runs until it reaches the number of cycles chosen by the programmer. The oven is then allowed to cool before the user handles the swirlplates. The data flows from the computer at start-up to the relays and ends up with temperature data being sent to files for later use.

C. DATA INTERPRETATION

Upon completion of a run, which consists of 30 cycles of 30 minutes each, the system was turned off and allowed to cool. The data extraction was then performed in steps of exact sequence each time. The sequence and description of each investigative step is explained in detail below.

The plates were first placed in the flow measurement set-up, seen in Figure 8, where measurements were taken using a Top-Trak, digital, electronic flow meter. Air from an O_2 cylinder was sent through a regulator, pressure gage, flow meter, pressure transducer, voltmeter and nozzle. Readings from the flow meter, voltmeter and a thermocouple were recorded. The reason that the flow measurement was chosen as the first step was to eliminate any loose clinging fuel deposits that would contribute to false high weight measurements and would be blown off by the fuel air mixture during normal operation.

Using equation (7) along with the following numbers:

$$\gamma = \frac{C_P}{C_V} = 1.4 \qquad \rho = 1.292 kg/m^3 \qquad R = 287 J/kgK$$

a relationship for the swirlplate's hole surface area, $S = \frac{\dot{m}}{0.04042} \times \frac{\sqrt{T_o}}{P_o}$ **(10)** can be obtained. To improve the accuracy of the gage pressure value, P, the calibration chart for the pressure transducer is used and intermediate voltage values are pulled off the chart, shown in Figure 9. A table of values for the pressure transducer calibration process

are given in Table 1. The absolute pressure is then calculated by adding the measurement to the atmospheric pressure for the time of the experiment.

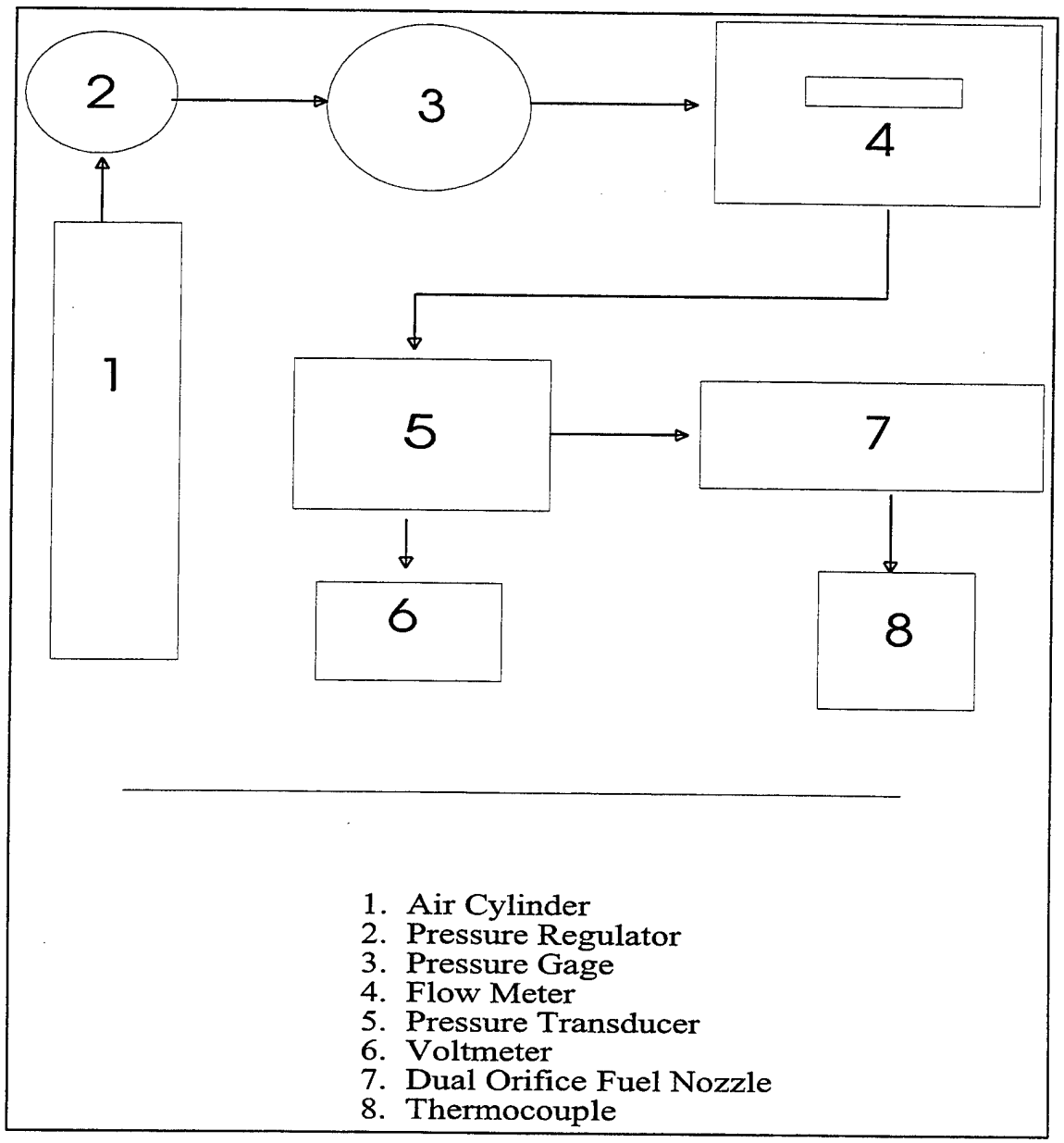

Figure 8: Schematic of the flow measurement experiment set-up.

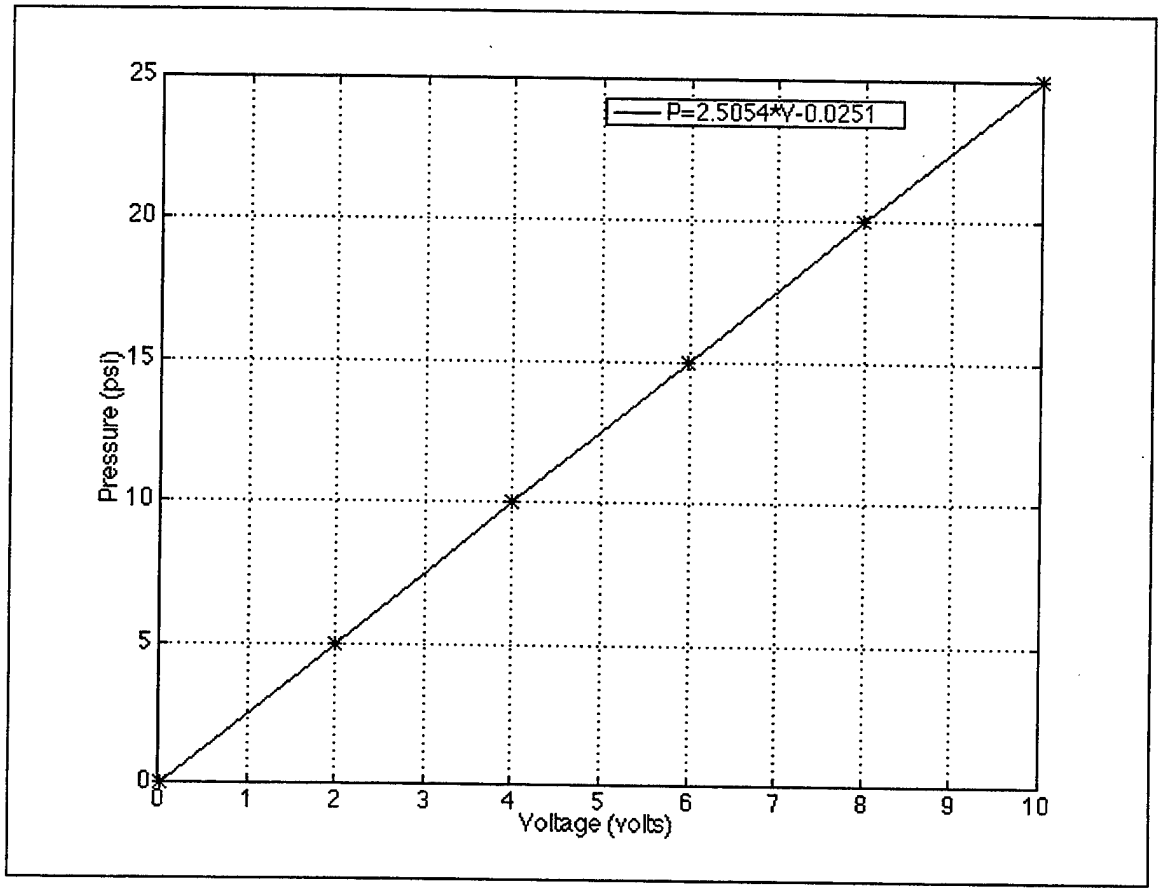

Figure 9: Pressure transducer calibration curve.

Psi	0.00	25.00	0.00	5.00	10.00	15.00	20.00	25.00	15.00	5.00	0.00
volts	0.016	10.00	0.023	2.00	3.99	5.99	7.99	10.00	5.99	2.01	0.023

Table 1: Pressure transducer calibration data

The pressure transducer calibration curve is linear and follows the equation:

$$P = 2.5054 \times V - 0.0251 \qquad \text{with} \quad \text{P: psi} \qquad \text{V: volts}$$

The samples must then be weighed using the METLER AT digital balance. The weights are then recorded and compared to the weights of the virgin samples and a percent increase in weight is calculated. Both the flow and weight measurements are accomplished after each 30 cycle run.

Optical microscopy is also accomplished after each run. The swirlplates are examined using a Zeiss optical microscope with an attached camera. Optical pictures are taken with an IMAGE PRO software package. Pictures of the 12, 3 ,6 and 9 o'clock hole positions were taken each time. Additional pictures of any specific feature of any hole were taken as needed.

Scanning Electron Microscope (SEM) examination is accomplished periodically to investigate the surface or inner side of the holes. This examination reveals where the coking is occurring and can be used to determine if preferential coking is occurring. This procedure is also a reliable method of verifying the data obtained from the weight and flow measurements. Pictures were also taken in this part of the experiment and compared to the pictures of the respective virgin samples.

All of the methods described above are ways of verifying, comparatively, the swirlplate that best resists fuel deposits. The experiments cannot determine the reason for the coking but each part can support the previous in determining the best choice of swirlplates.

III. RESULTS

A. GENERAL

Following is a collection of data retrieved during present testing as well as data retrieved from prior investigations by Vassiloyanakopoulos [Ref. 13] and Dr. Crooks [Ref. 1]. This data will be used to show the usefulness of the new test rig that was completed by Vassiloyanakopoulos [Ref. 13] as well as to verify the results of the initial work by Dr. Crooks [Ref. 1]. The data accumulated from the previous test will provide a starting point for the current testing. The comparative nature of these tests will lead to conclusions of generality and not to conclusions of absolutes. It will lead to the focusing of future studies toward the optimal swirl plate surface coating for maximum resistance to coking.

B. WEIGHT MEASUREMENTS

First and foremost, the data completed prior to this investigation was reviewed. The following data represents initial tests from the old test rig as well as testing by Vassiloyanakopoulos [Ref. 13] on the new test rig. The nomenclature used to represent certain surface finishes, with Production Swirl Plate labeled PSP, is shown in Table 2. All future references to surface finishes will use these labels.

PSP only - no polishing, no coating	A
PSP with surface polished to 50 microns and no coating	A'
PSP with surface polished and hole polished, no coating	B
PSP with surface and hole polished and coated with amorphous diamond coat	B-md
PSP with a silicon coating	A-sil
PSP with amorphous diamond coating	A-md

Table 2 : Nomenclature for Swirlplates

1. A vs. A'.

The first two swirlplates, A22 and A'27, tested by Dr. Crooks [Ref. 1] were a production swirlplate and a production swirlplate that had been polished to 30 microns. The weight gains obtained from Dr. Crooks runs, consisting of 27 cycles at 50 minutes per cycle, are shown below in Tables 3 and 4. Figure 10 is a plot of the weight gains of each of the swirlplates and indicates that no real difference in coking rates can be concluded from this data.

With so few data points it is difficult to see any significant pattern. However, it's evident that there is not much difference between the two swirlplates from the data presented.

Cycles	0	27	54	81
Weight (milligrams)	822.27	822.51	822.67	822.89
Weight increase	-	0.24	0.40	0.68

Table 3: Weight measurements of A22 from initial test of old test rig.

Cycles	0	27	54	81
Weight (milligrams)	762.3	762.99	763.19	763.47
Weight increase	-	0.26	0.46	0.74

Table 4: Weight measurements of A'27 from initial test of old test rig.

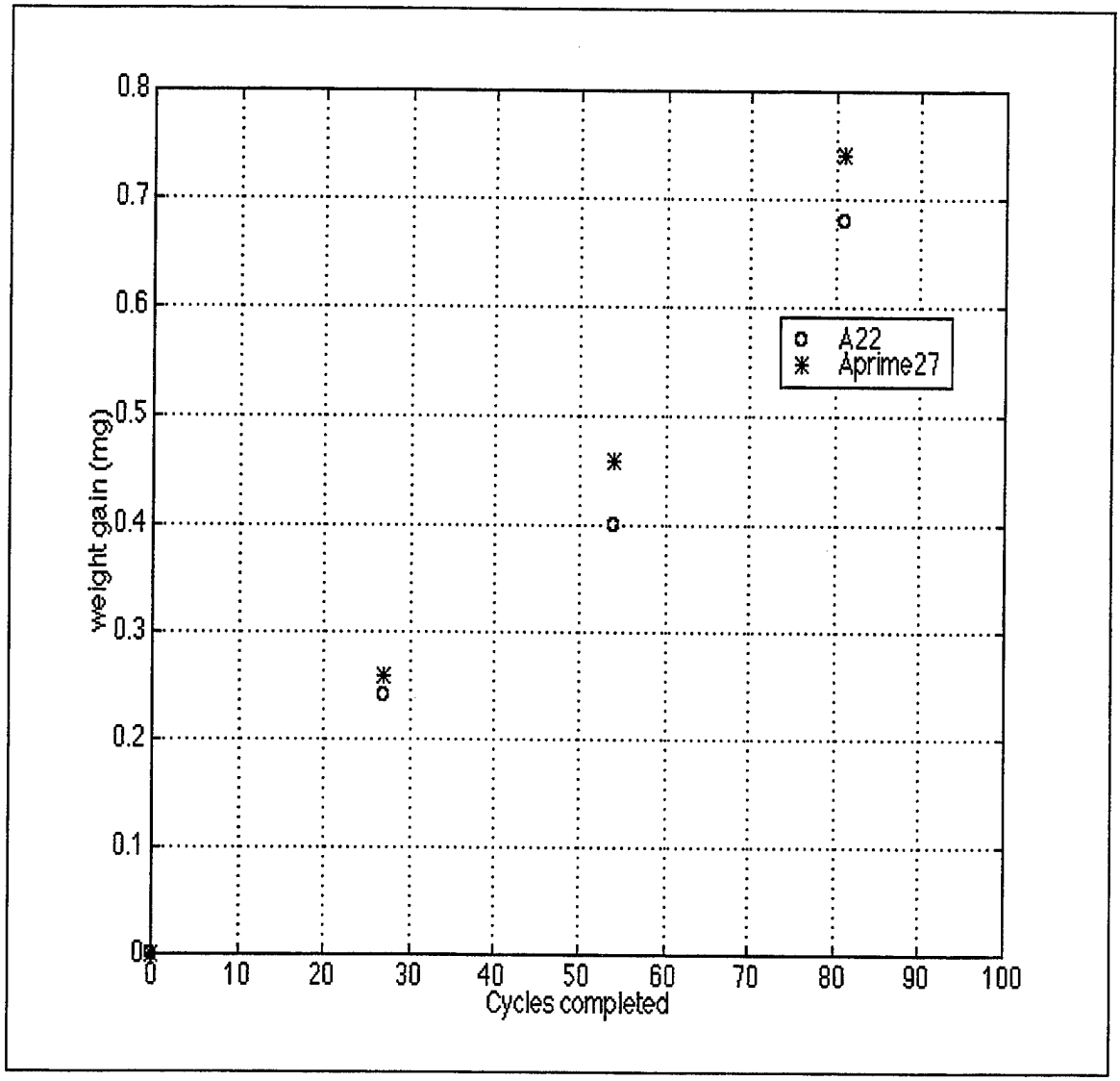

Figure 10: Weight increase versus number of cycles completed by A22 and A'27.

2. A vs. B.

Tables 5 an 6 are data from the work of Vassiloyanakopoulos and the new testing rig. The data from these tables are plotted in Figure 11 where it is very apparent that there is a significantly lower deposition rate for the B18 swirlplate. These tests were conducted using runs of 25 cycles of 30 minutes per cycle.

Cycles	0	25	50	75	100	125	150
Weight (milligrams)	826.3	826.93	827.18	827.40	827.52	827.70	827.90
Weight increase	-	0.66	0.88	1.10	1.22	1.40	1.60

Table 5: Weight measurements of A27 from initial tests with new test rig.

Cycles	0	25	50	75	100	125	150
Weight (milligrams)	852.50	852.74	852.91	852.95	853.01	853.16	853.33
Weight increase	-	0.24	0.41	0.45	0.51	0.65	0.80

Table 6: Weight measurements of B18 from initial tests with new test rig.

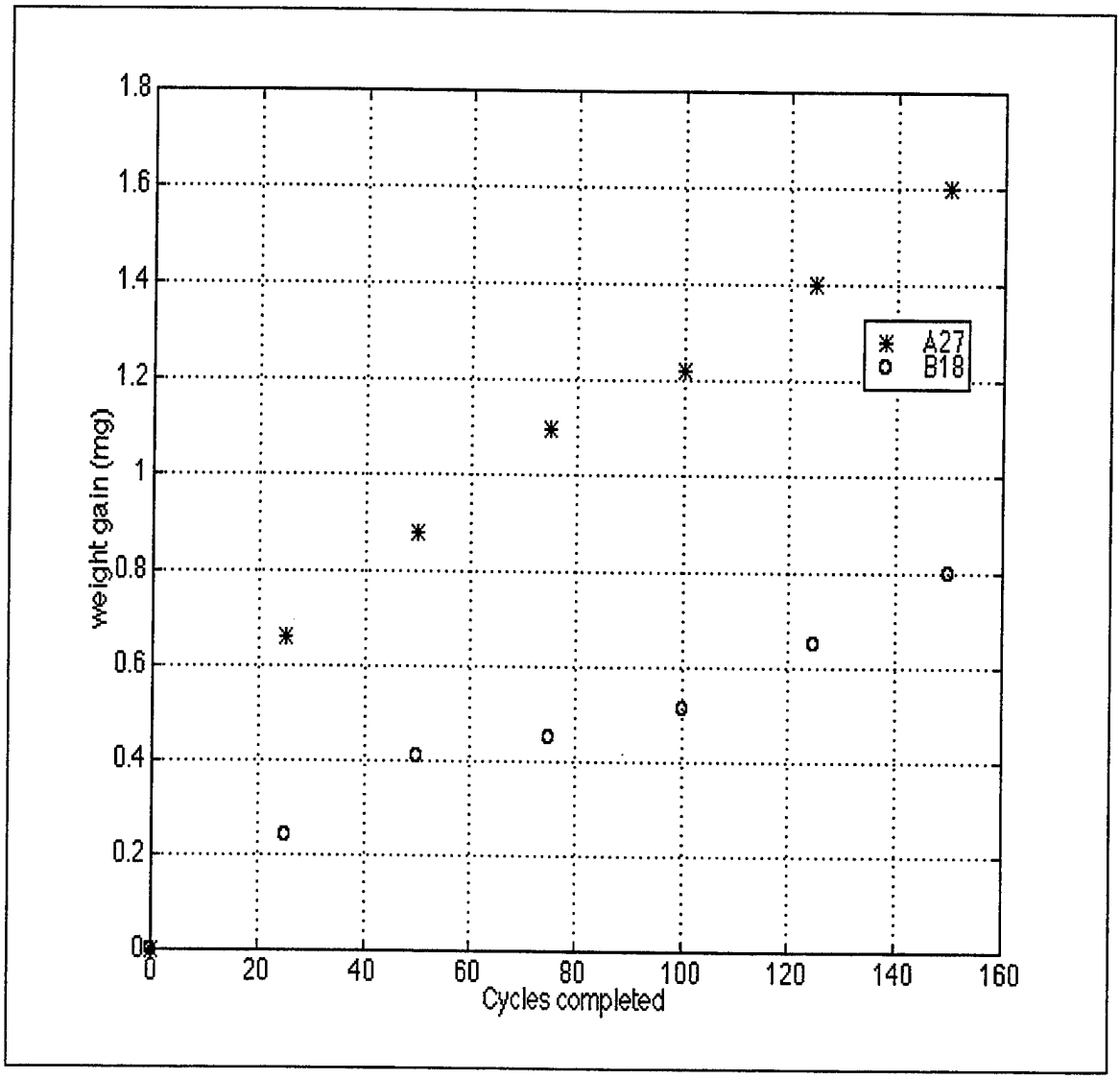

Figure 11: Weight increase versus number of cycles completed by A27 and B18.

3. A vs. A'.

This test again provided a comparison of a production plate with a polished production plate, which is important as the polished plates have been accepted as a temporary solution. This comparison helps to verify that the polished plate does in fact provide additional resistivity to coking. All work from this point forward will comprise of runs of 30 cycles, each cycle consisting of 30 minutes.

Cycles	0	30	60	90	120	150
Weight (milligrams)	819.70	820.01	820.22	820.37	820.49	820.81
Weight increase	-	0.31	0.52	0.67	0.79	1.11

Table 7: Weight measurements of A01.

Cycles	0	30	60	90	120	150
Weight (milligrams)	750.35	750.53	750.76	750.90	751.05	751.18
Weight increase	-	0.18	0.41	0.55	0.70	0.83

Table 8: Weight measurements of A'01.

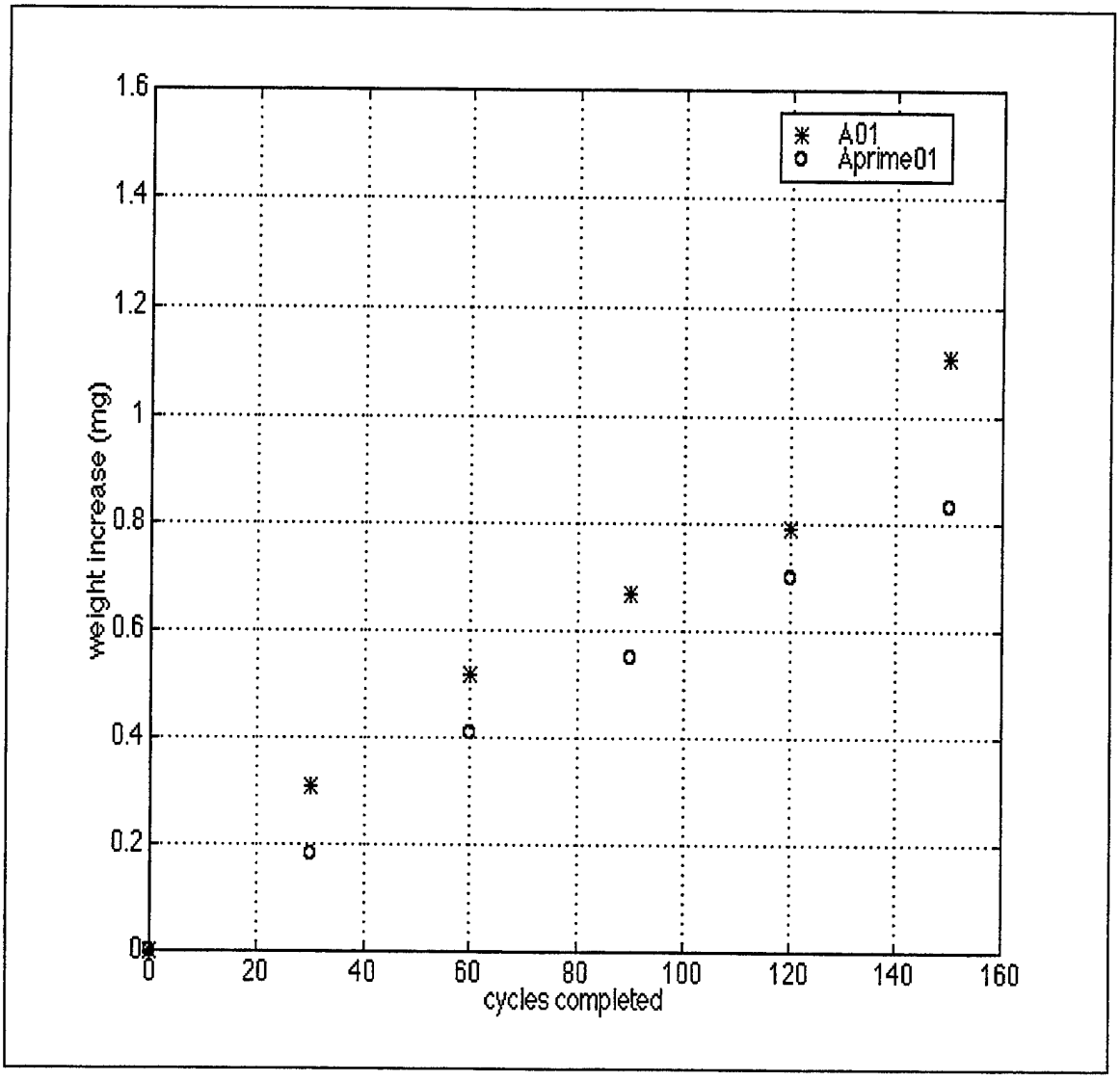

Figure 12: Weight increase versus number of cycles completed by A01 and A'01.

4. B vs. B-md.

The swirl plates chosen, B17 and B-md20, represent the first test of the viability of new alternate coatings. Testing a B type swirl plate helped to verify if a consistency between the present work and that of Vassiloyanakopoulos existed, while allowing the B type plate to act as the control in the testing of the amorphous diamond coated swirl plate.

Cycles	0	30	60	90	120	150
Weight (milligrams)	856.87	857.05	857.46	857.63	857.74	857.84
Weight increase	-	0.18	0.59	0.76	.87	.97

Table 9: Weight measurements of B17.

Cycles	0	30	60	90	120	150
Weight (milligrams)	851.79	852.06	852.16	852.34	852.64	853.06
Weight increase	-	0.27	0.37	0.55	0.85	1.27

Table 10: Weight measurements of B-md20.

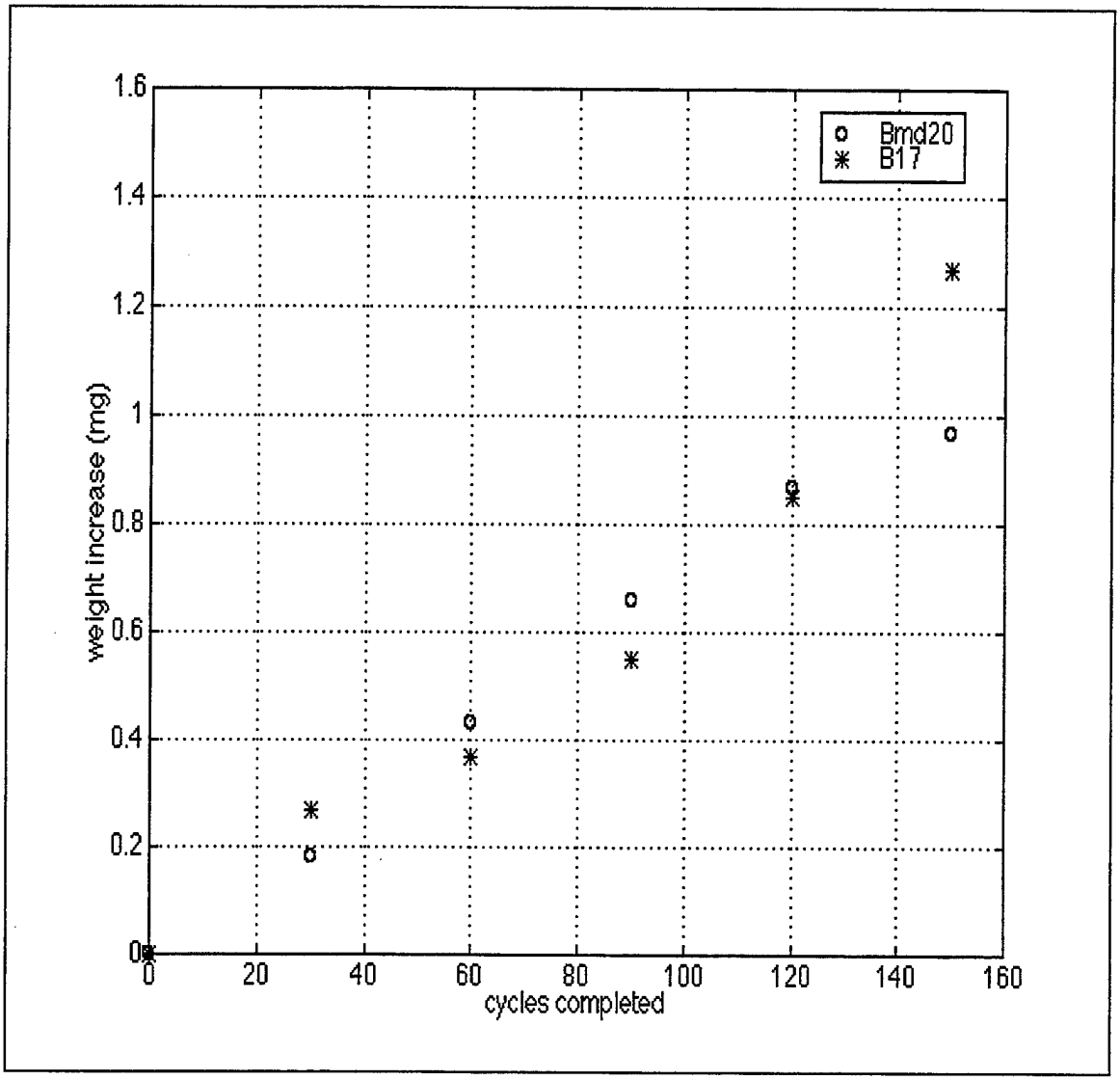

Figure 13: Weight increase versus number of cycles completed by B17 and B-md20.

5. B vs. A-md.

An additional B plate was tested in order to solidify the earlier results. The other swirl plate tested wais a regular production swirl plate coated with amorphous diamond. Earlier tests indicated that the amorphous diamond coating worked well up until the 150 cycle point. Using the diamond coating on a normal production plate shed additional insight into the reliability of the coating.

Cycles	0	30	60	90	120	150
Weight (milligrams)	855.89	855.91	856.18	856.27	856.36	856.58
Weight increase	-	0.02	0.29	0.38	0.47	0.69

Table 11: Weight measurements of B10.

Cycles	0	30	60	90	120	150
Weight (milligrams)	827.91	828.03	828.28	828.43	828.58	828.83
Weight increase	-	0.13	0.37	0.52	0.67	0.93

Table 12: Weight measurements of A-md25.

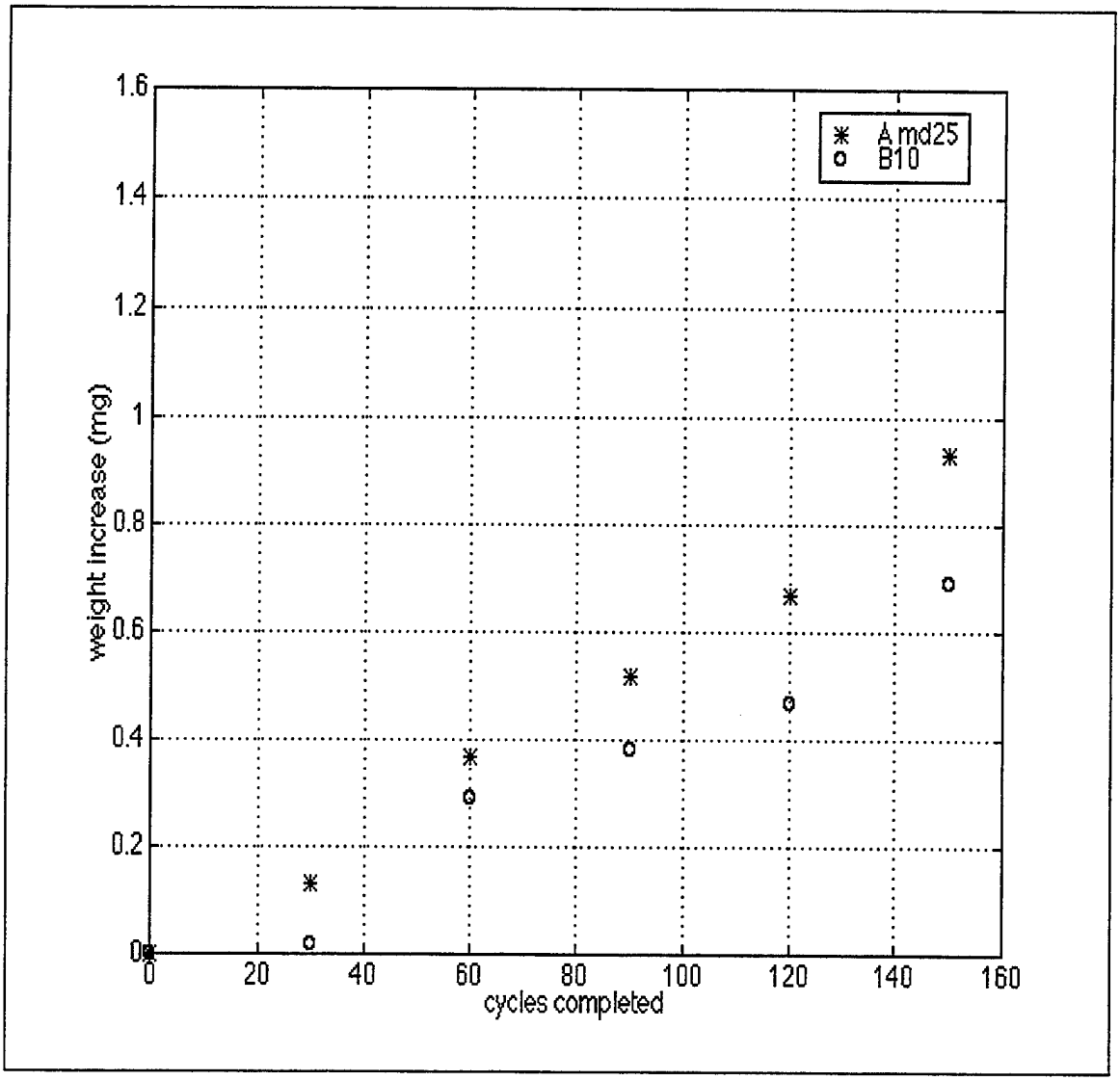

Figure 14: Weight increase versus number of cycles completed by B10 and A-md25.

6. A vs. A-sil.

Another surface finish chosen was a silicon coating that was tested with an original production swirl plate. This test verified previous work done on the original production plate while allowing the production swirl plate to act as a control for the silicon coated swirl plate in order to determine the increase in resistivity due to the silicon. The weight gains of the two swirl plates, labeled A28 and A-sil23, are shown below in tables 13 and 14 while Figure 15 gives a graphical representation of that data.

Cycles	0	30	60	90	120	150
Weight (milligrams)	819.78	820.08	820.40	820.71	820.91	821.19
Weight increase	-	0.30	0.61	0.92	1.13	1.40

Table 13: Weight measurements of A28.

Cycles	0	30	60	90	120	150
Weight (milligrams)	819.54	819.86	820.13	820.31	820.52	820.68
Weight increase	-	0.33	0.59	0.78	0.98	1.15

Table 14: Weight measurements of A-sil23.

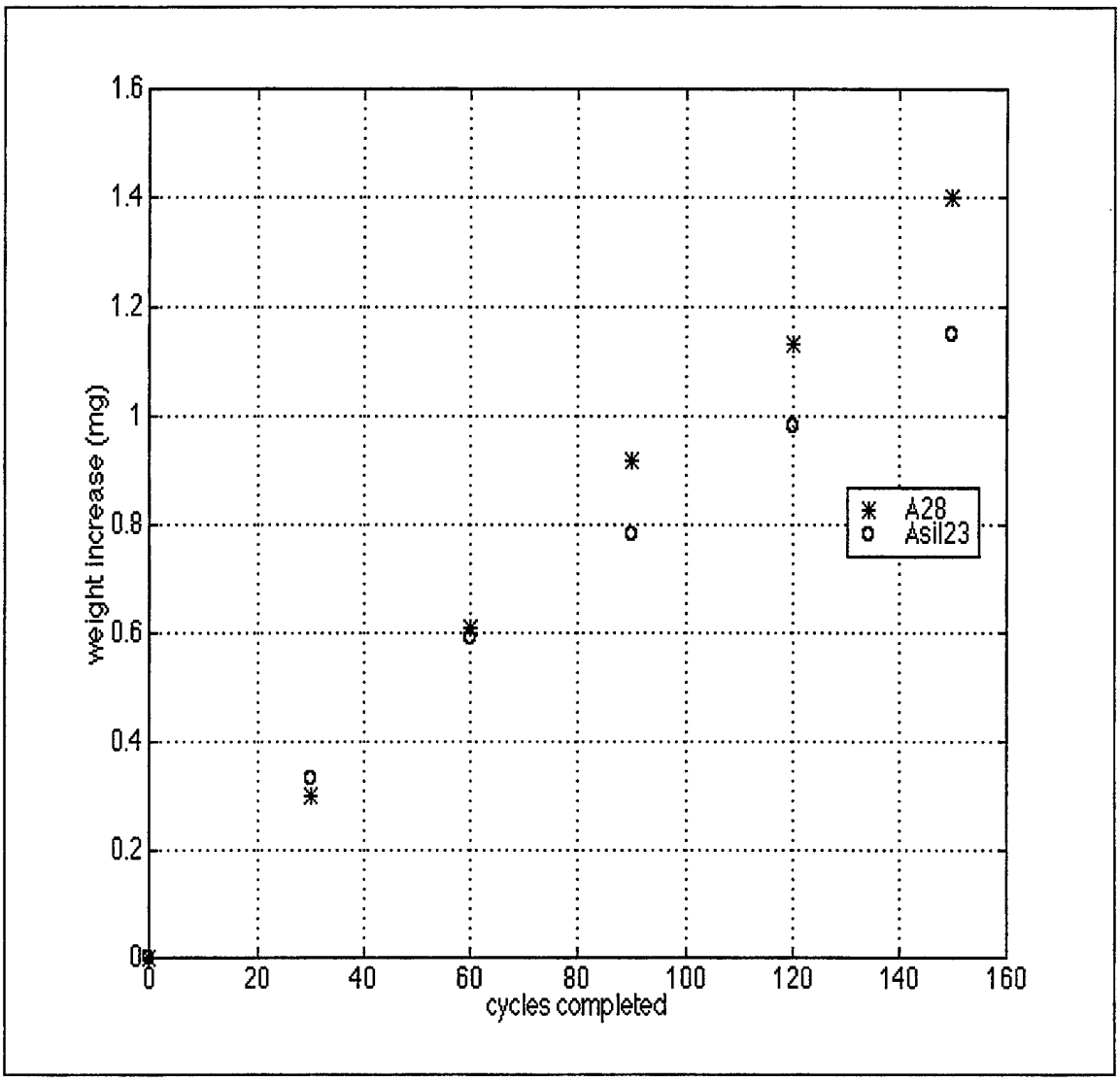

Figure 15: Weight increase versus number of cycles completed by A28 and A-sil23.

7. B vs. A-sil.

A silicon coated swirl plate as well as an additional B plate were tested in this run. This test produced additional data for the silicon coating, again on a production swirl plate, while providing more data for the B type plates.

Cycles	0	30	60	90	120	150
Weight (milligrams)	850.75	850.87	850.94	850.99	851.14	851.28
Weight increase	-	0.12	0.19	0.24	0.39	0.53

Table 15: Weight measurements of B12.

Cycles	0	30	60	90	120	150
Weight (milligrams)	819.53	819.57	819.85	820.10	820.14	820.30
Weight increase	-	0.04	0.31	0.56	0.61	0.76

Table 16: Weight measurements of A-sil24.

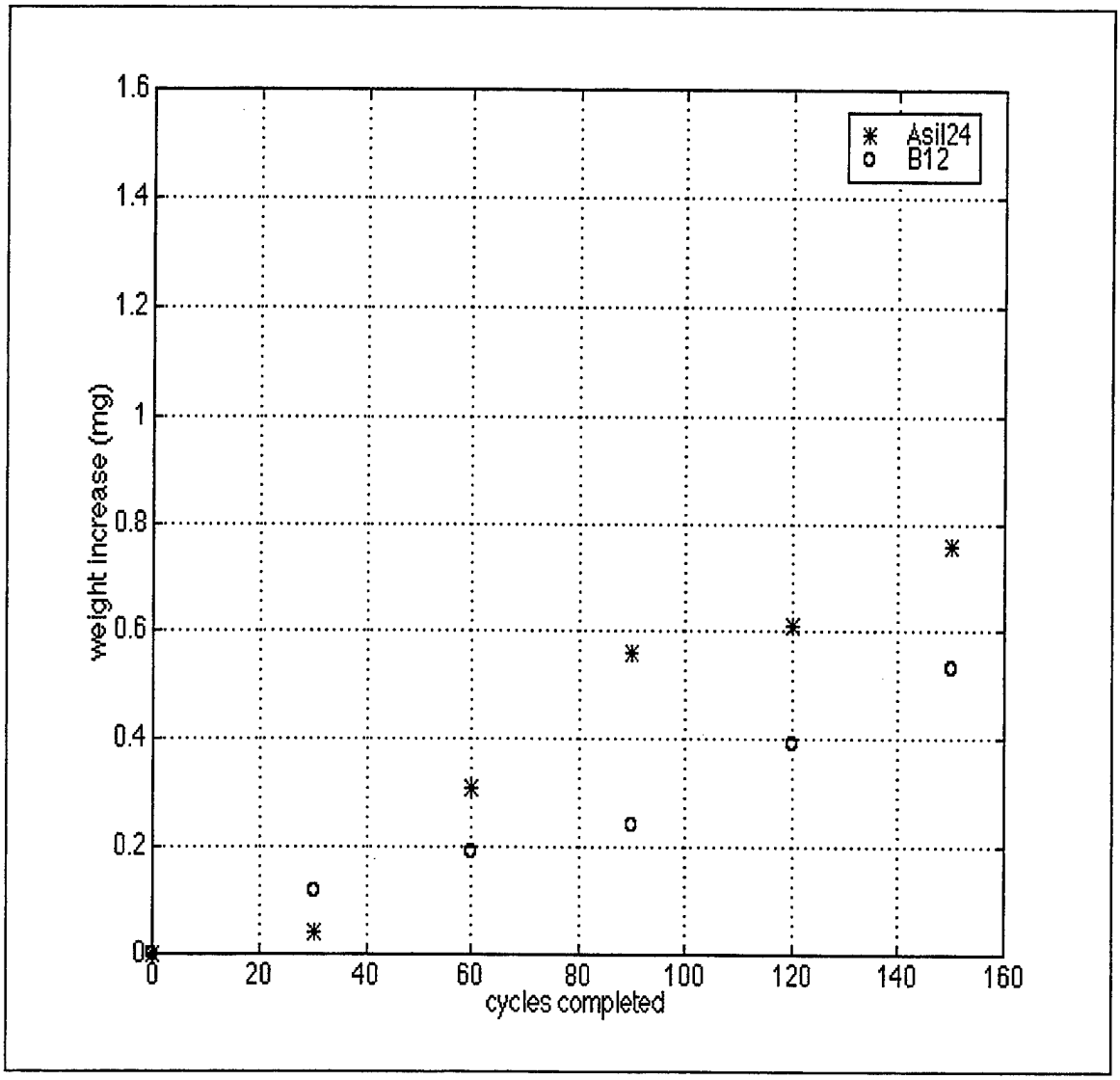

Figure 16: Weight increase versus number of cycles completed by B12 and A-sil24.

8. B vs. B.

Two B plates were chosen as the final test in order to gain additional data points to support the results found previously. Tables 17 and 18 have the weight gain data while Figure 17 displays it graphically.

Cycles	0	30	60	90	120	150
Weight (milligrams)	841.22	841.36	841.47	841.70	841.79	841.96
Weight increase	-	.14	.25	.48	.57	.74

Table 17: Weight measurements of B13.

Cycles	0	30	60	90	120	150
Weight (milligrams)	855.60	855.73	855.90	856.02	856.19	856.32
Weight increase	-	.13	.20	.42	.59	.72

Table 18: Weight measurements of B14.

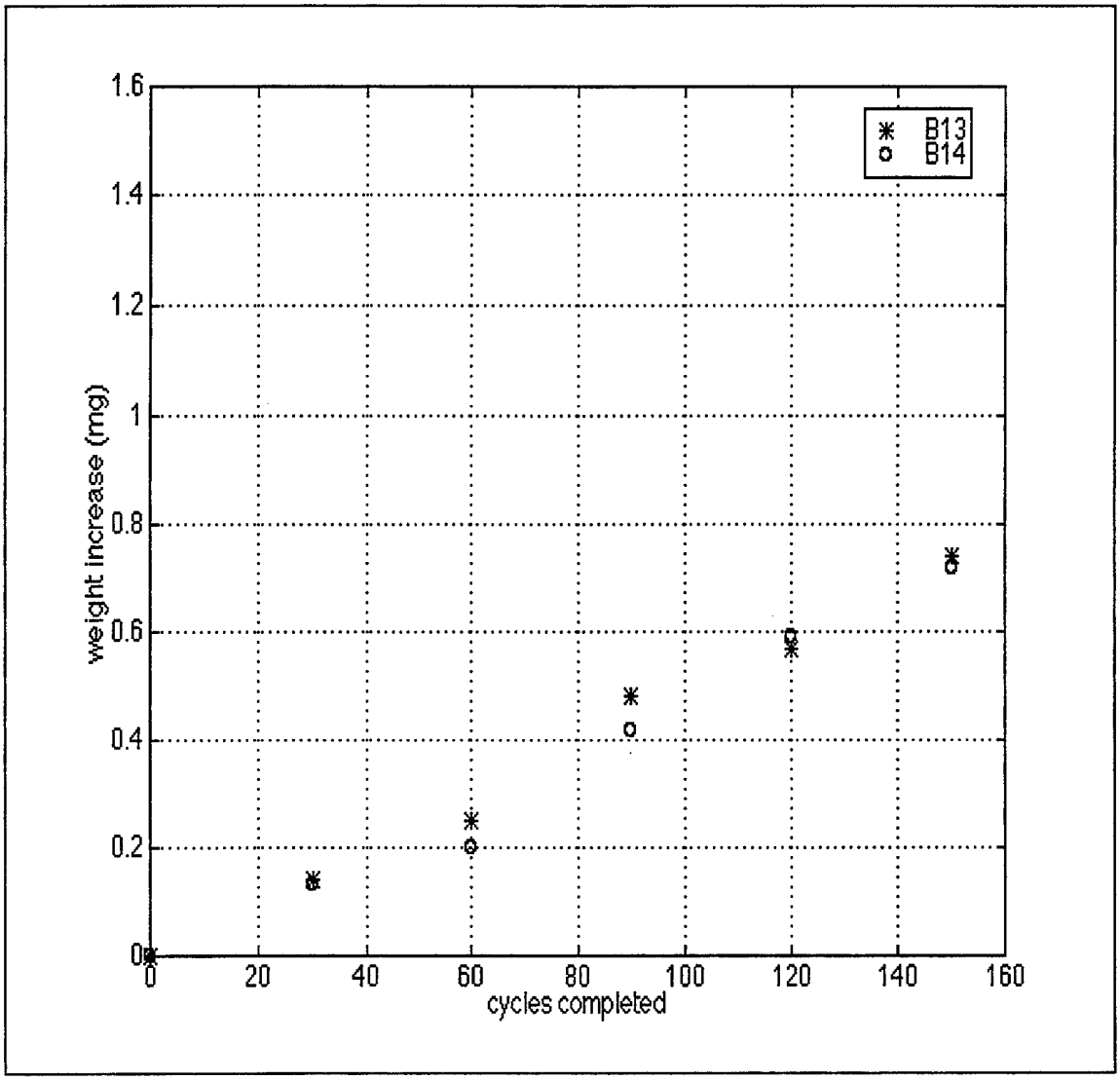

Figure 17: Weight increase versus number of cycles completed by B13 and B14.

C. OPTICAL MICROSCOPY

After each complete run, photographs of the swirlplates were taken using the IMAGE-PRO software package previously described. Photos were taken of the 12 o'clock and 6 o'clock positions as well as any other holes that may show particular signs of coking. The photos help to indicate whether the weight gains are due to coking on the surfaces of the plates or in the holes. They were used in a supporting role to the weight gain and flow measurements.

The optical photos of the runs accomplished in previous work will not be shown here as they were shown in detail in work accomplished by Vassiloyanakopoulos [Ref. 13]. The photos will be shown in order of the runs indicated previously. The first set of photos are from run 1 with A01 versus A'01. Each photo caption indicates the plate number, hole position and number of cycles completed.

Figures 18 through 23 do not clearly indicate any dominant plate with reference to coking resistivity nor do they show any indication of position preference. All additional photos will be shown as follows:

1. A01 vs. A'01, Figures 18 - 23 .
2. B17 vs. B-md20, Figures 24 - 33.
3. B10 vs. A-md25, Figures 34 - 45
4. A28 vs. A-sil23, Figures 46 - 59
5. B12 vs. A-sil24, Figures 60 - 67
6. B13 vs. B14, Figures 68 - 75

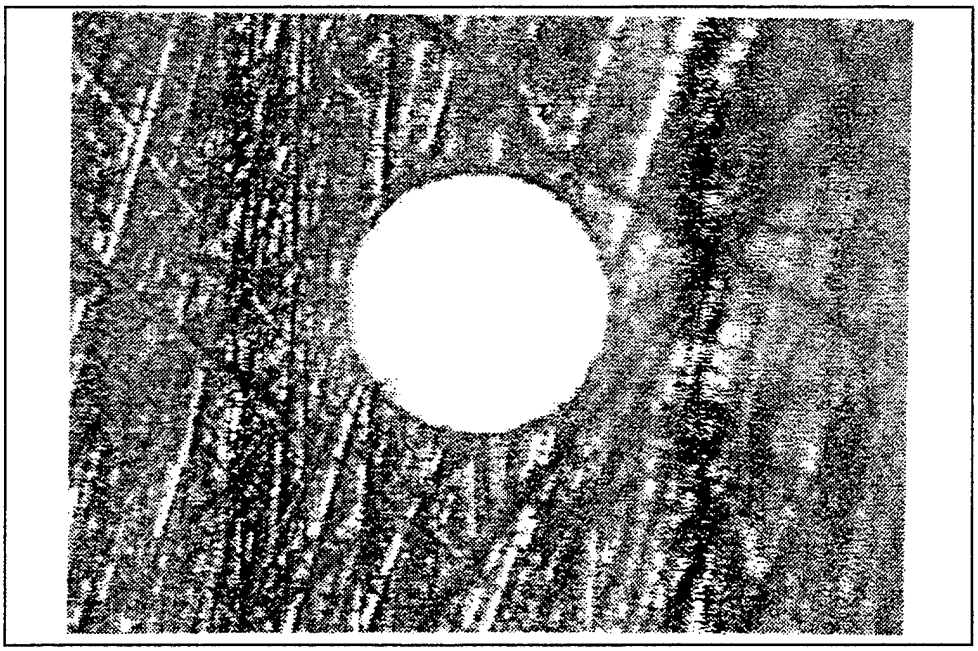

Figure 18: Optical photo of A01, 12 o'clock, zero cycles.

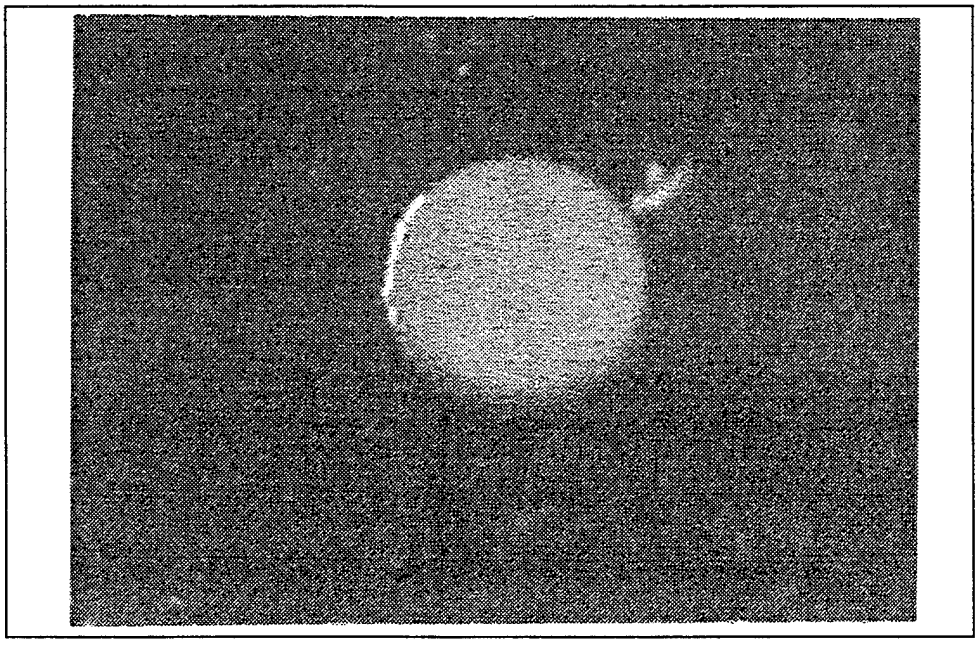

Figure 19: Optical photo of A'01, 12 o'clock, zero cycles.

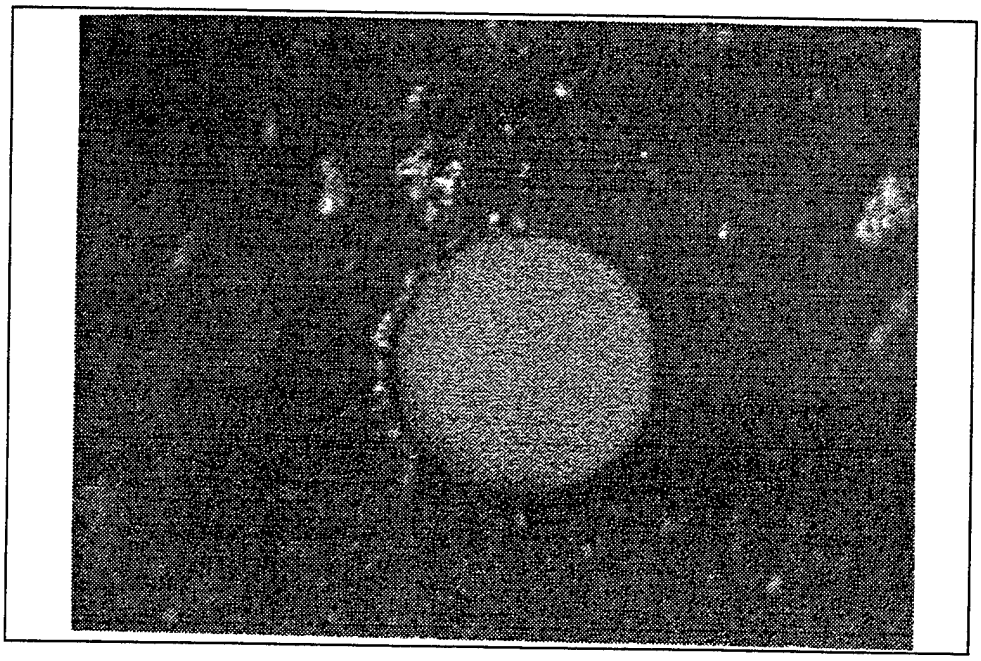

Figure 20: Optical photo of A01, 12 o'clock, 150 cycles.

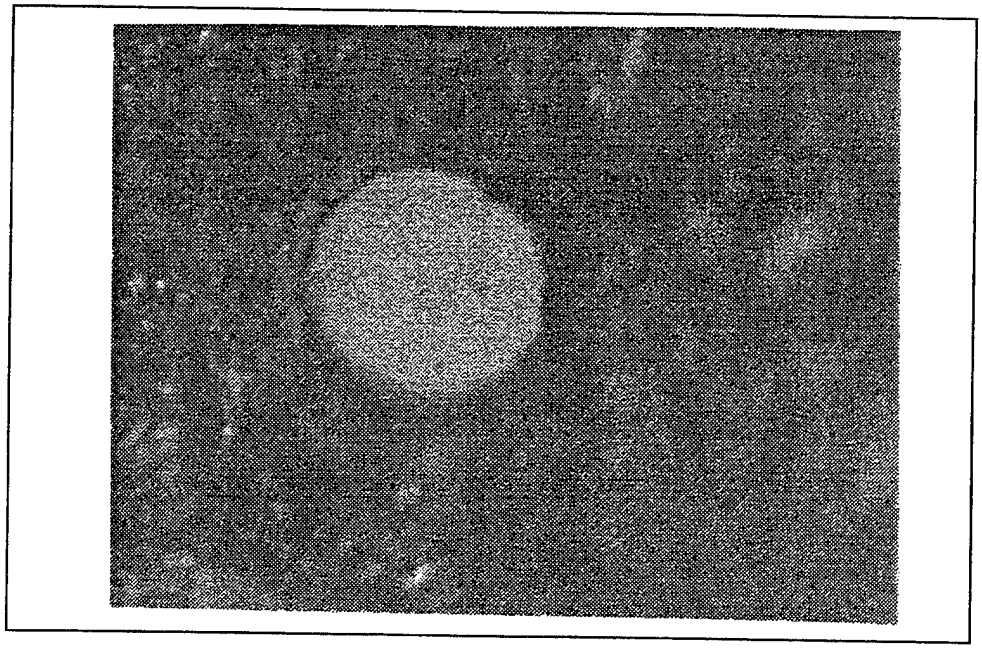

Figure 21: Optical photo of A'01, 12 o'clock, 150 cycles.

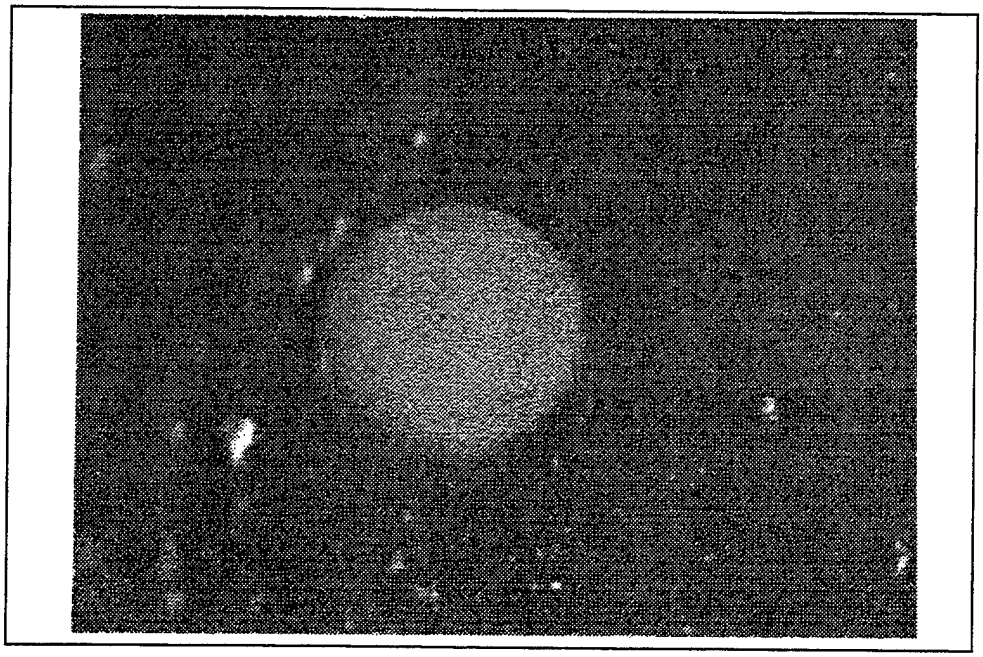

Figure 22: Optical photo of A01, 6 o'clock, 150 cycles.

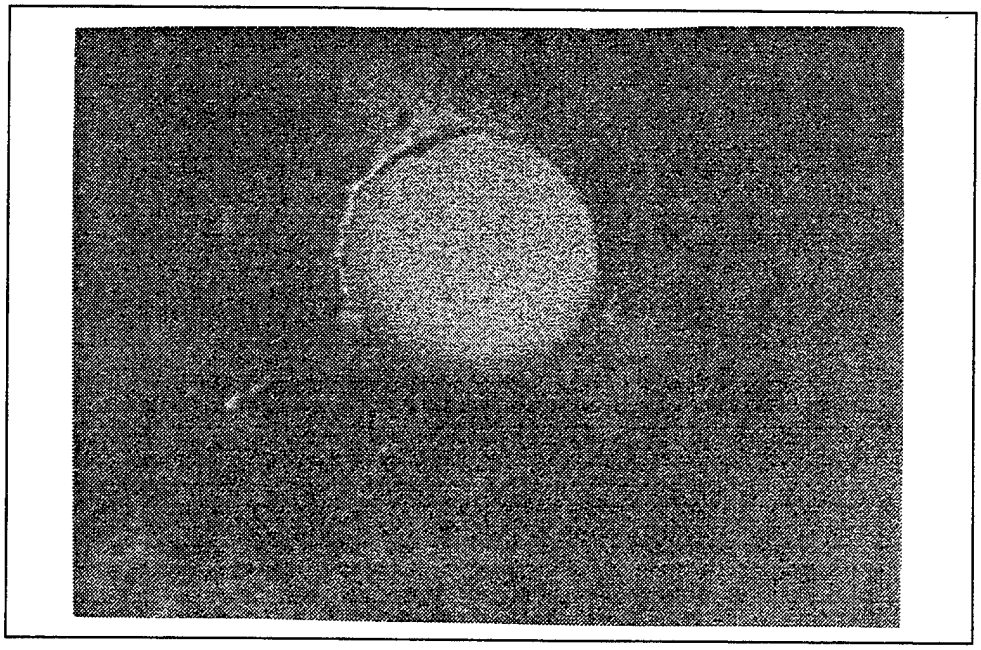

Figure 23: Optical photo of A'01, 6 o'clock, 150 cycles.

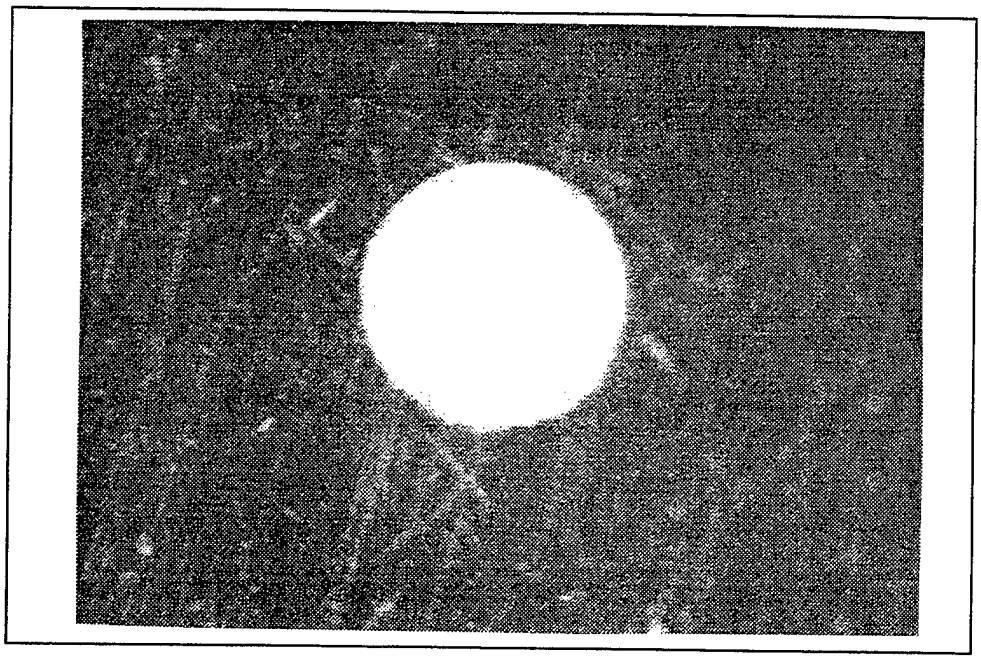

Figure 24: Optical photo of B17, 12 o'clock, zero cycles.

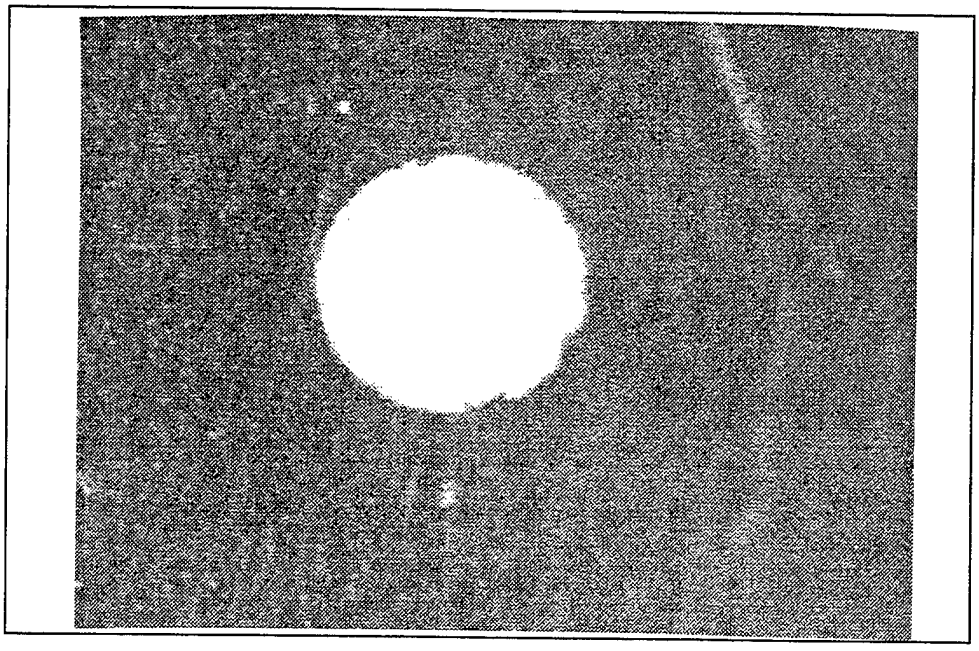

Figure 25: Optical photo of B-md20, 12 o'clock, zero cycles.

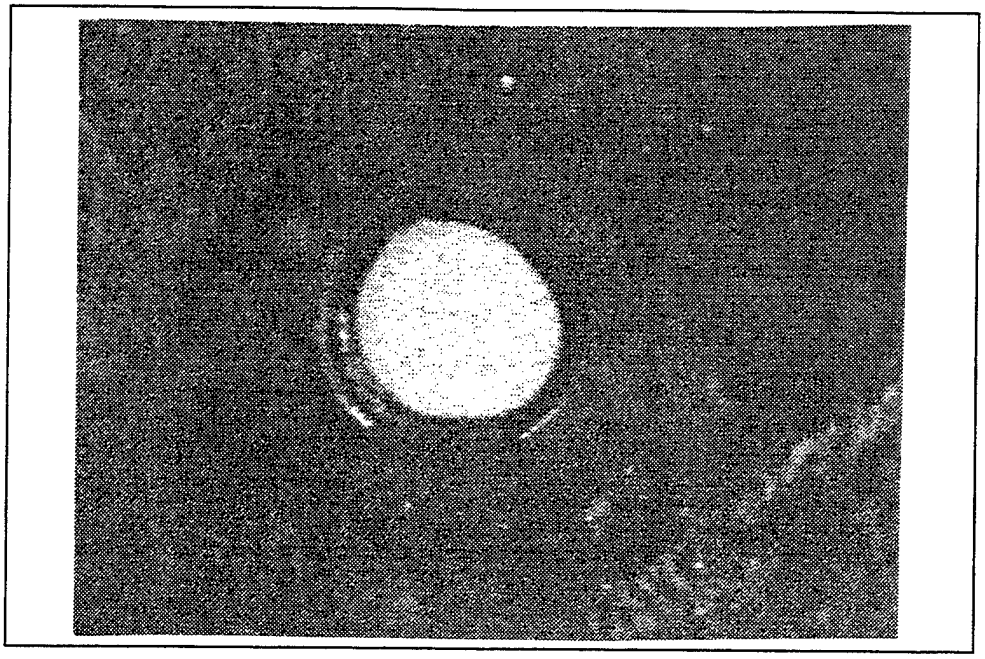

Figure 26: Optical photo of B17, 12 o'clock, 90 cycles.

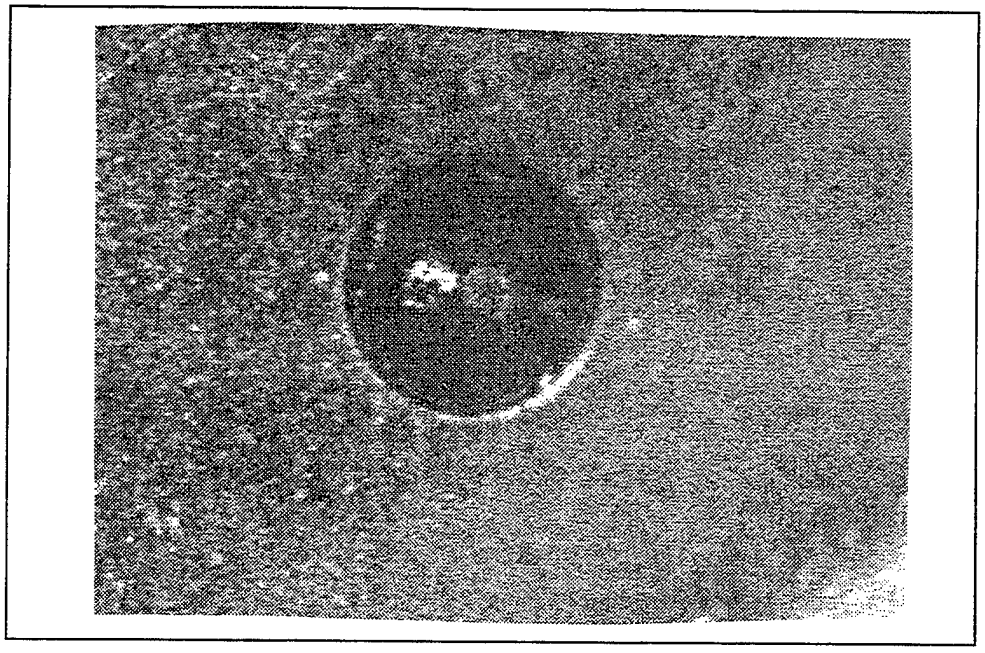

Figure 27: Optical photo of B-md20, 12 o'clock, 60 cycles.

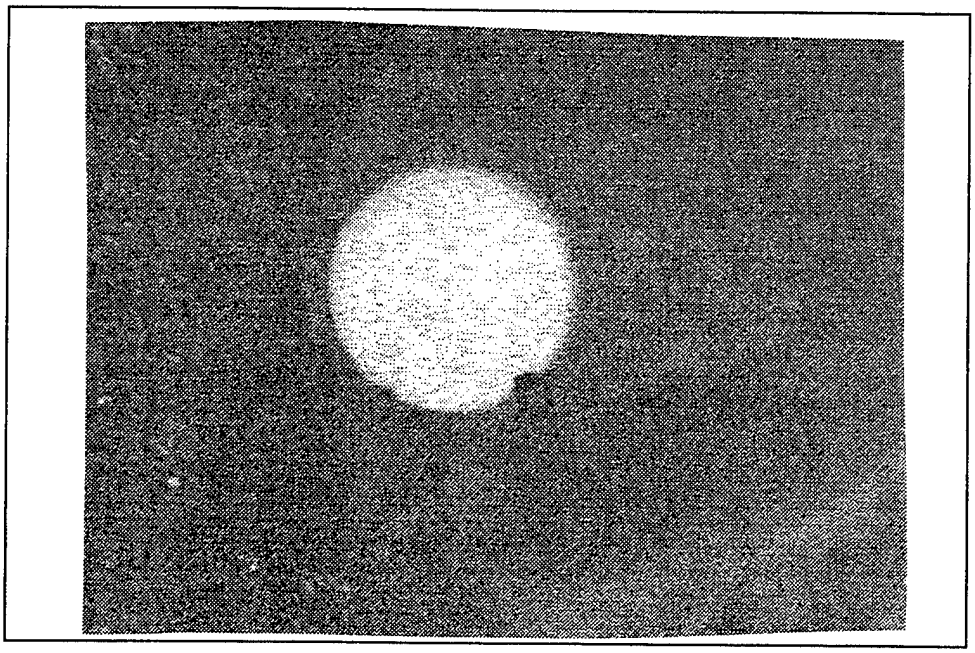

Figure 28: Optical photo of B17, 6 o'clock, 90 cycles.

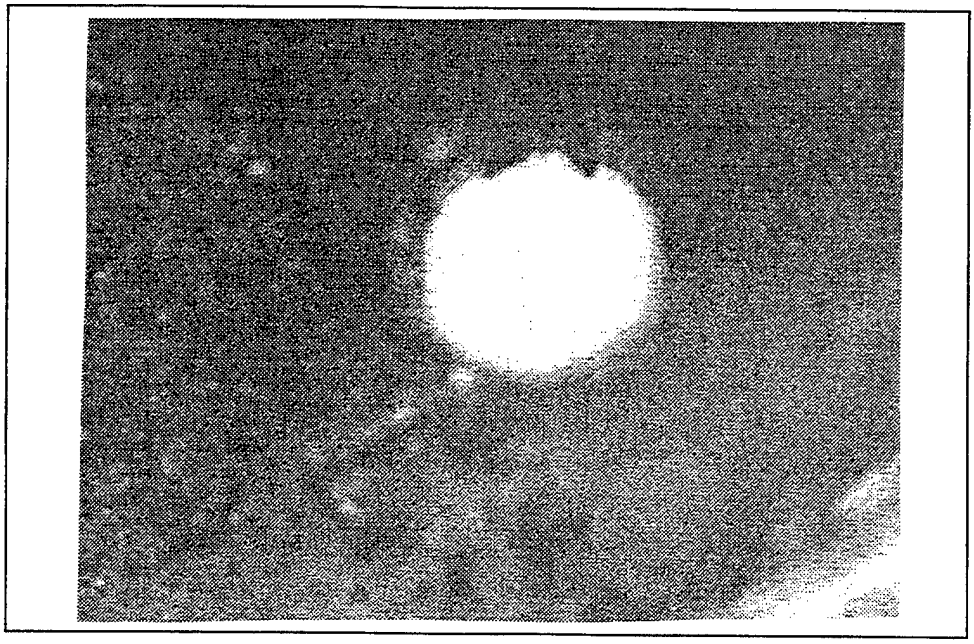

Figure 29: Optical photo of B-md20, 6 o'clock, 60 cycles.

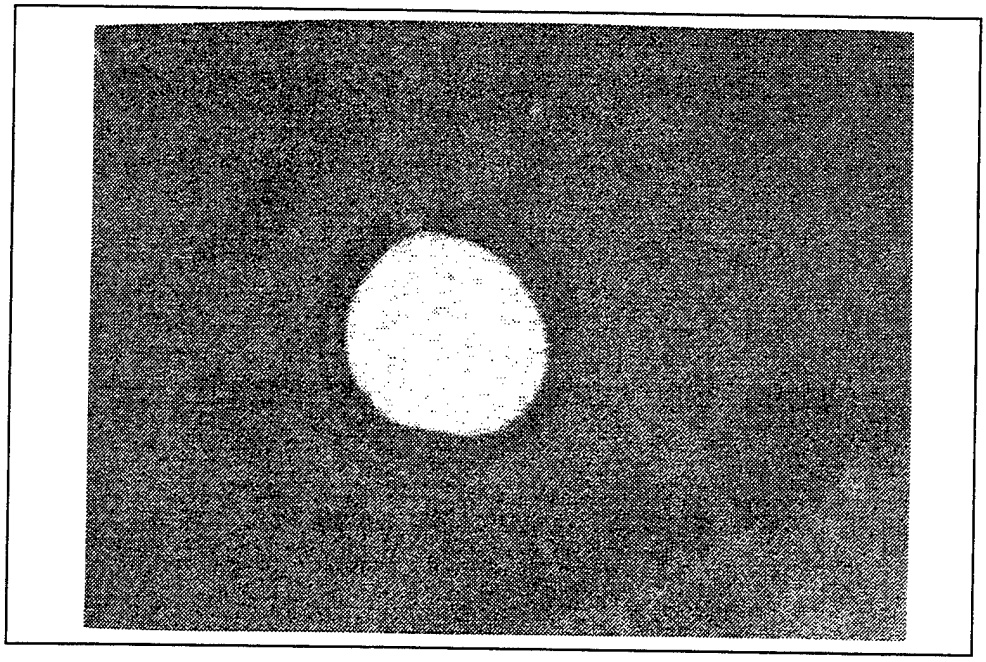

Figure 30: Optical photo of B17, 12 o'clock, 150 cycles.

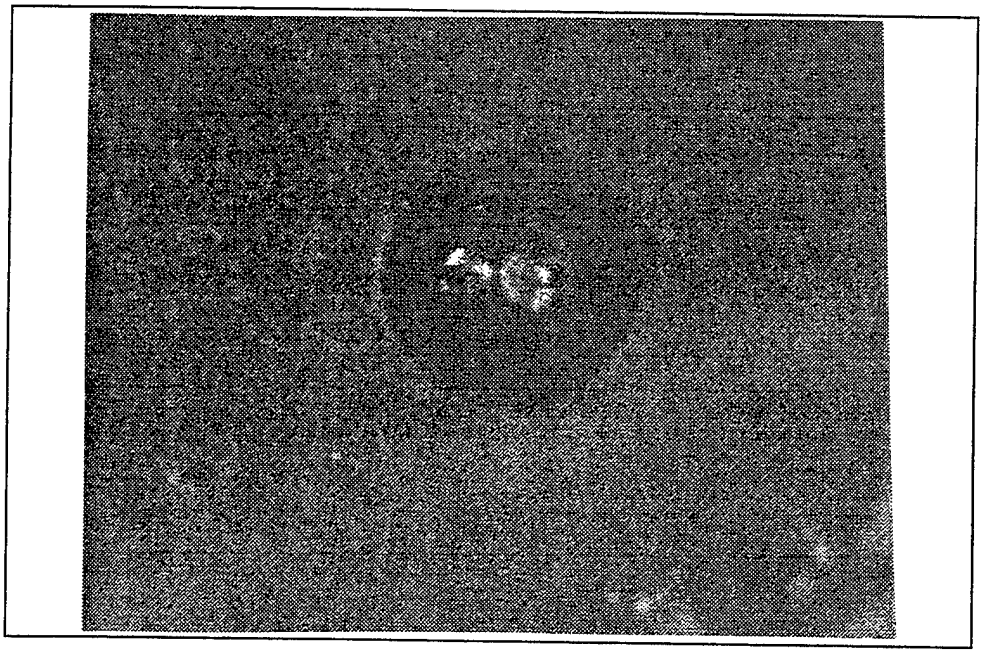

Figure 31: Optical photo of B-md20, 12 o'clock, 150 cycles.

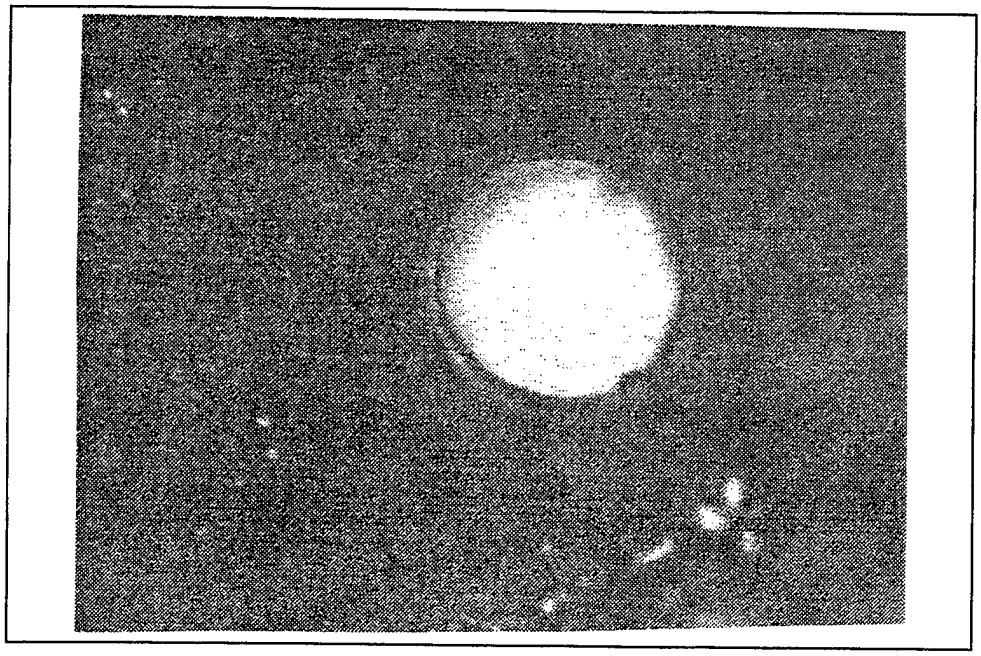

Figure 32: Optical photo of B17, 6 o'clock, 150 cycles.

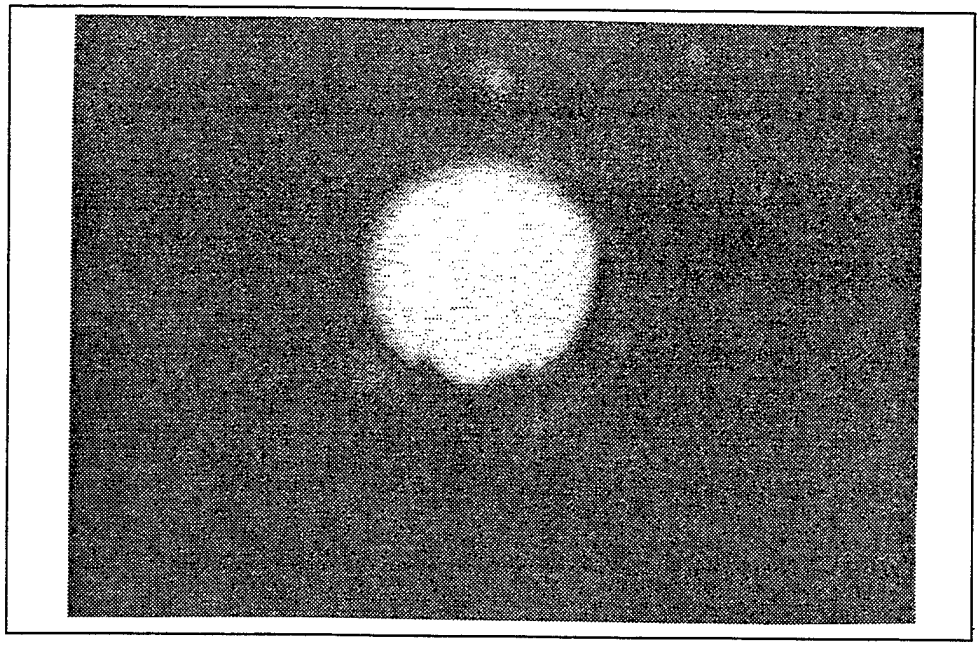

Figure 33: Optical photo of B-md20, 6 o'clock, 150 cycles.

Figures 24 through 33 lead to some very useful observations. The amorphous diamond coating appears to offer no improvement on the non-coated B-type plate. It has allowed the entire hole to be coked over. Additionally, the 12 o'clock position appears to be preferential to the 6 o'clock hole. Initial observations show that the coking is far greater in the 12 o'clock position then in the 6 o'clock. After 150 cycles, the 6 o'clock positions have very little coking present.

The next set of photos compares another B-type plate with an A-type plate coated with amorphous diamond coating. Figures 34 through 45 indicate that the B-type plate has excellent potential. The amorphous diamond coating again appears to have failed. Several hole became severely blocked. Both 12 o'clock and 6 o'clock positions on the B-type swirl plate showed little coking. The A-md25 plate showed preferential coking at the top of the plate near the 12 o'clock position while very little coking was present near the bottom of the swirl plate. The final two photos, figures 44 and 45, show that the holes around the 12 o'clock hole are preferentially coked.

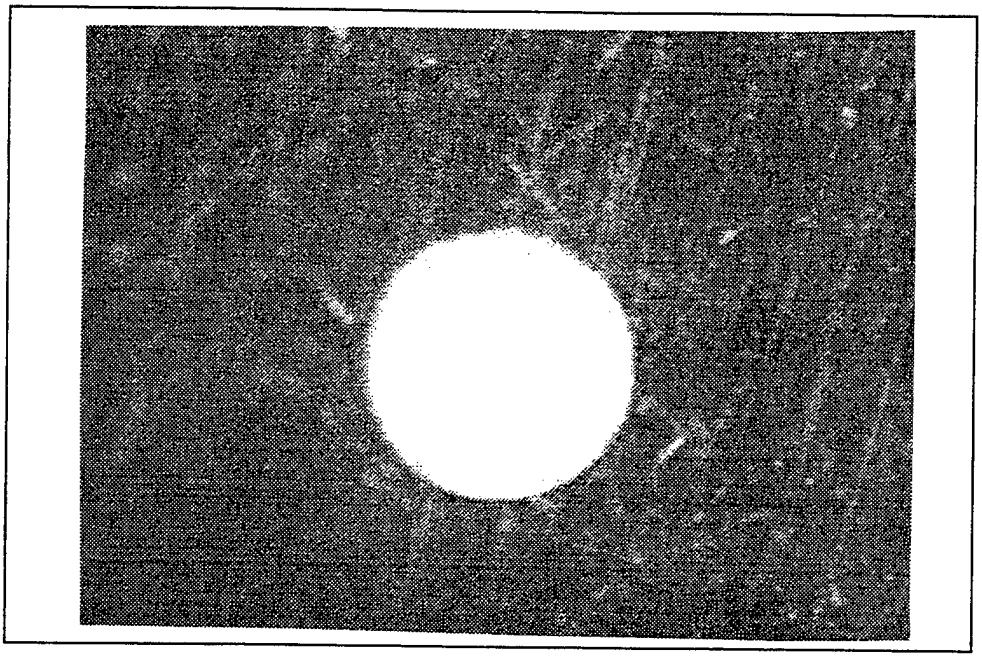

Figure 34: Optical photo of B10, 12 o'clock, zero cycles.

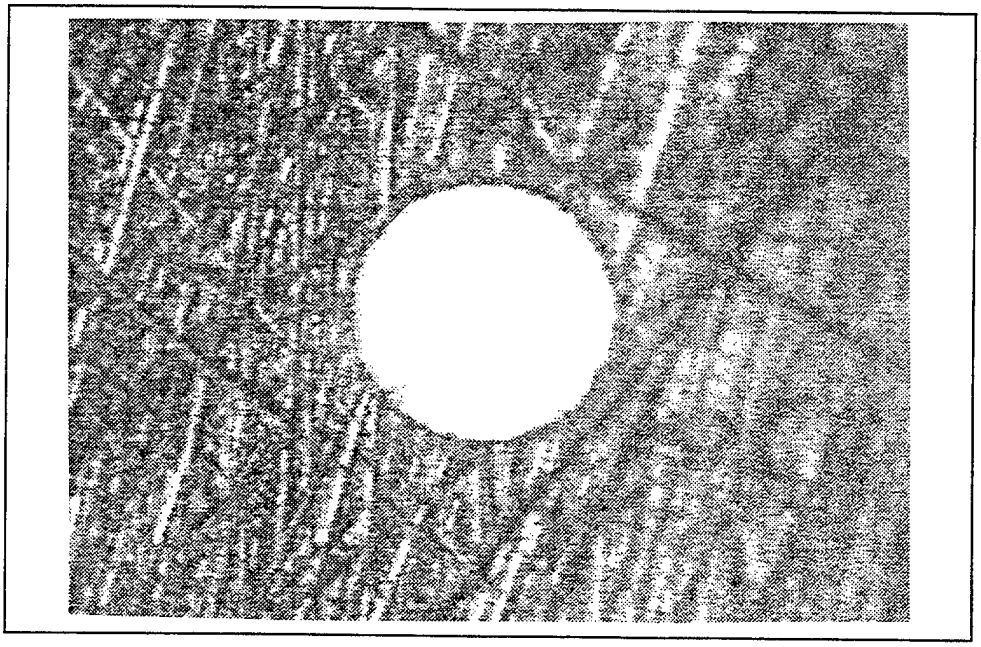

Figure 35: Optical photo of A-md25, 12 o'clock, zero cycles.

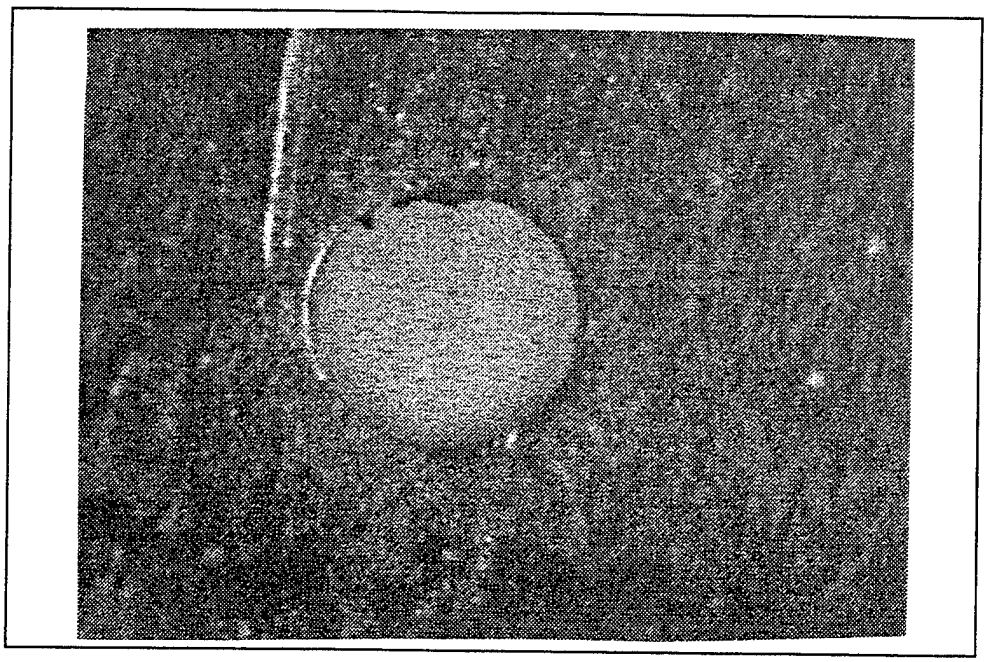

Figure 36: Optical photo of B10, 12 o'clock, 60 cycles.

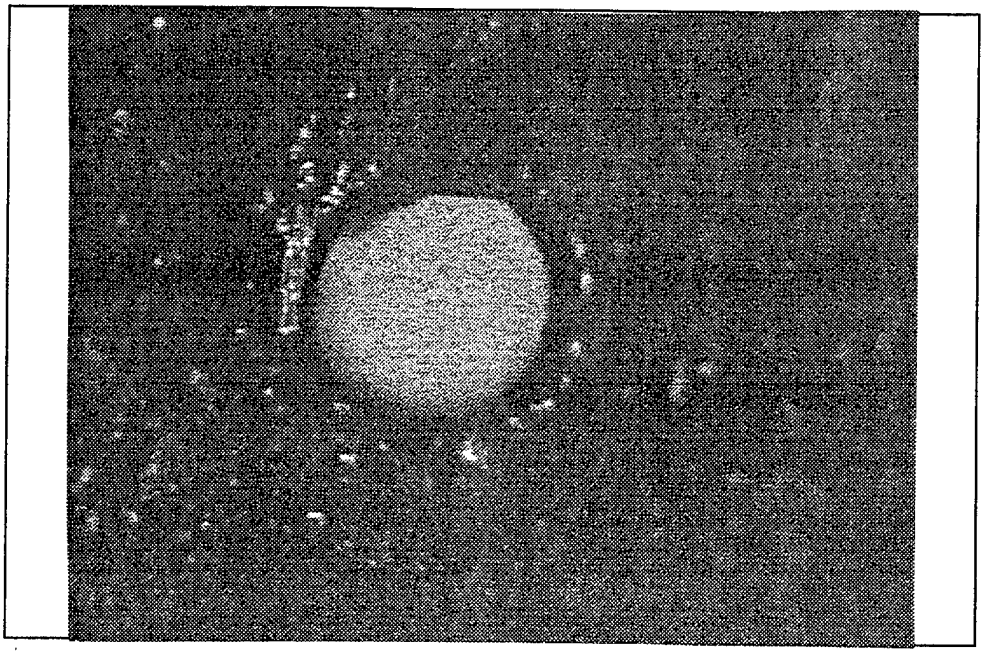

Figure 37: Optical photo of A-md25, 12 o'clock, 60 cycles.

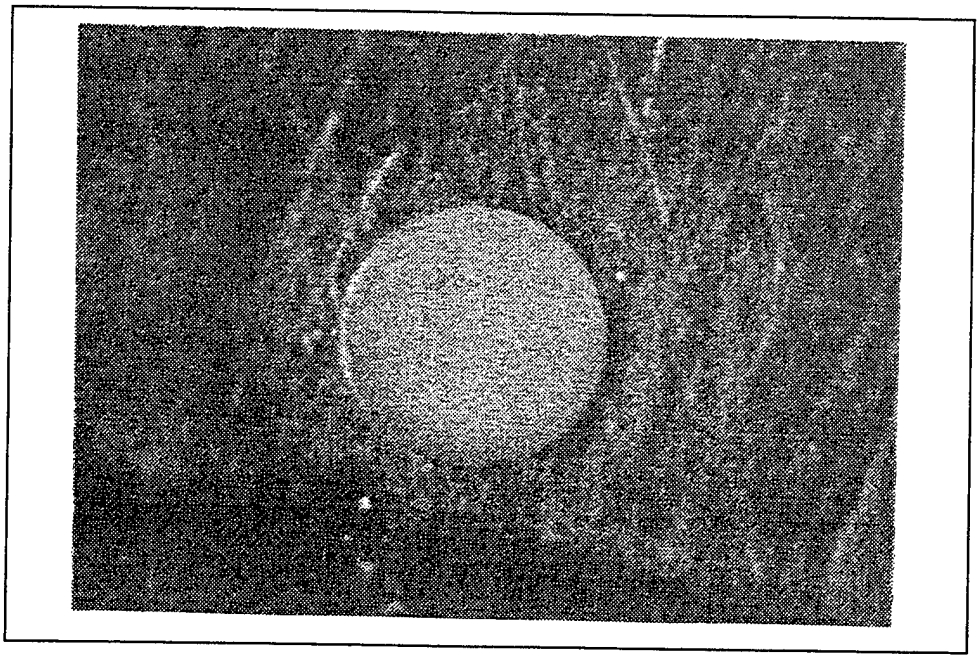

Figure 38: Optical photo of B10, 6 o'clock, 60 cycles.

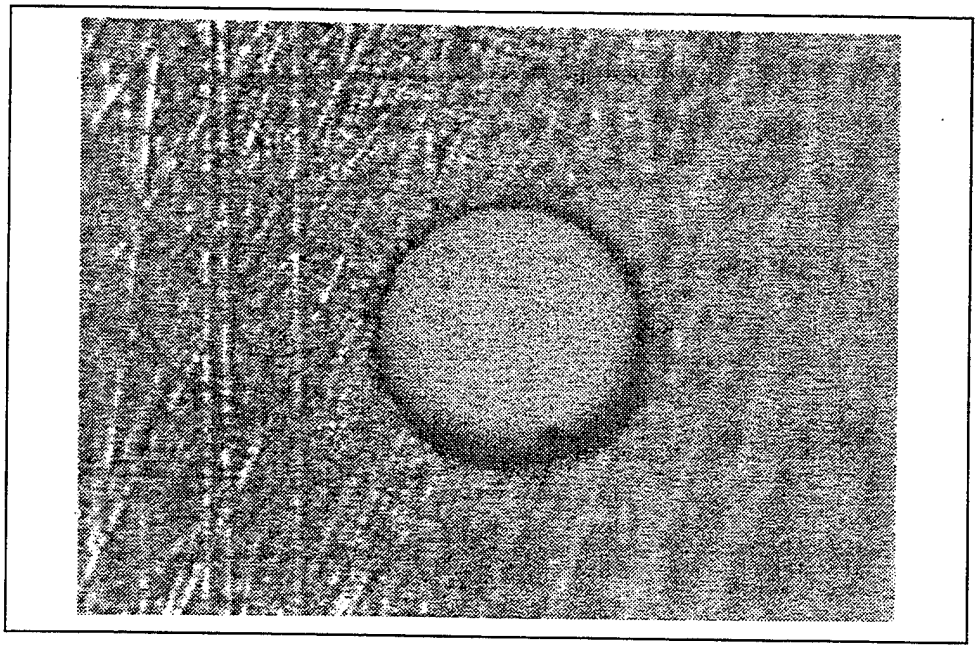

Figure 39: Optical photo of A-md25, 6 o'clock, 60 cycles.

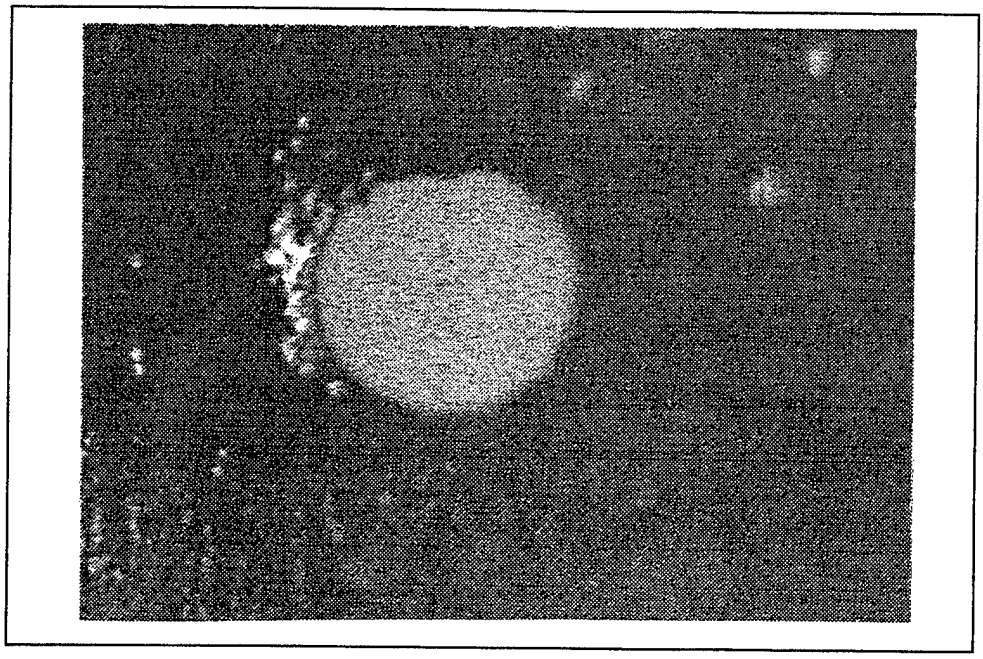

Figure 40: Optical photo of B10, 12 o'clock, 150 cycles.

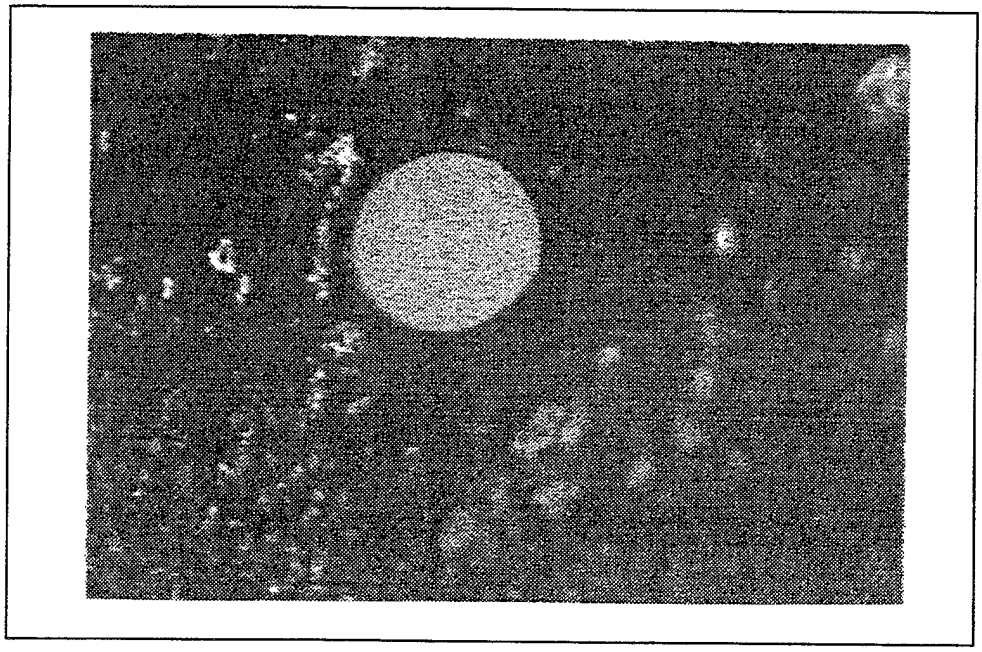

Figure 41: Optical photo of A-md25, 12 o'clock, 150 cycles.

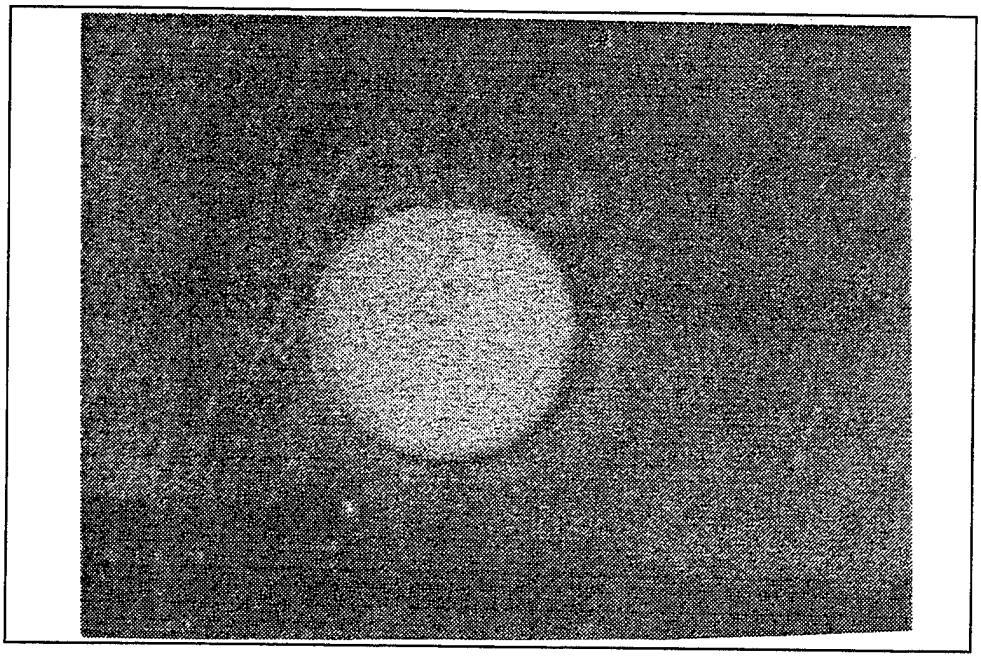

Figure 42: Optical photo of B10, 6 o'clock, 150 cycles.

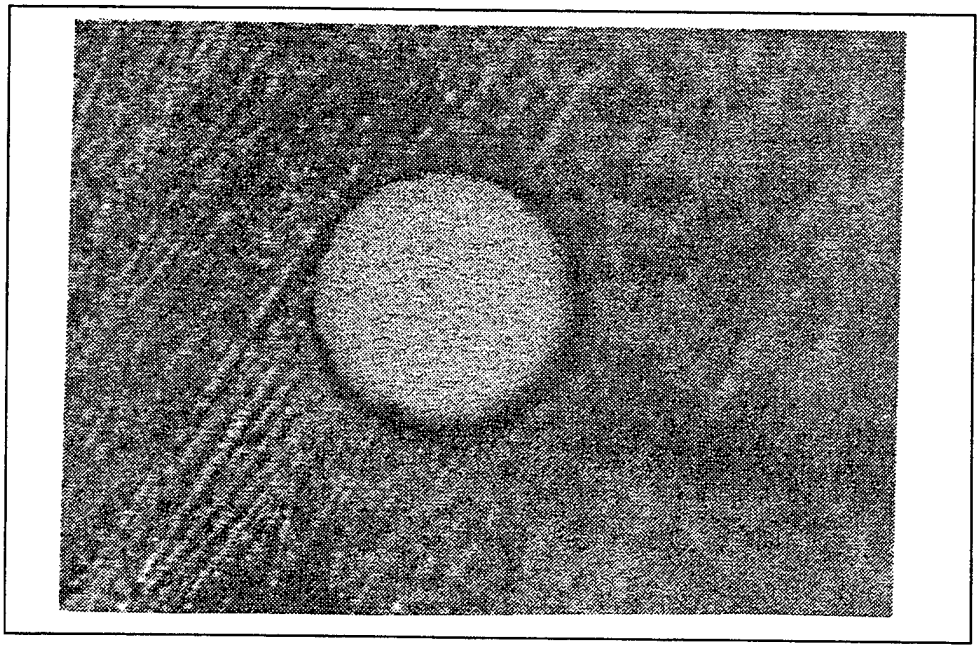

Figure 43: Optical photo of A-md25, 6 o'clock, 150 cycles.

Figure 44: Optical photo of A-md25, 2 o'clock, 150 cycles.

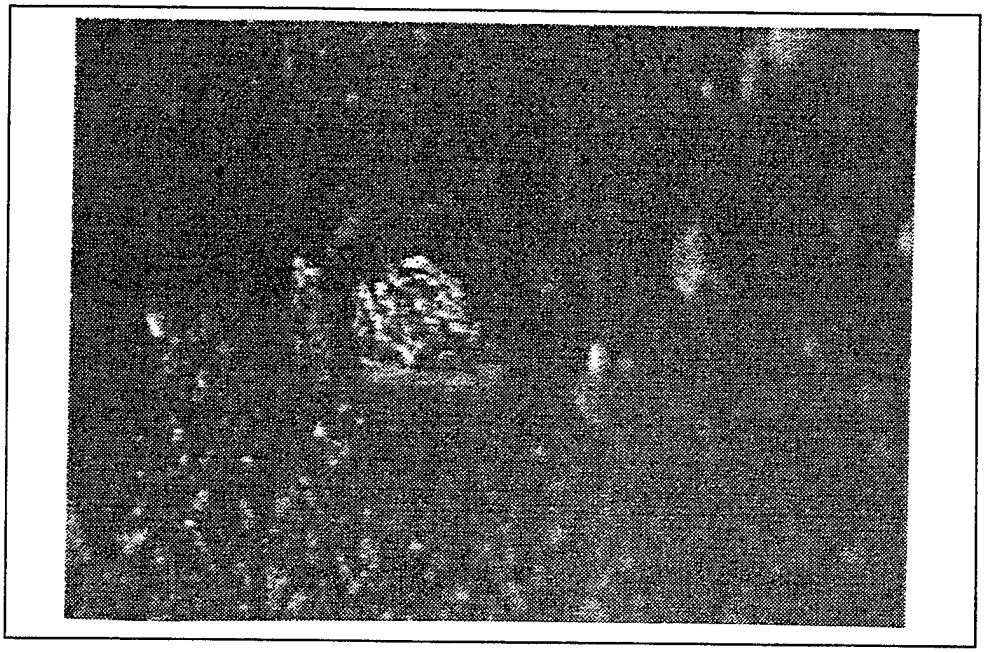

Figure 45: Optical photo of A-md25, 10 o'clock, 150 cycles.

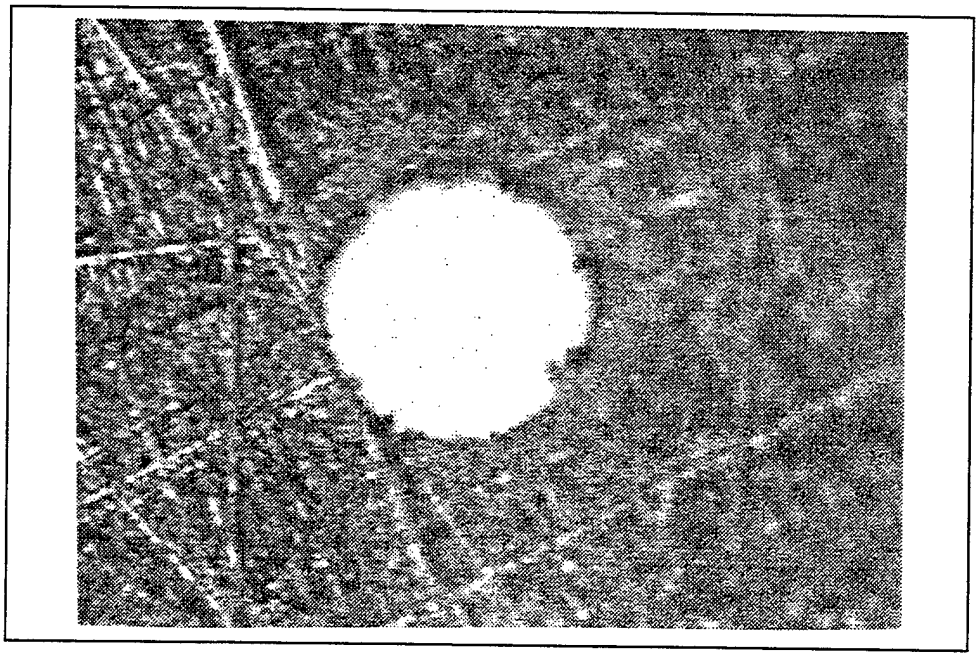

Figure 46: Optical photo of A28, 12 o'clock, zero cycles.

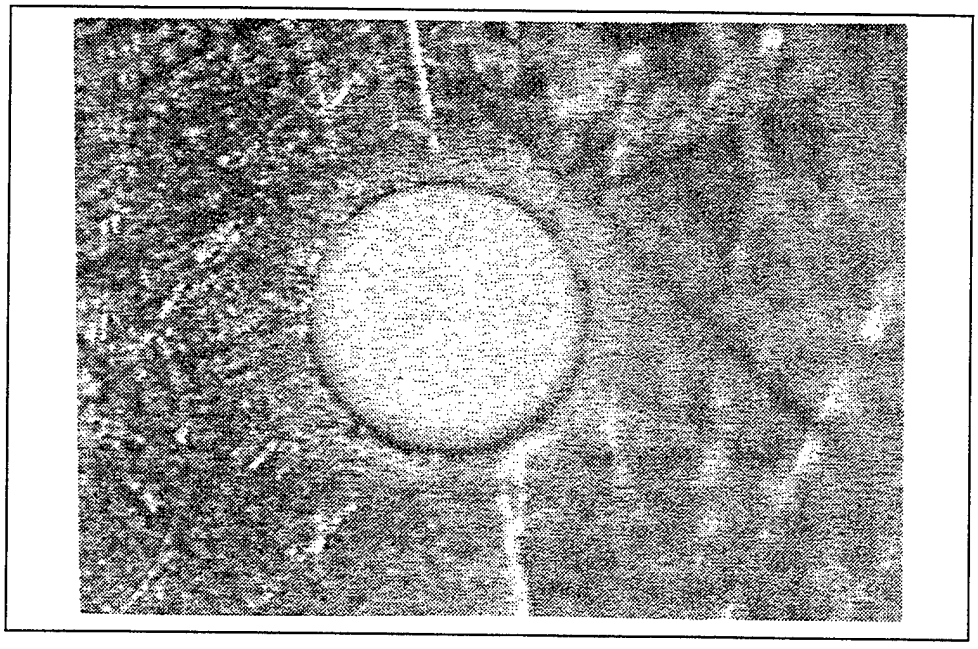

Figure 47: Optical photo of A-sil23, 12 o'clock, zero cycles.

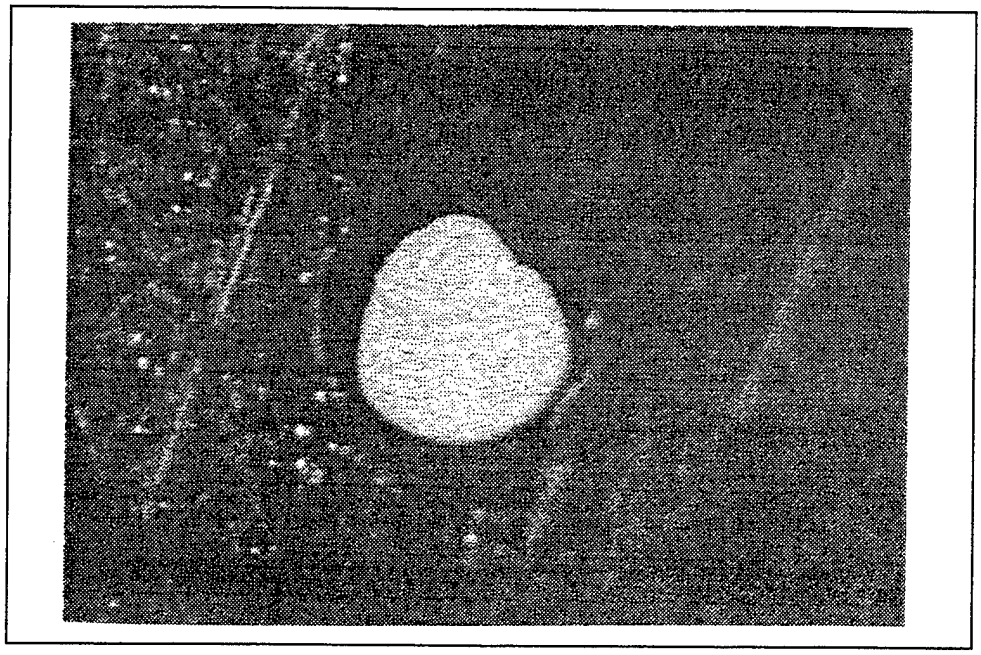

Figure 48: Optical photo of A28, 12 o'clock, 60 cycles.

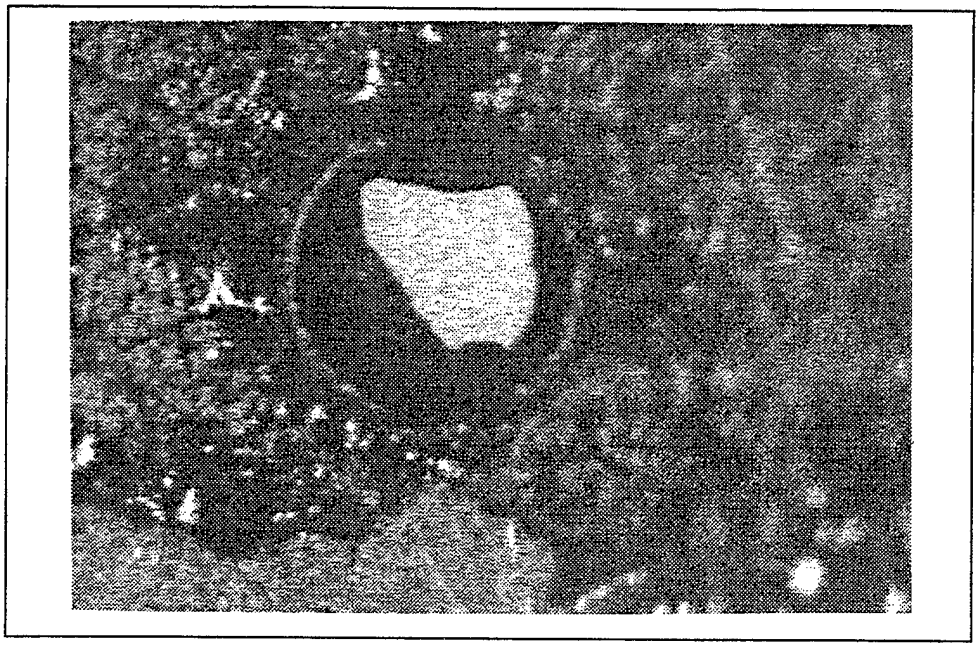

Figure 49: Optical photo of A-sil23, 12 o'clock, 60 cycles.

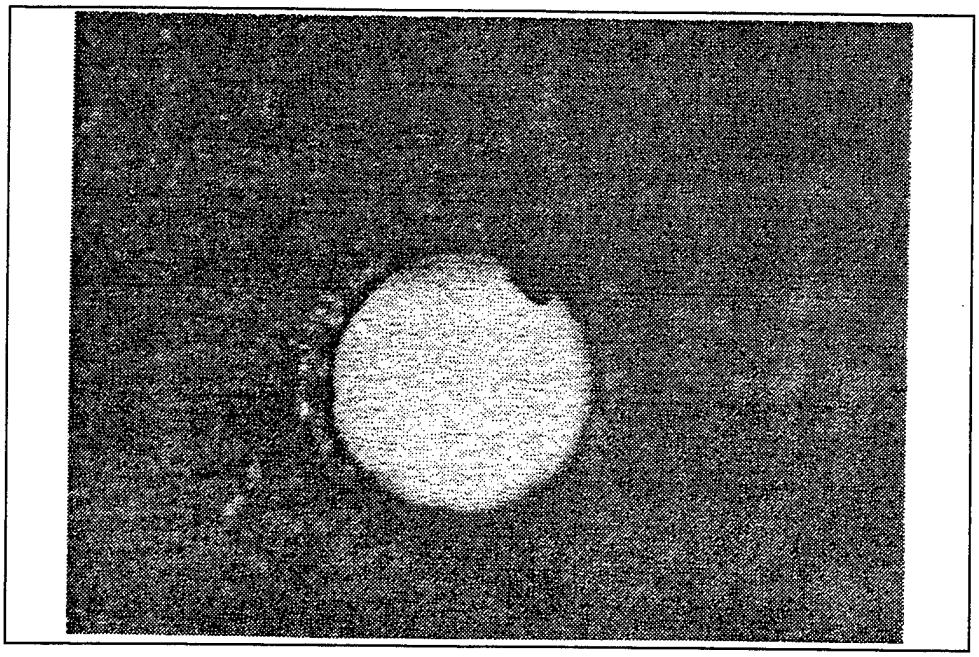

Figure 50: Optical photo of A28, 6 o'clock, 60 cycles.

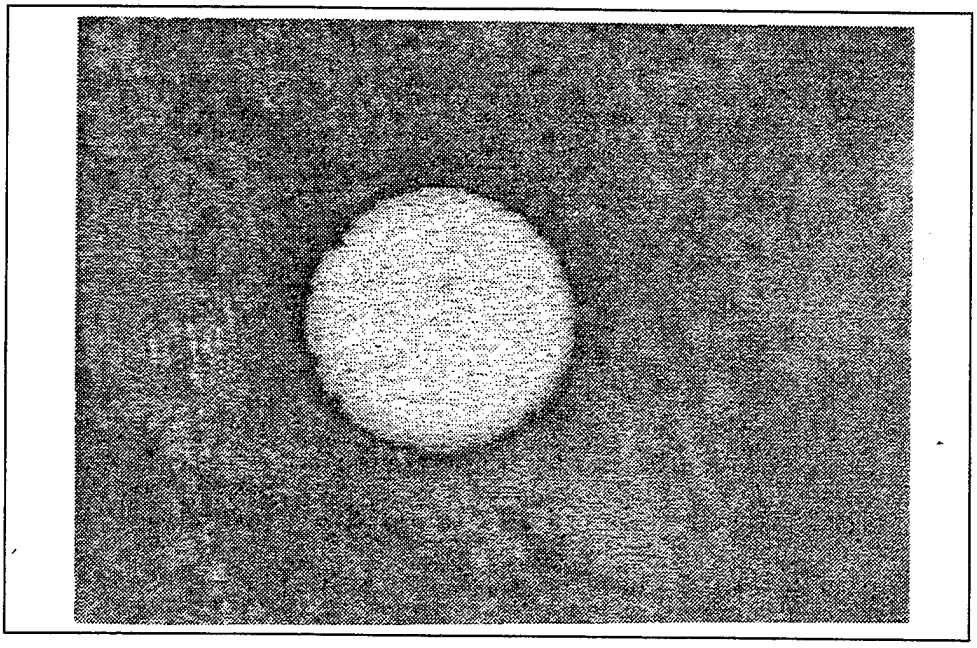

Figure 51: Optical photo of A-sil23, 6 o'clock, 60 cycles.

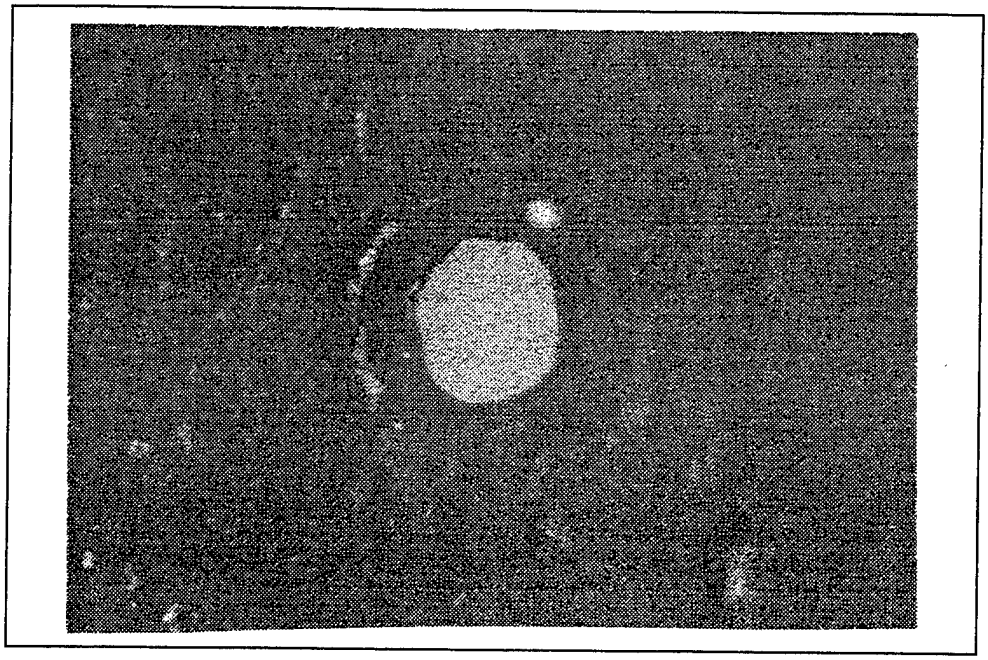

Figure 52: Optical photo of A28, 12 o'clock, 150 cycles.

Figure 53: Optical photo of A-sil23, 12 o'clock, 150 cycles.

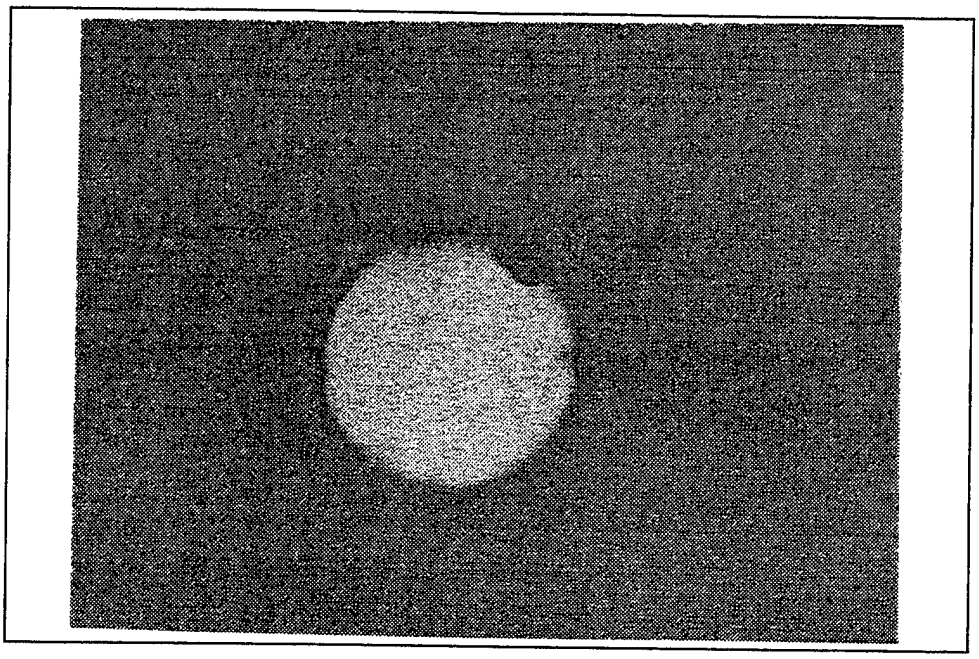

Figure 54: Optical photo of A28, 6 o'clock, 150 cycles.

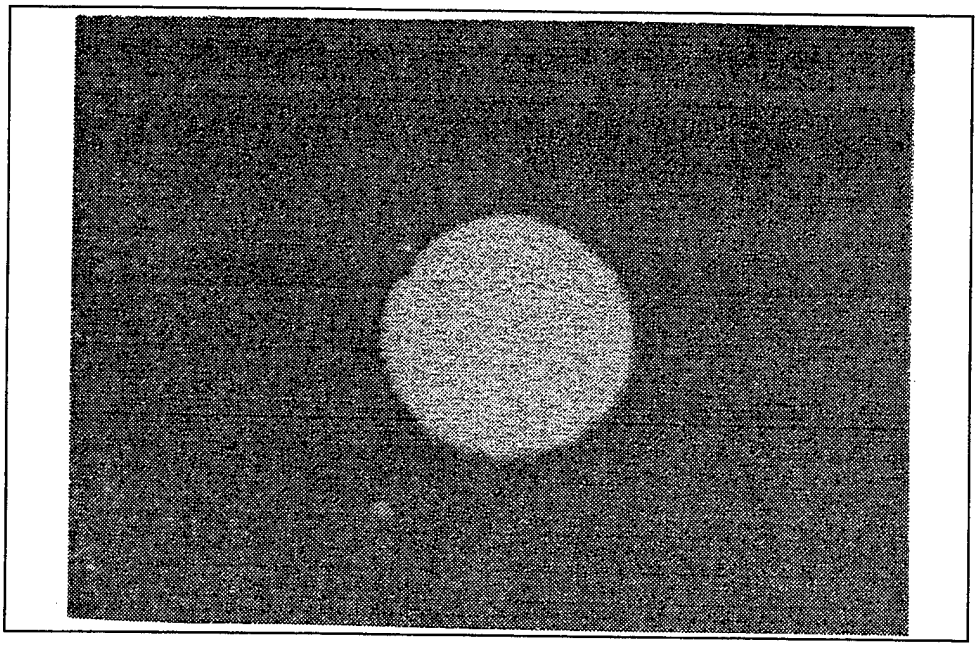

Figure 55: Optical photo of A-sil23, 6 o'clock, 150 cycles.

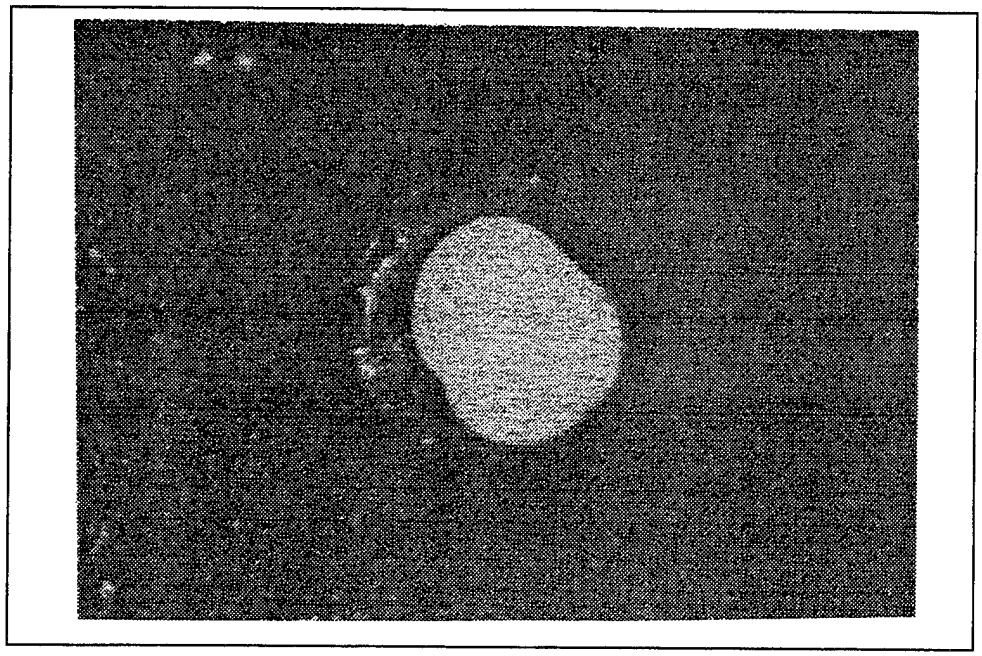

Figure 56: Optical photo of A28, 1 o'clock, 150 cycles.

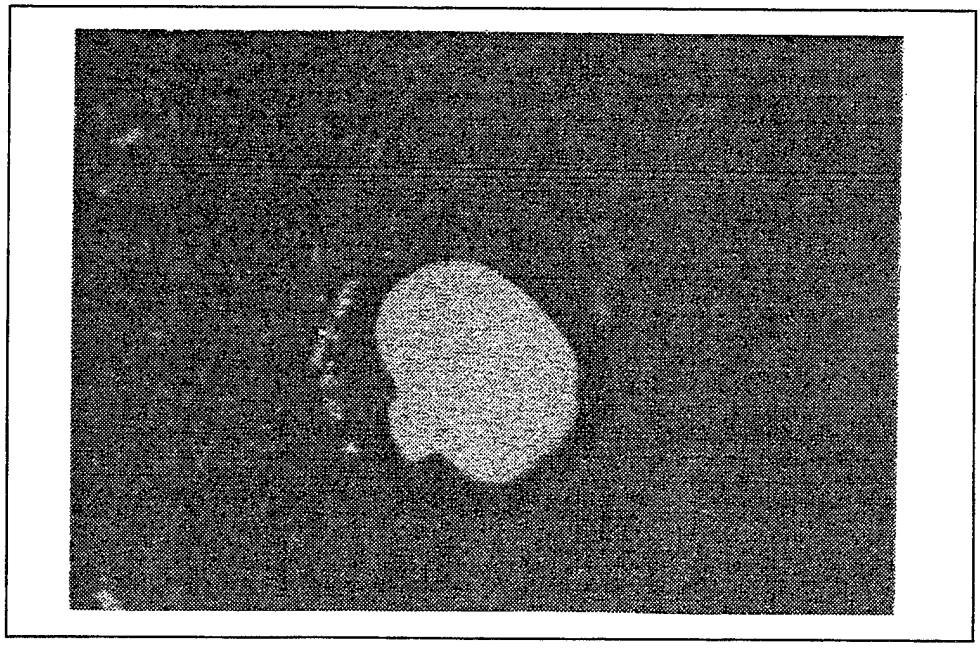

Figure 57: Optical photo of A-sil23, 2 o'clock, 150 cycles.

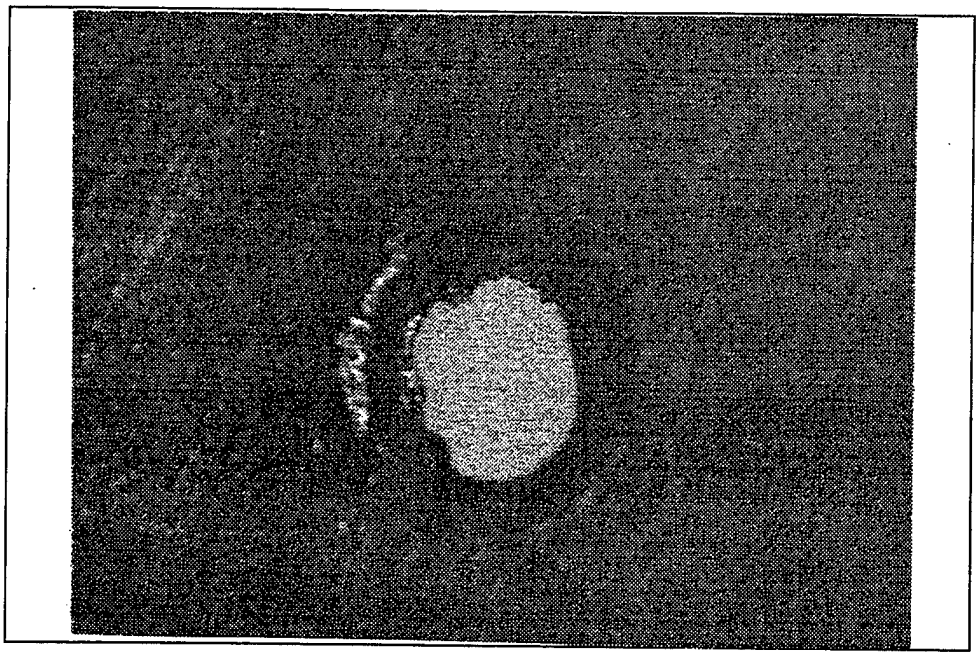

Figure 58: Optical photo of A28, 10 o'clock, 150 cycles.

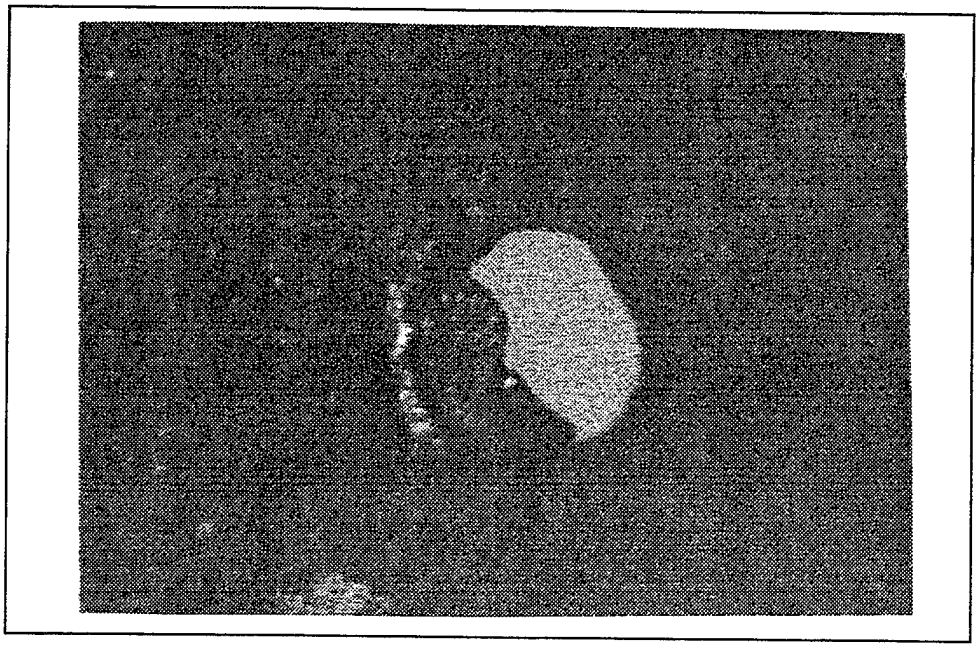

Figure 59: Optical photo of A-sil23, 3 o'clock, 150 cycles.

Figures 46 through 59 illustrate preferential coking in the region near the top of the swirlplate. Swirlplate A-sil23 appears to provide some additional resistance to coking though the photos show minimal evidence of this fact. It is quite evident that the original swirlplate used is very prone to coking. Since the two most promising candidates as replacement swirlplates thus far are the B-type and some type coated with silicon, the next photos will show a B-type plate versus an A-type coated with silicon. This way the true effect of the silicon can be seen since any improvement in the A-type plate must be the result of the coating.

Figures 60 through 67 show that the B-type swirlplate again appears to resists coking greatly. However, the A-sil plate does show that the silicon provides some protection over the A-type plate alone. There is some preferential coking around the 12 o'clock position but overall there appears to be a reduction in coking with the silicon coating.

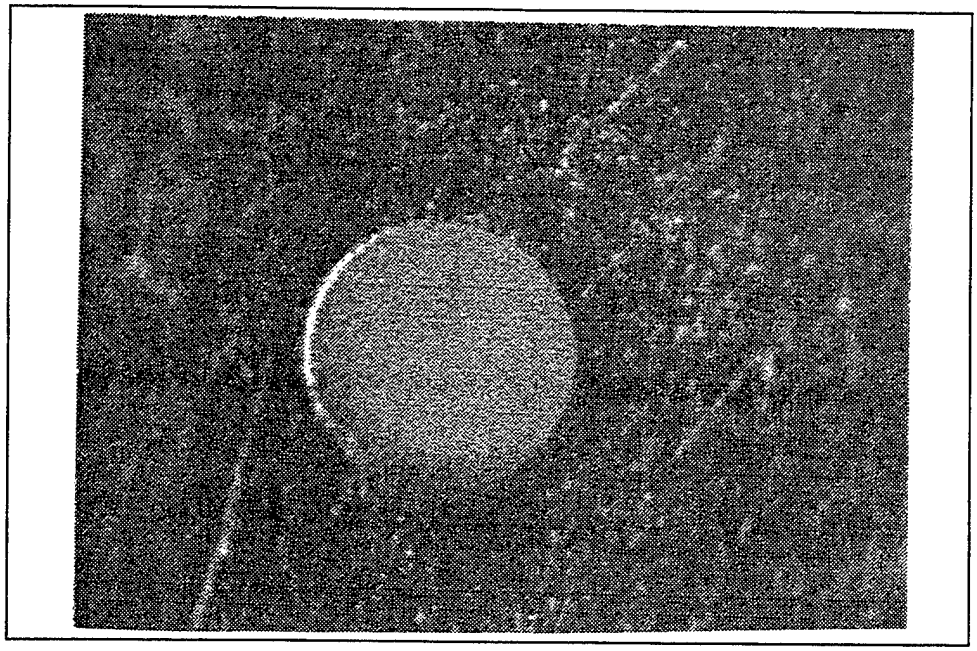

Figure 60: Optical photo of B12, 12 o'clock, zero cycles.

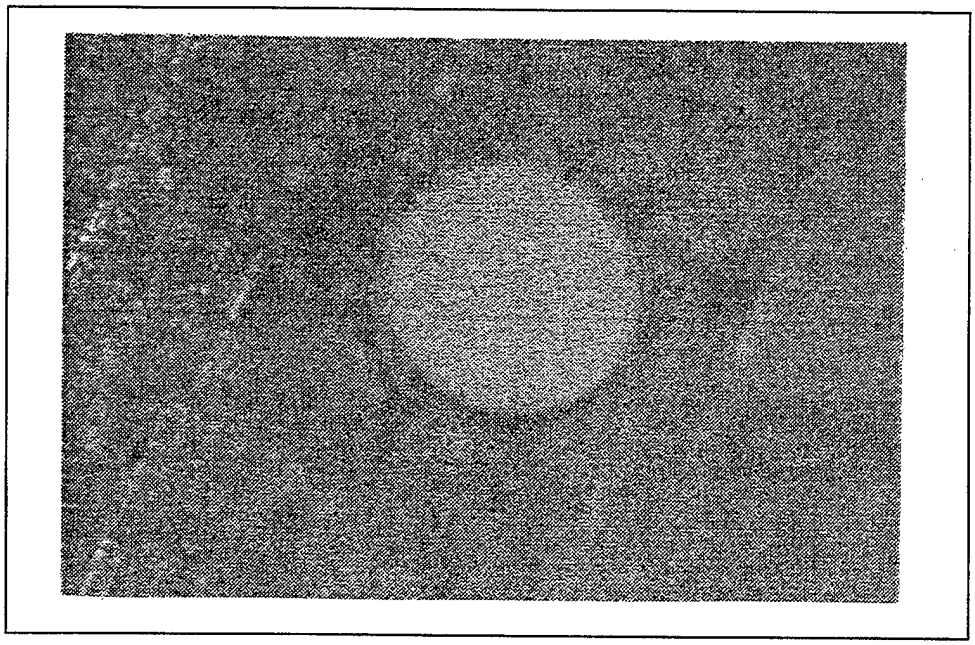

Figure 61: Optical photo of A-sil24, 12 o'clock, zero cycles.

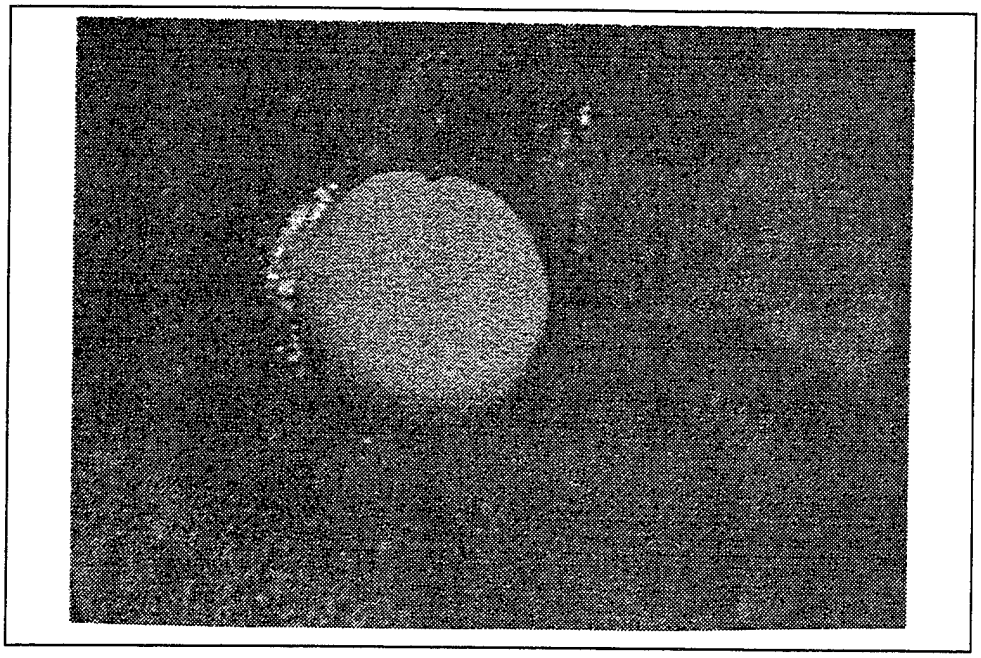

Figure 62: Optical photo of B12, 12 o'clock, 90 cycles.

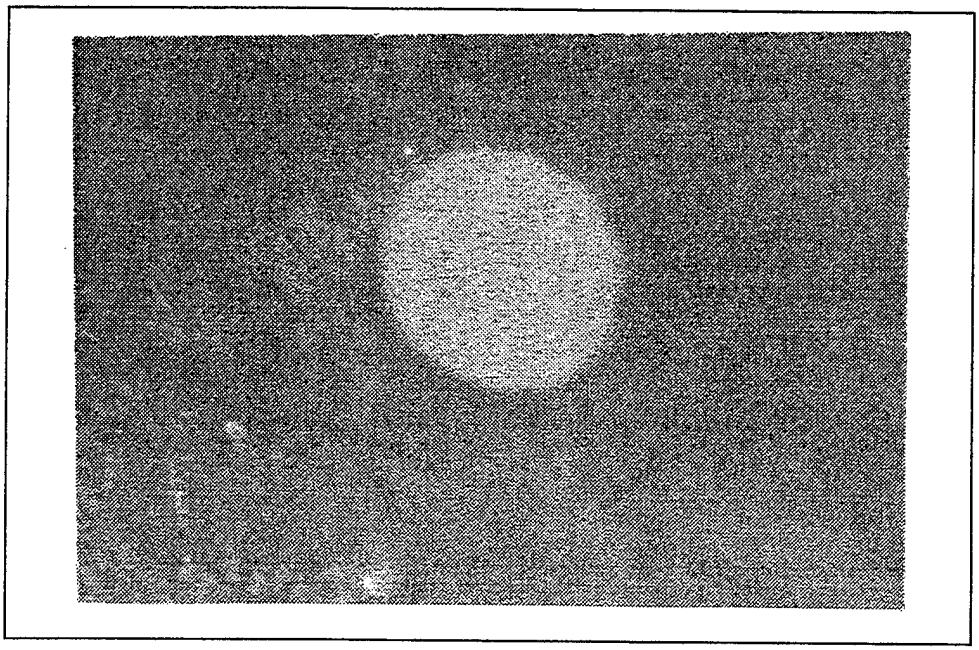

Figure 63: Optical photo of A-sil24, 12 o'clock, 90 cycles.

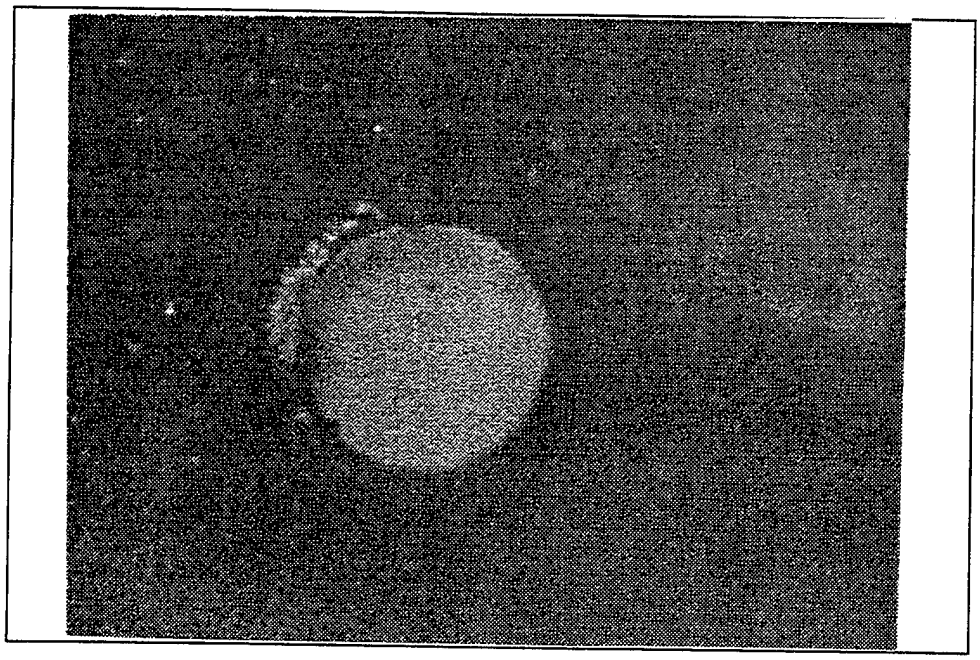

Figure 64: Optical photo of B12, 12 o'clock, 150 cycles.

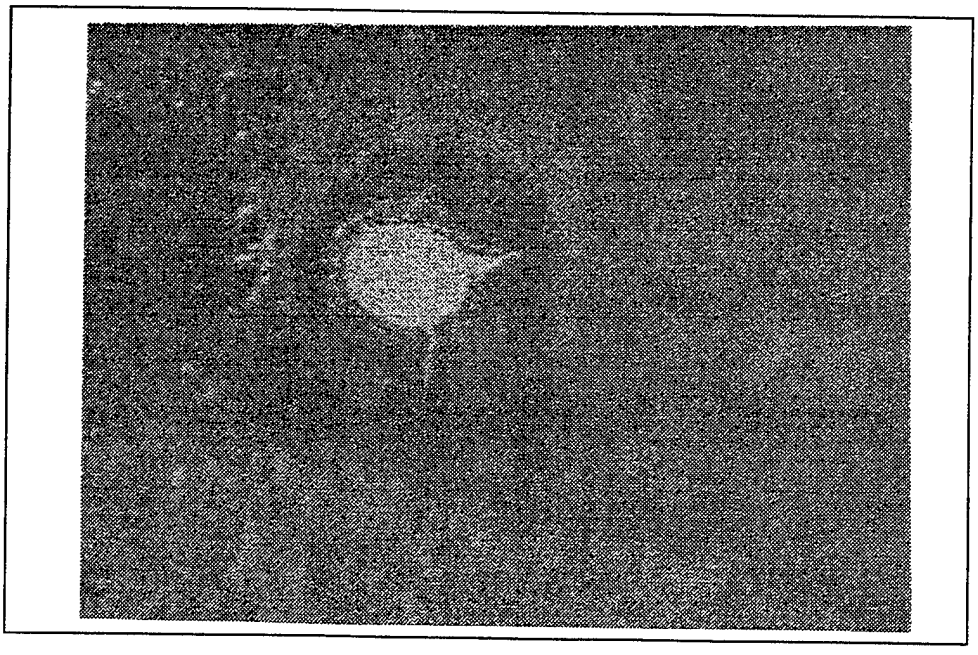

Figure 65: Optical photo of A-sil24, 1 o'clock, 150 cycles.

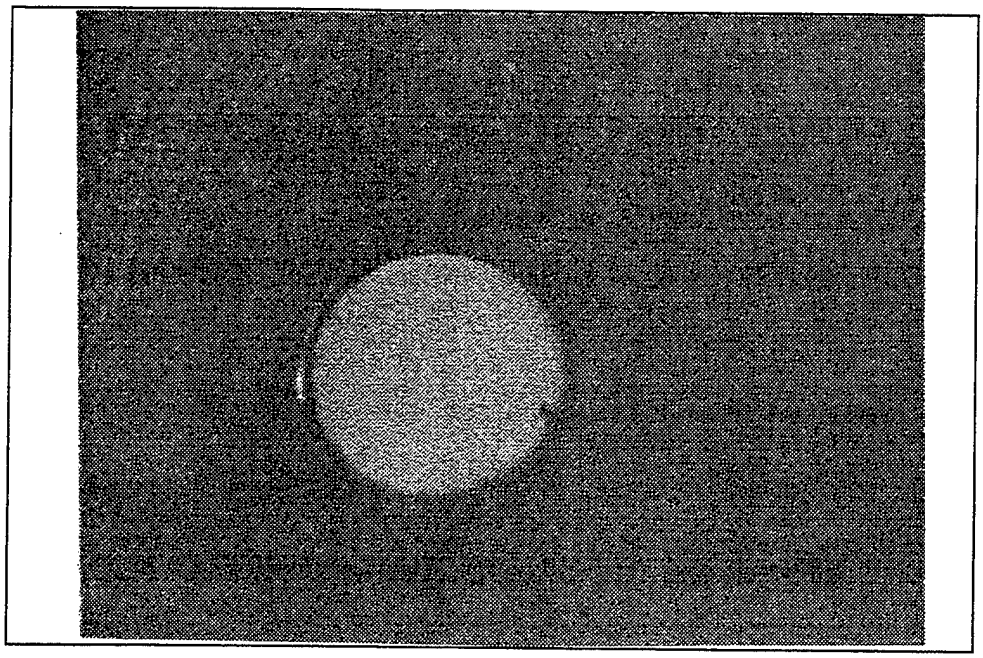

Figure 66: Optical photo of B12, 6 o'clock, 150 cycles.

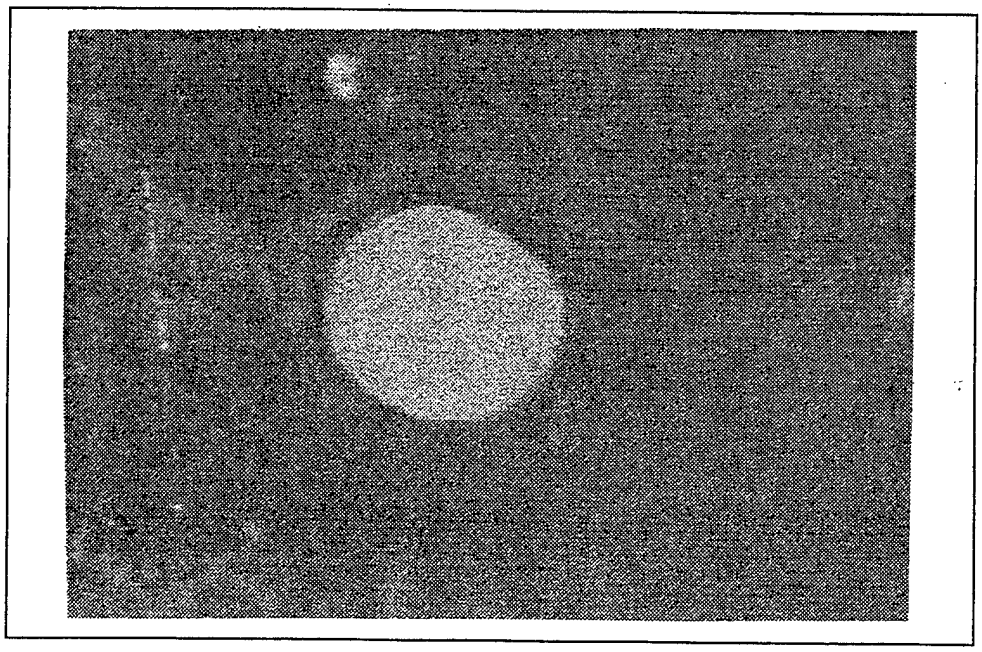

Figure 67: Optical photo of A-sil24, 6 o'clock, 150 cycles.

The last set of pictures focuses on the B-type swirl plates alone. Since these plates have shown the most promising results throughout, they will be tested against one another to provided additional data points to support the analysis. Figures 68 through 75 show both plates provide excellent resistance to coking. Some preferential coking can be seen but it is difficult to say to what degree as very little coking is present anywhere.

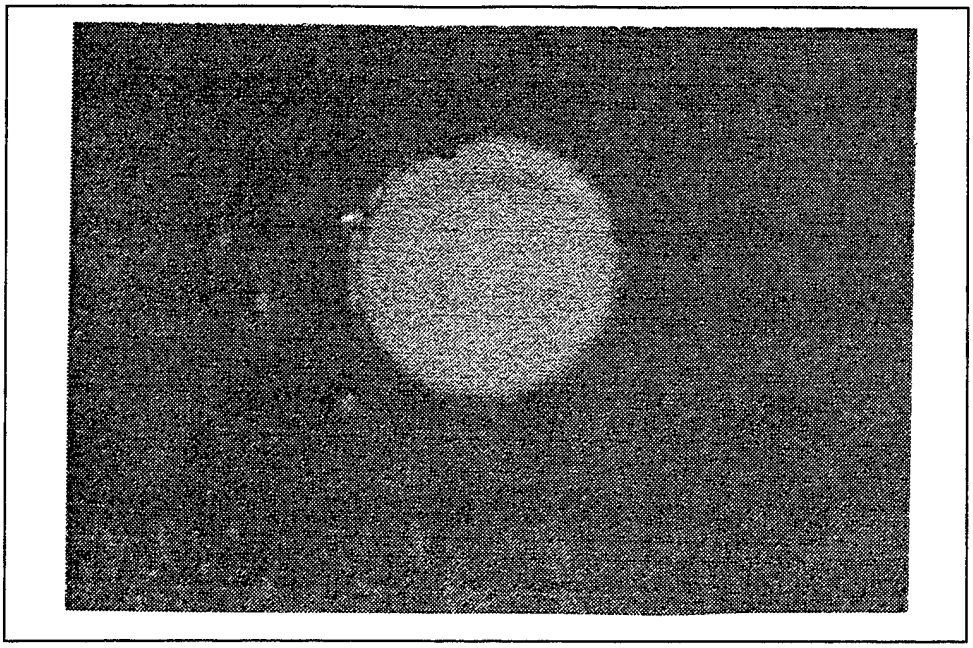

Figure 68: Optical photo of B13, 12 o'clock, 60 cycles.

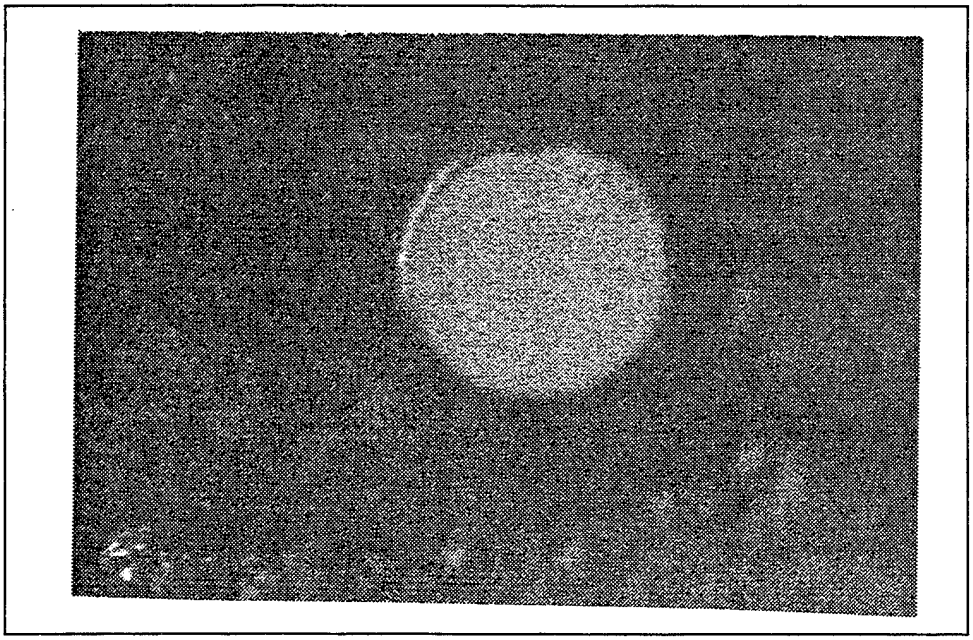

Figure 69: Optical photo of B14, 12 o'clock, 60 cycles.

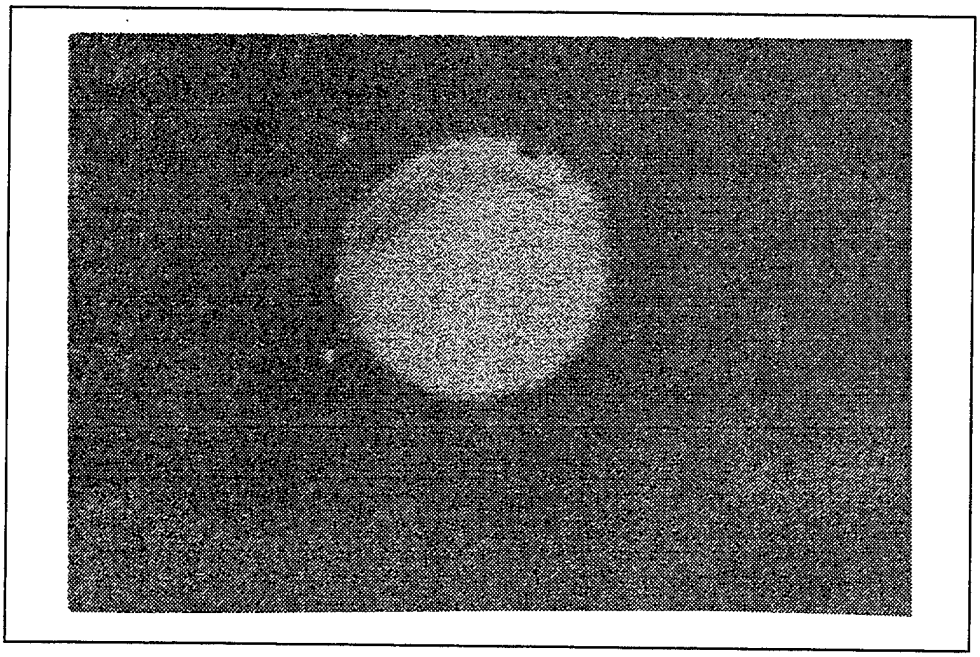

Figure 70: Optical photo of B13, 6 o'clock, 60 cycles.

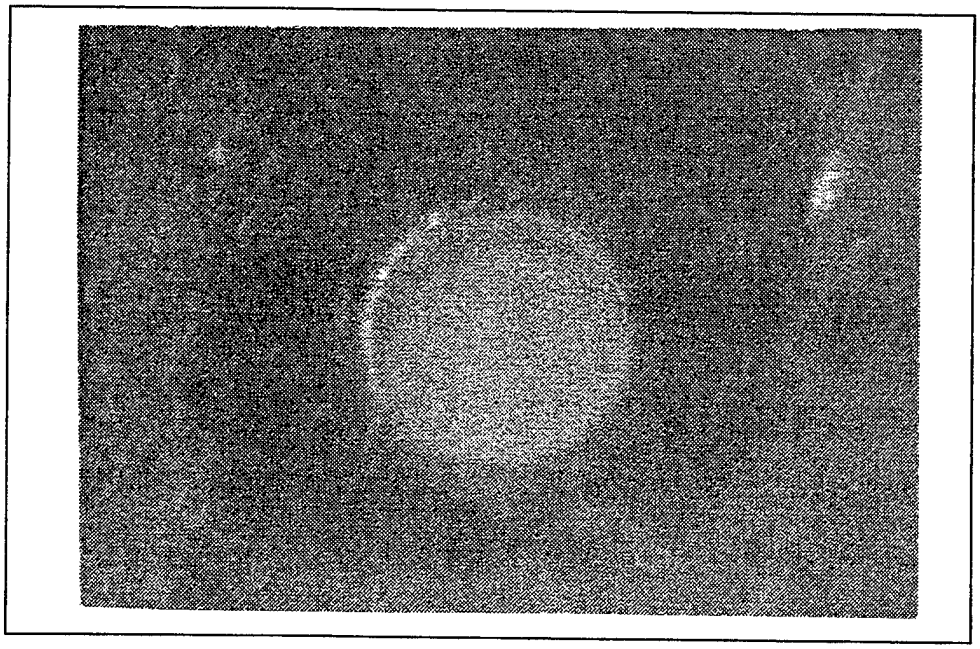

Figure 71: Optical photo of B14, 6 o'clock, 60 cycles.

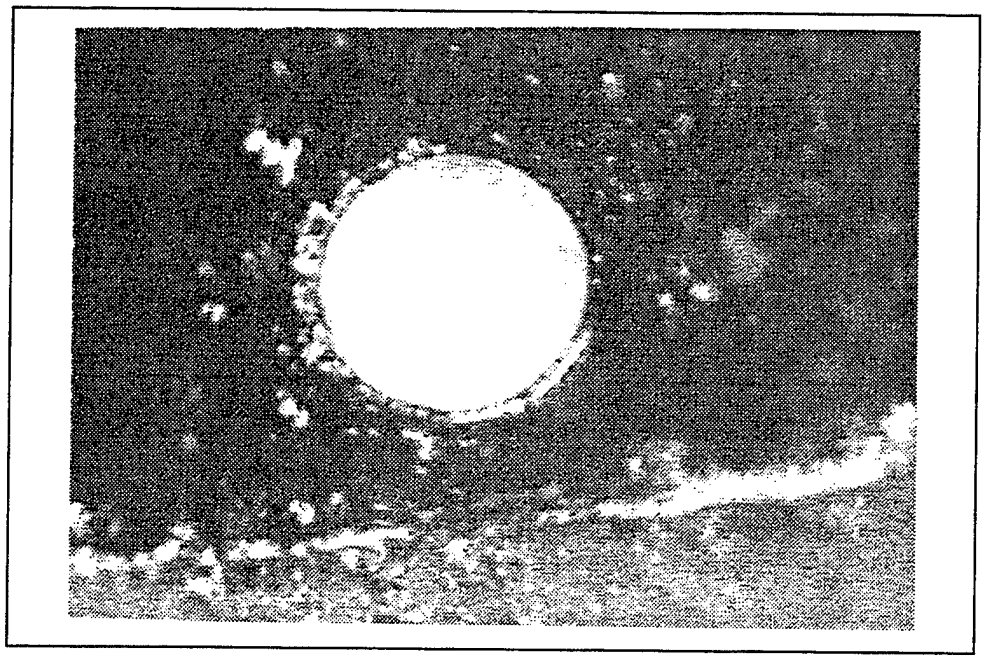

Figure 72: Optical photo of B13, 12 o'clock, 150 cycles.

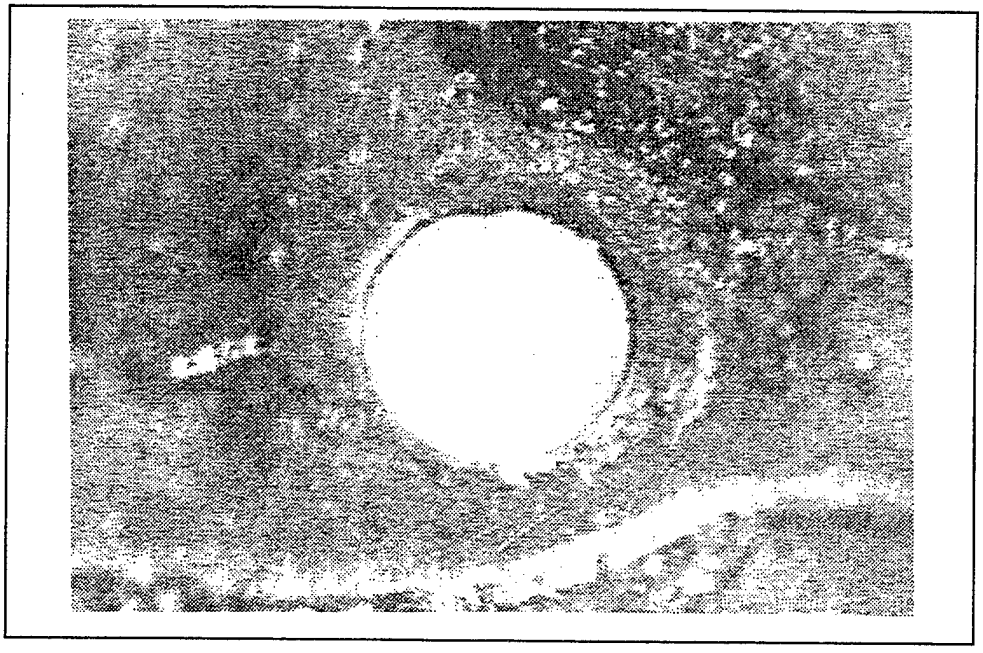

Figure 73: Optical photo of B14, 12 o'clock, 150 cycles.

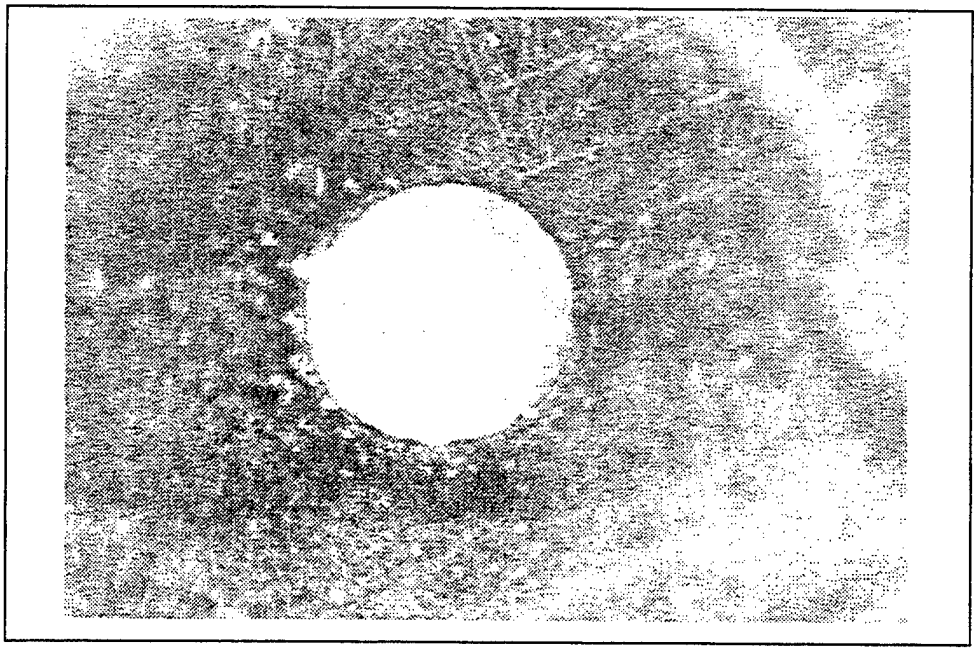

Figure 74: Optical photo of B13, 6 o'clock, 150 cycles.

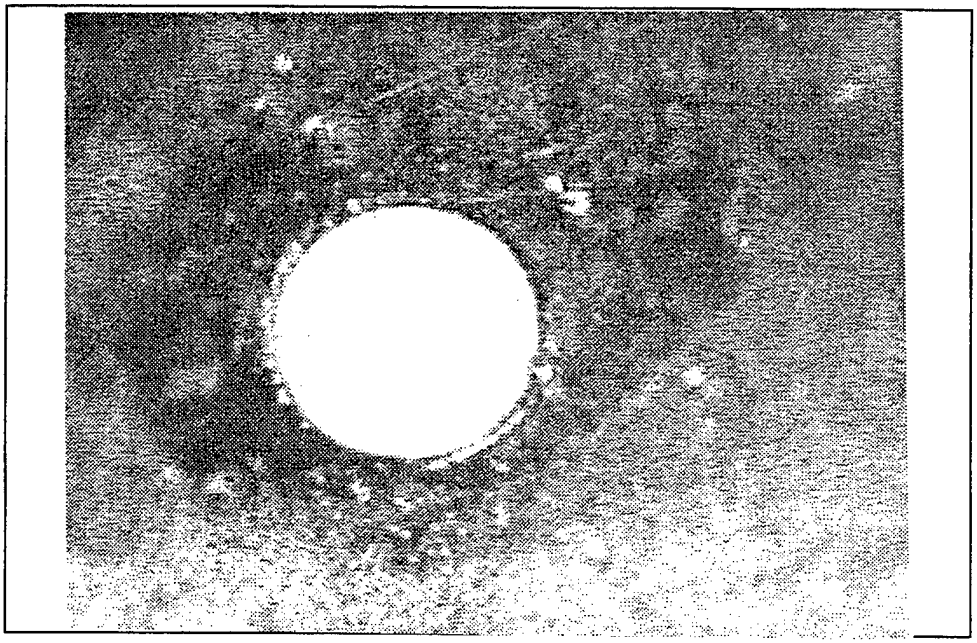

Figure 75: Optical photo of B14, 6 o'clock, 150 cycles.

D. SCANNING ELECTRON MICROSCOPE PHOTO ANALYSIS

While optical photos were taken of each plate after each run, SEM analysis of the plates was done periodically. The SEM analysis shows where coking is occurring and the extent to which it affects the flow through the hole by examining the surface of the plate and the hole at great magnification. Photos of the swirl plates help to verify the analyses completed previously.

The photos of the swirl plates from the SEM analysis will be presented in a similar manner to that of the optical pictures. The captions are of the same format with comments on observations dispersed throughout the figures. The figures are presented as follows:

1. Typical hole and edge photos, Figures 76 - 80.
2. A01 vs. A'01, Figures 81 - 90.
3. B17 vs. B-md20, Figures 91 - 94.
4. B10 vs. A-md25, Figures 95 - 103.
5. A28 vs. A-sil23, Figures 104 - 111.
6. B12 vs. A-sil24, Figures 112 - 123.
7. B13 vs. B14, Figures 124 -131.

The following figures depict typical swirl plate appearances and hole edge appearances for the various swirl plate types. Figures 76 through 78 show A, A' and B type holes and while figures 79 and 80 show the smoothness of the holes.

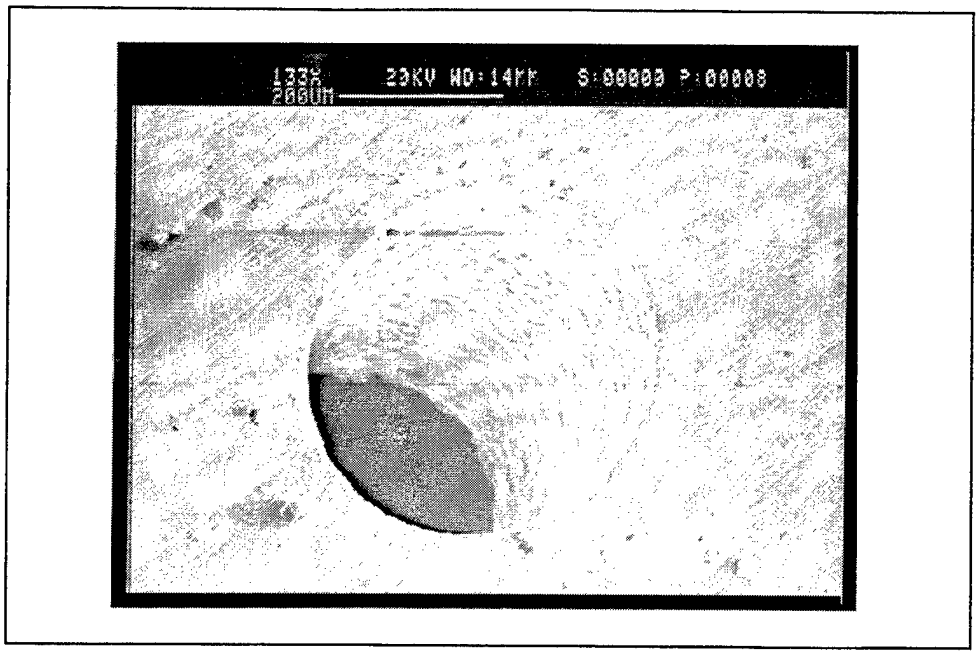

Figure 76: SEM photo of typical A swirlplate, magnification 133X.

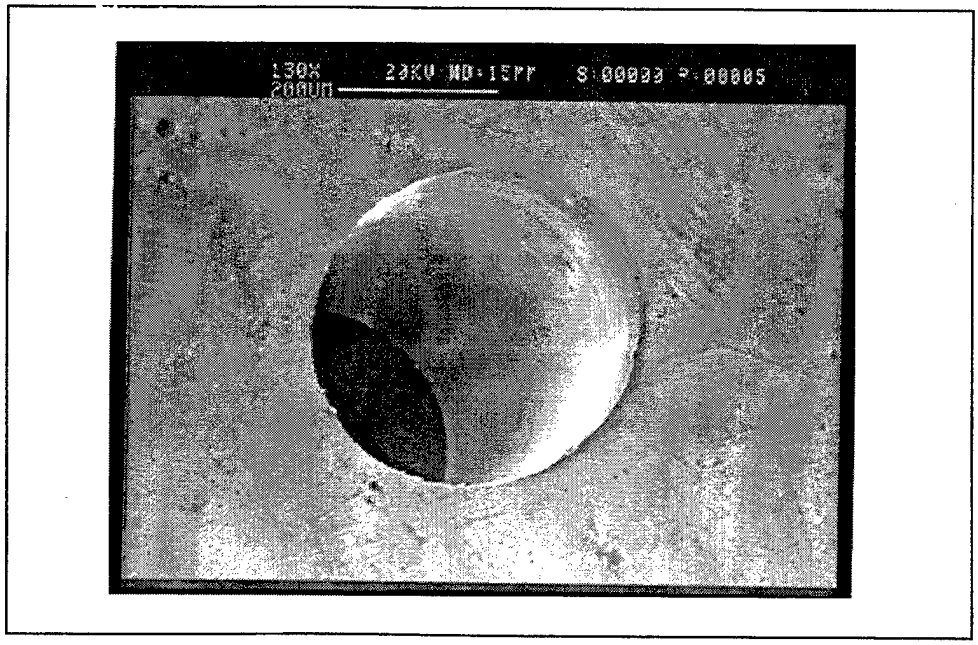

Figure 77: SEM photo of typical B swirlplate, magnification 130X.

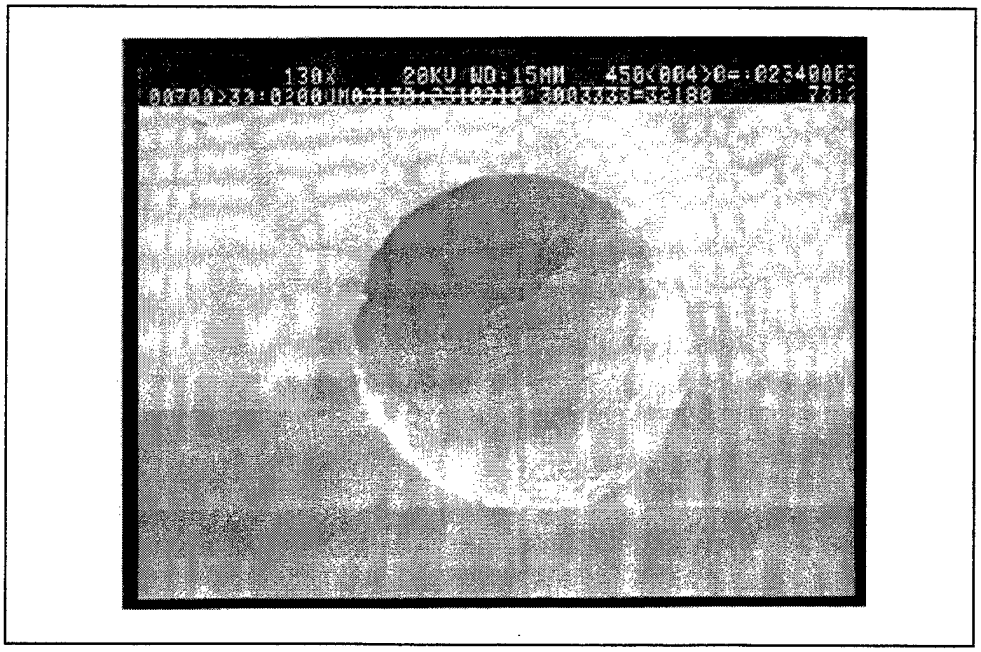

Figure 78: SEM photo of typical A' swirlplate, magnification 130X.

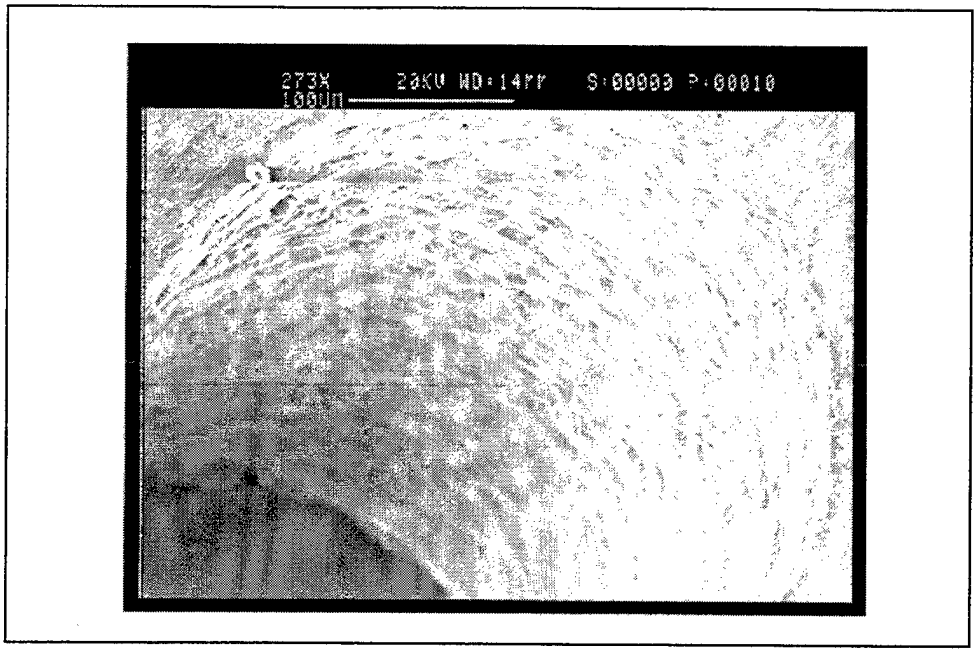

Figure 79: SEM photo of typical A swirlplate hole, magnification 273X.

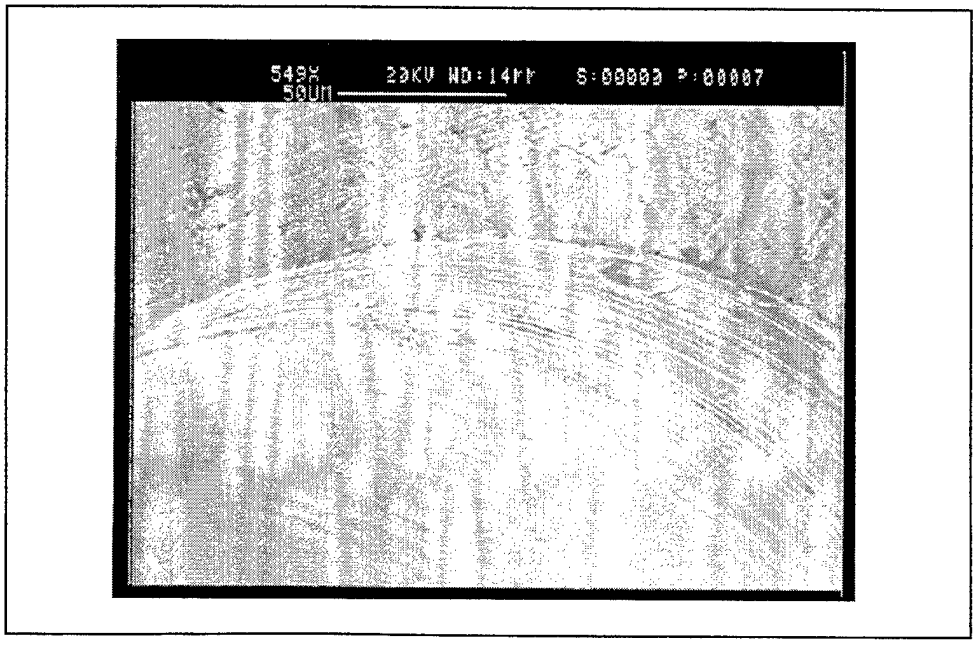

Figure 80: SEM photo of typical B swirlplate hole, magnification 549X.

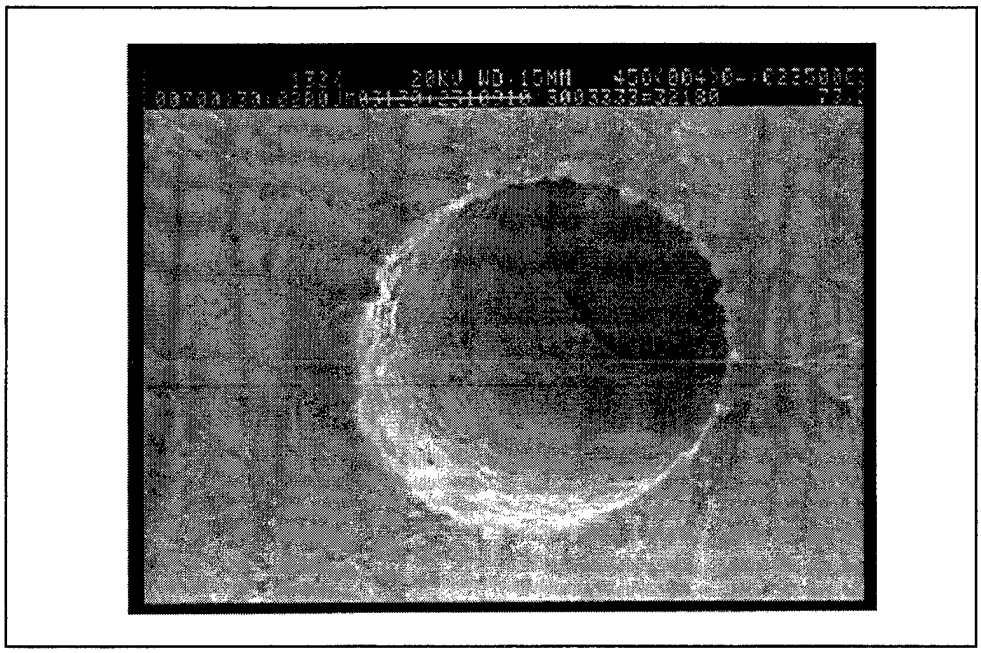

Figure 81: SEM photo of typical A01, 12 o'clock, zero cycles, magnification 132X.

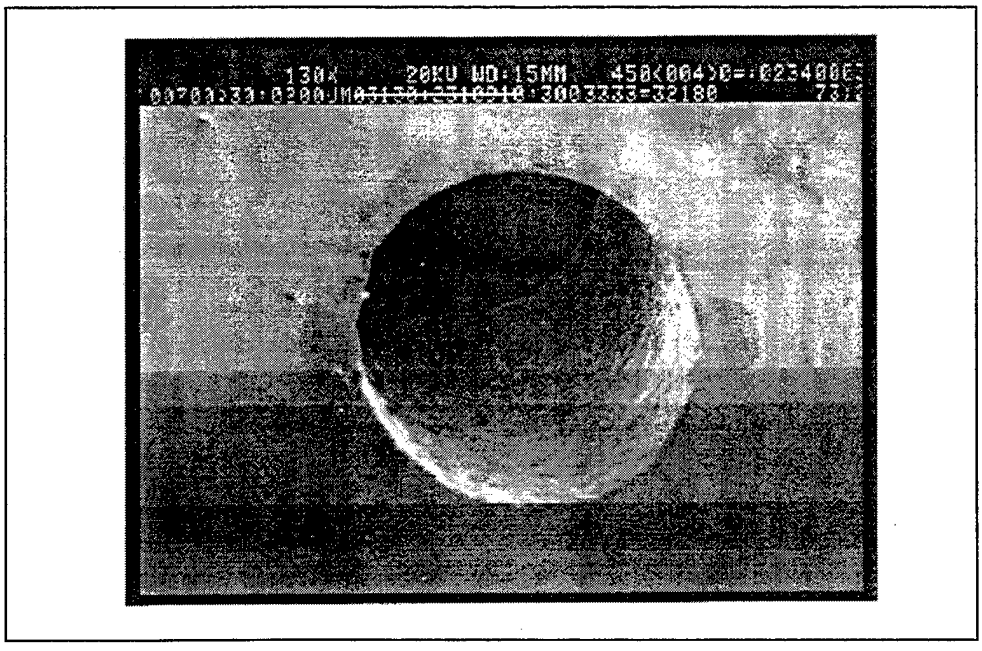

Figure 82: SEM photo of typical A'01, 12 o'clock, zero cycles, magnification 130X.

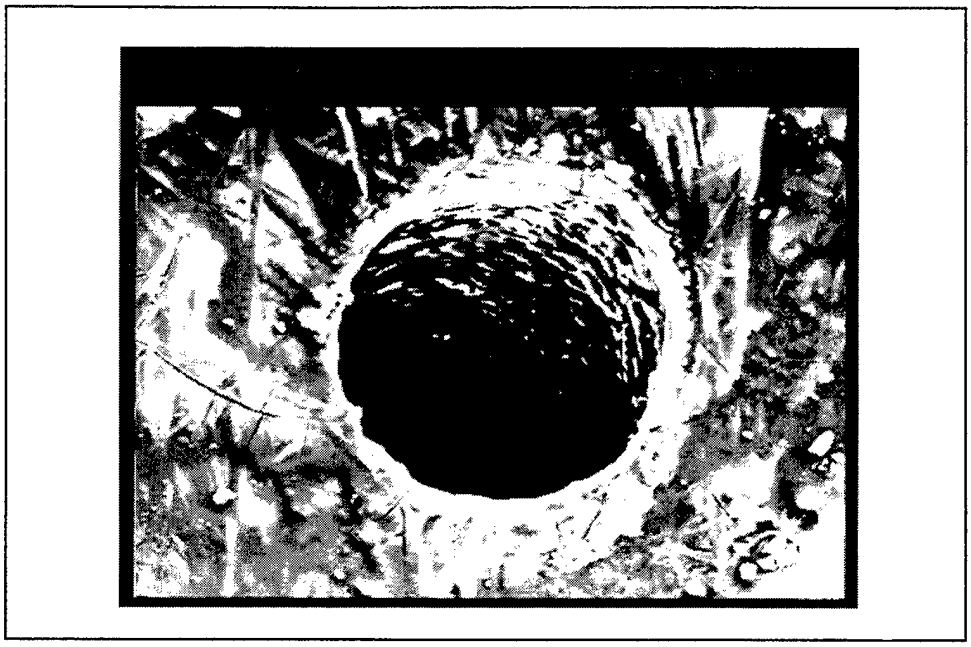

Figure 83: SEM photo of A01, 12 o'clock, 60 cycles, mag. 133X.

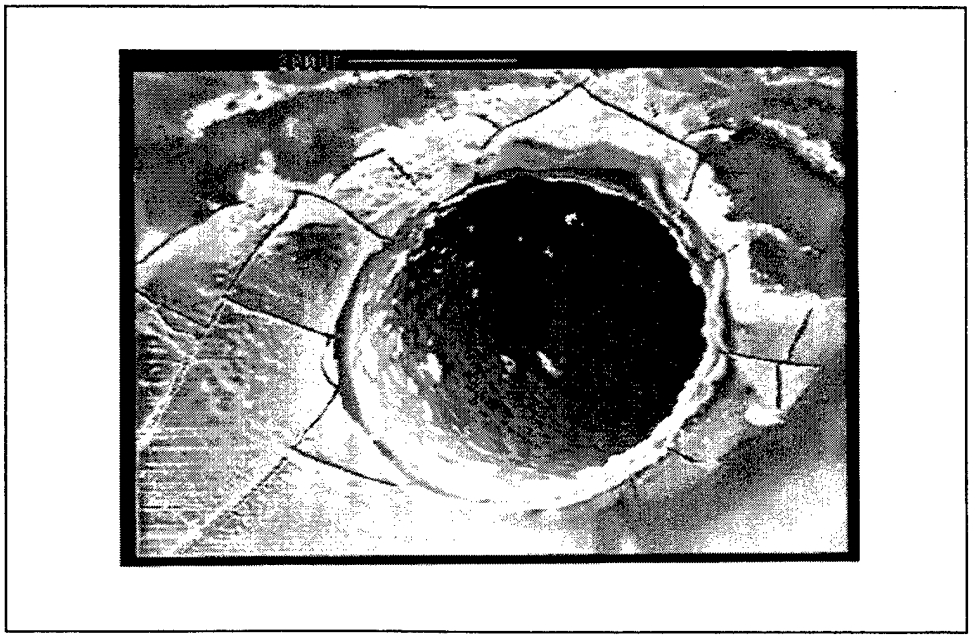

Figure 84: SEM photo of A'01, 12 o'clock, 60 cycles, mag. 130X.

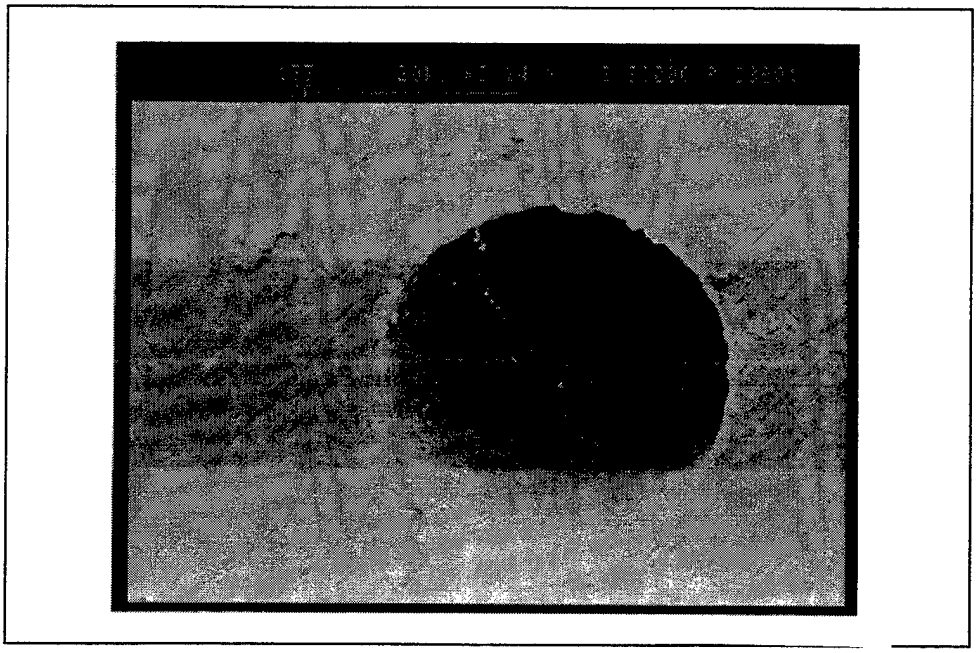

Figure 85: SEM photo of A01, 6 o'clock, 60 cycles, mag. 133X.

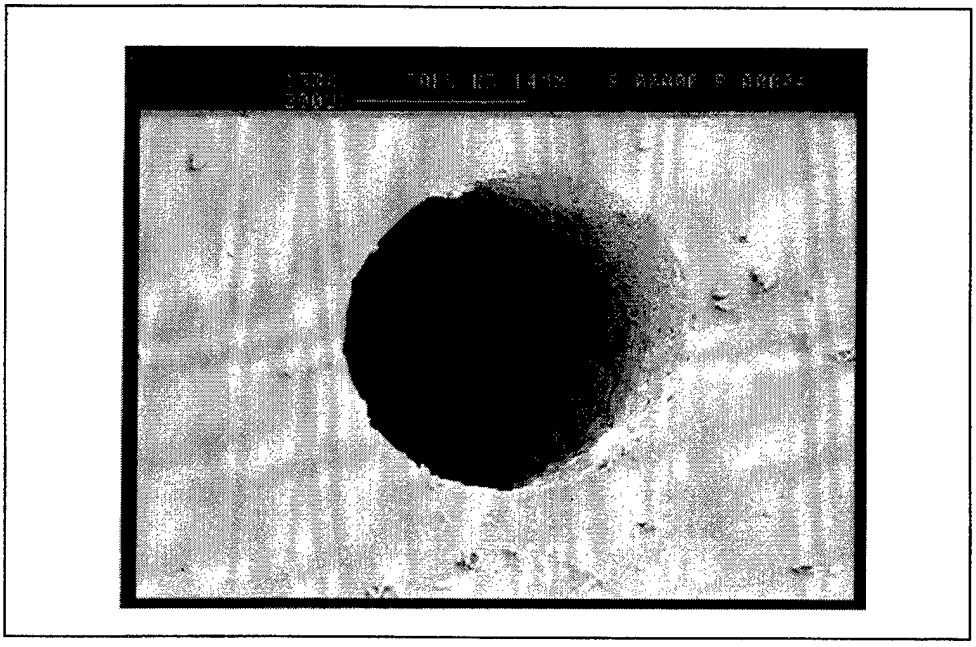

Figure 86: SEM photo of A'01, 6 o'clock, 60 cycles, mag. 133X.

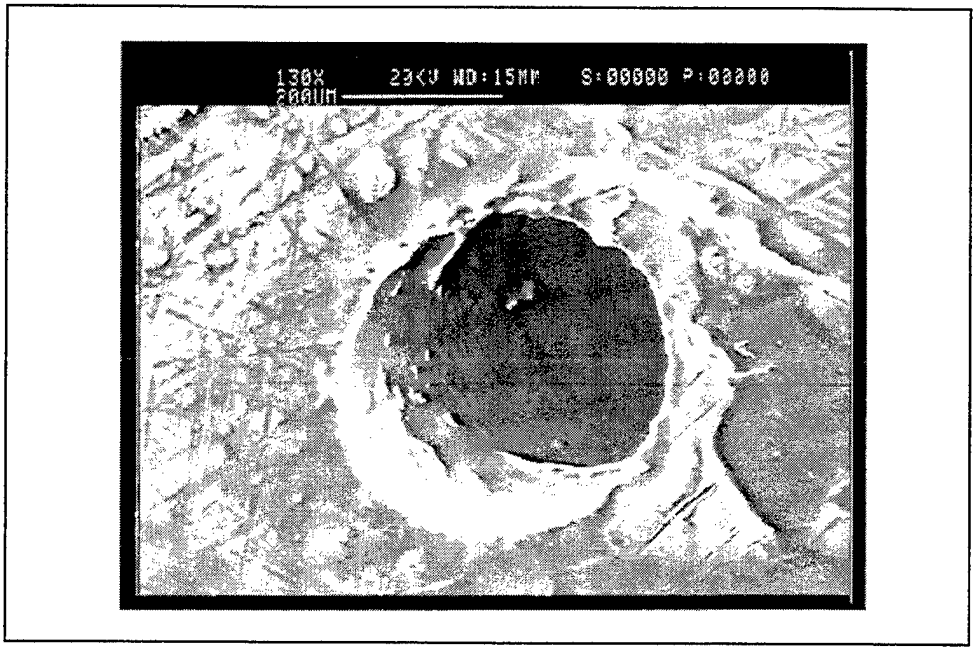

Figure 87: SEM photo of A01, 12 o'clock, 150 cycles, mag. 130X.

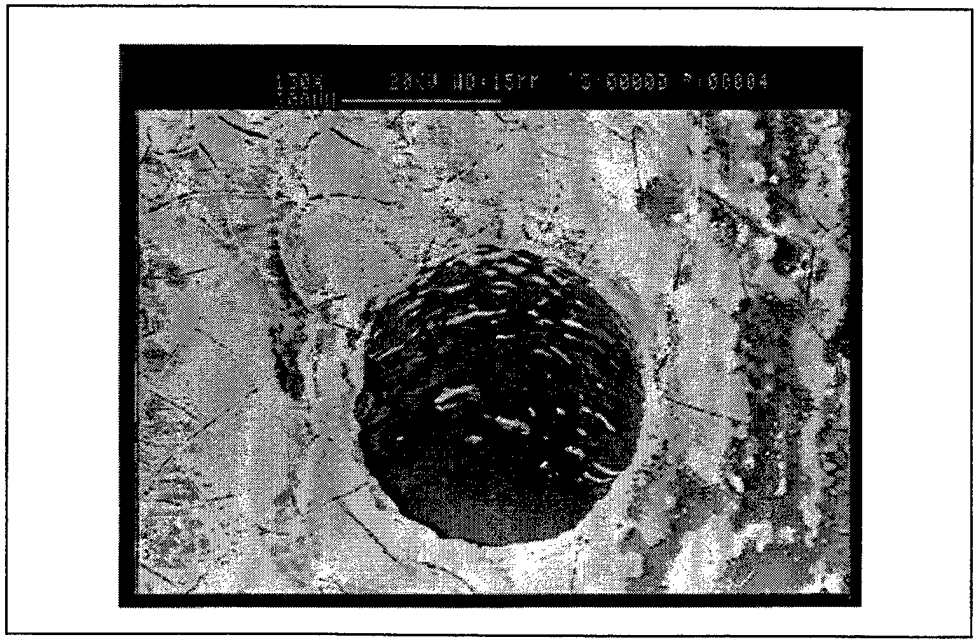

Figure 88: SEM photo of A'01, 12 o'clock, 150 cycles, mag. 130X.

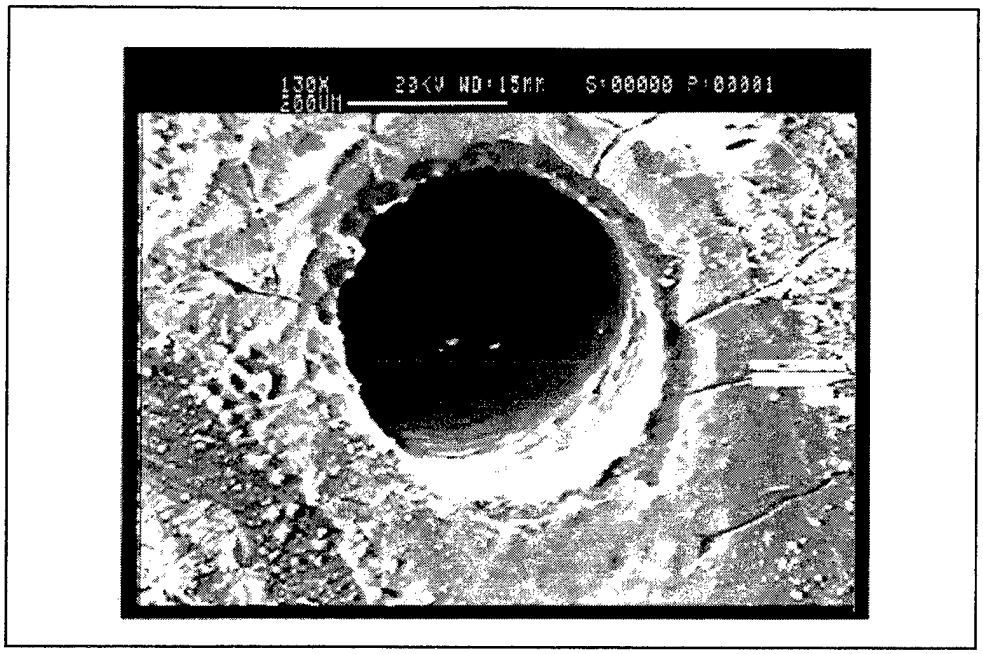

Figure 89: SEM photo of A01, 6 o'clock, 150 cycles, mag. 130X.

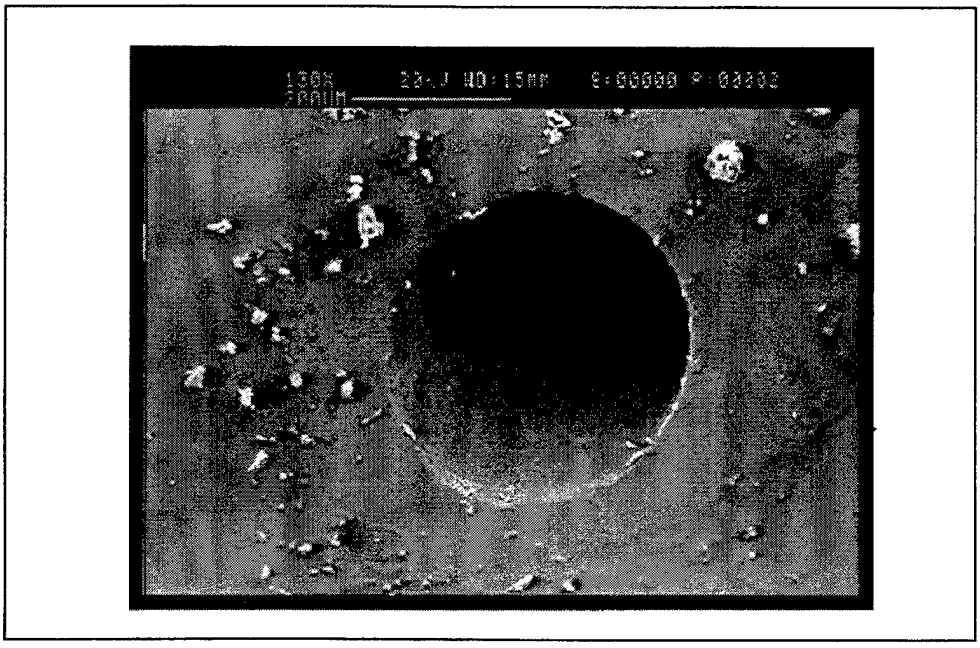

Figure 90: SEM photo of A'01, 6 o'clock, 150 cycles, mag. 130X.

Figures 81 through 90 show preferential coking around the edges of the holes. They also show that coking is indeed occurring in abundance near the 12 o'clock position vice the 6 o'clock position. These photos depict coking attached to the surface while little is attached to the holes. The A'01 swirlplate appears to have less coking on the surface.

As seen in figures 76 and 78 and again in figures 81 and 82, the surface of the A'01 plate is smoother than the A01. The reduced surface coking of the A'01 plate may indicate that surface effect plays an important role. Further photos of different coated swirlplates may help to clarify this assumption.

Figures 91 through 94 show the virgin swirlplates of B17 and B-md20 and then show the final photos after 150 cycles. These final two photos are included as they show excellent evidence of the coking mechanism occurring near the edge of the hole.

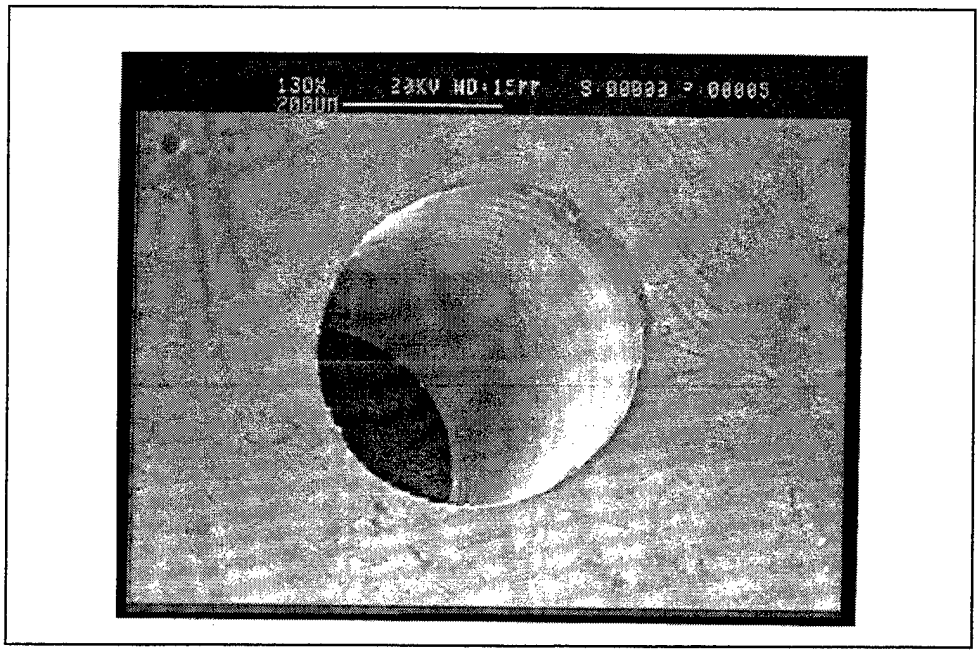

Figure 91: SEM photo of B17, 12 o'clock, zero cycles, mag. 130X.

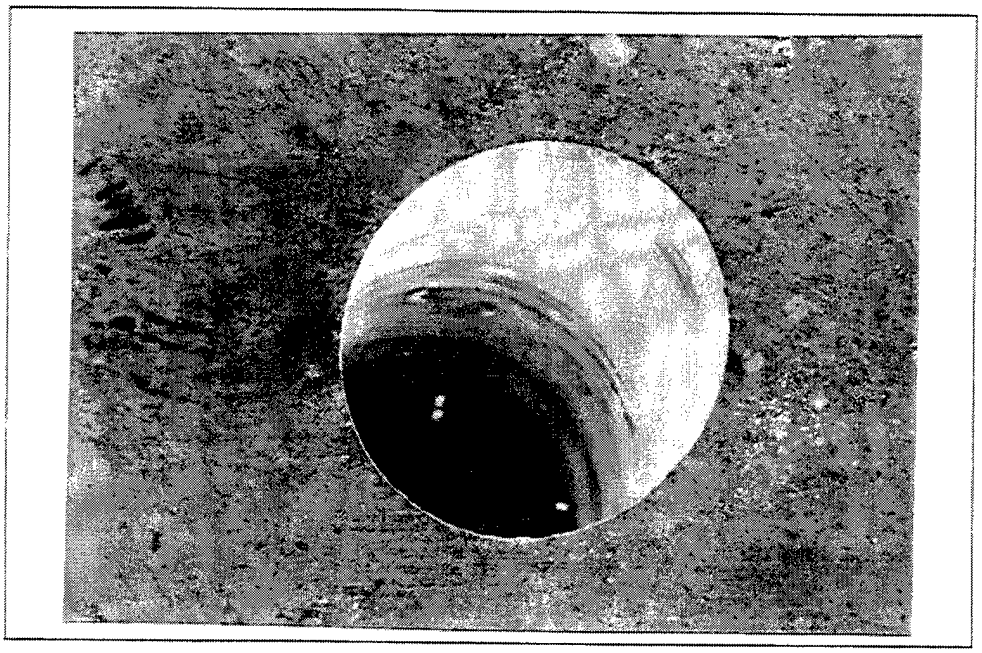

Figure 92: SEM photo of B-md20, 12 o'clock, zero cycles, mag. 130X.

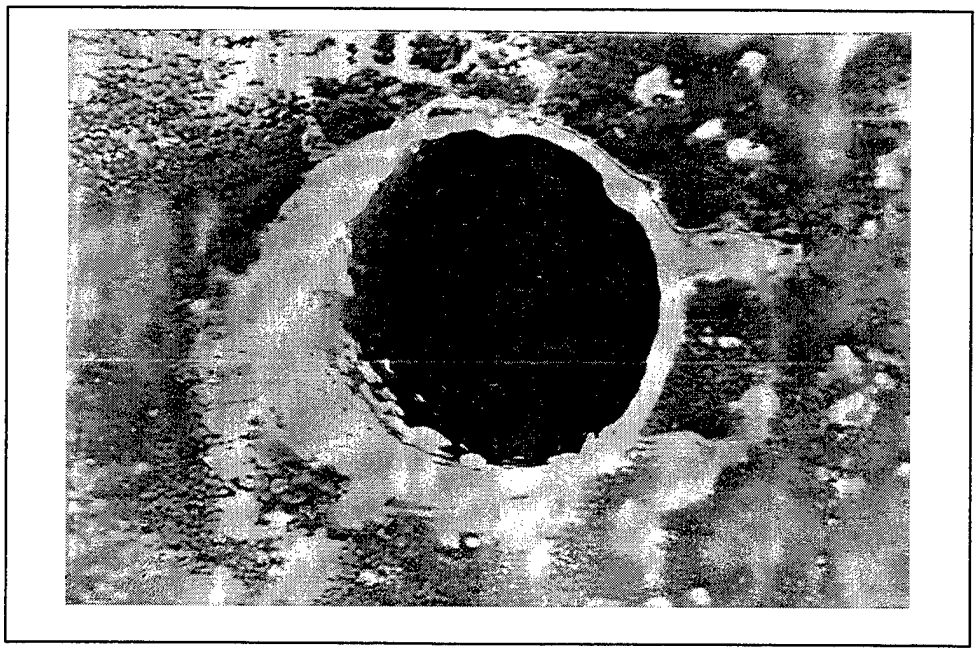

Figure 93: SEM photo of B17, 9 o'clock, 150 cycles, mag. 130X.

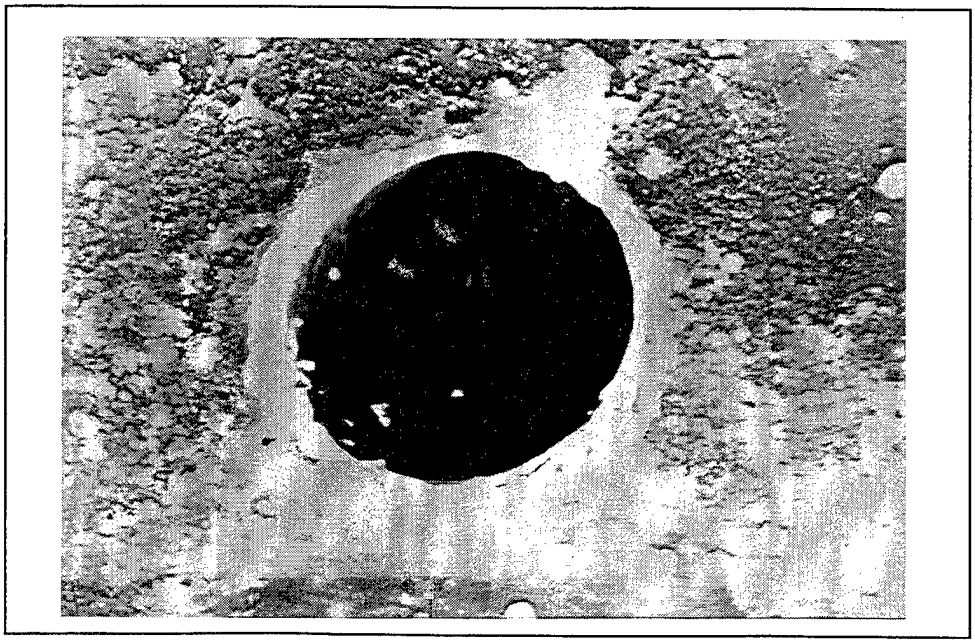

Figure 94: SEM photo of B-md20, 9 o'clock, 150 cycles, mag. 133X.

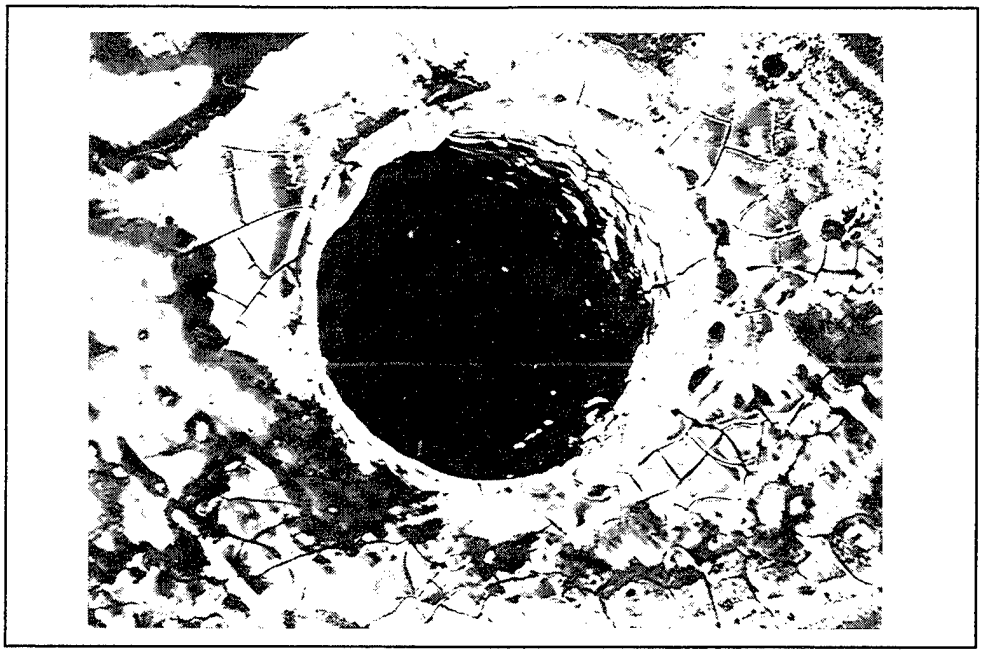

Figure 95: SEM photo of A-md25, 12 o'clock, 60 cycles, mag. 128X.

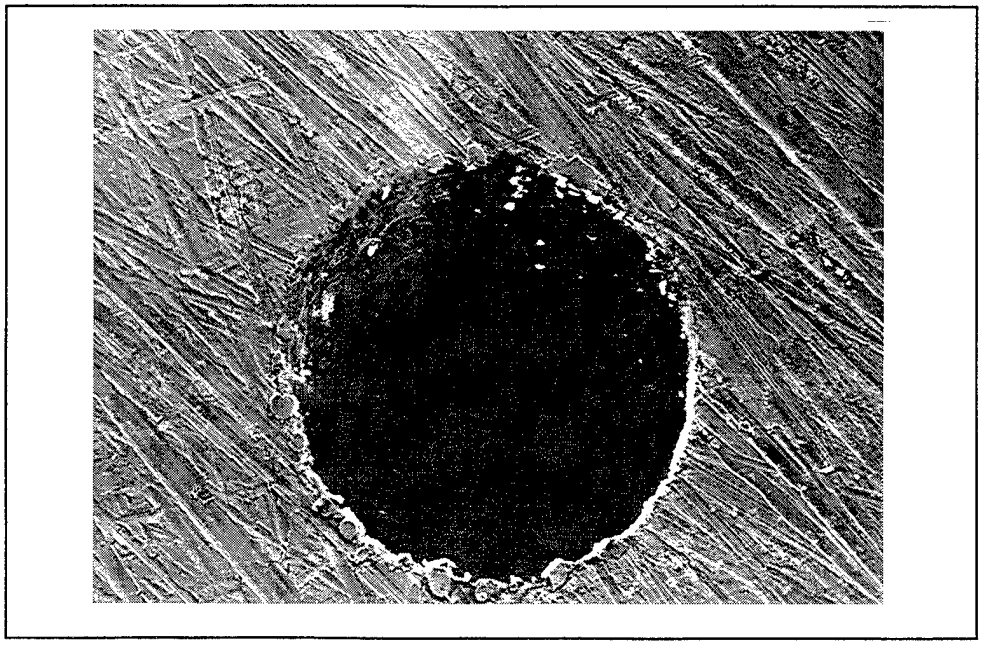

Figure 96: SEM photo of A-md25, 6 o'clock, 60 cycles, mag. 128X.

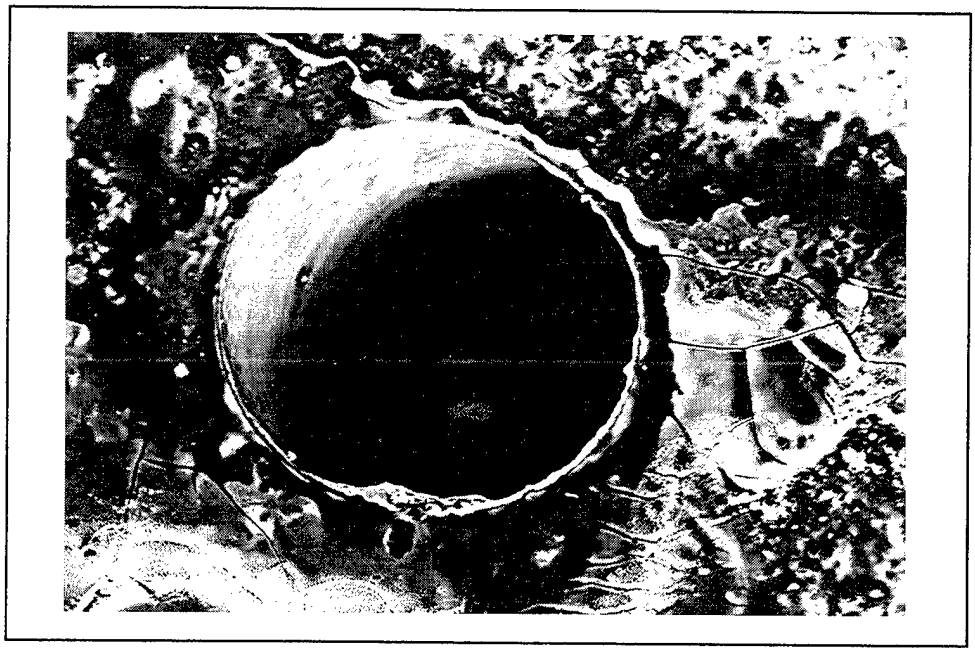

Figure 97: SEM photo of B10, 12 o'clock, 120 cycles, mag. 133X.

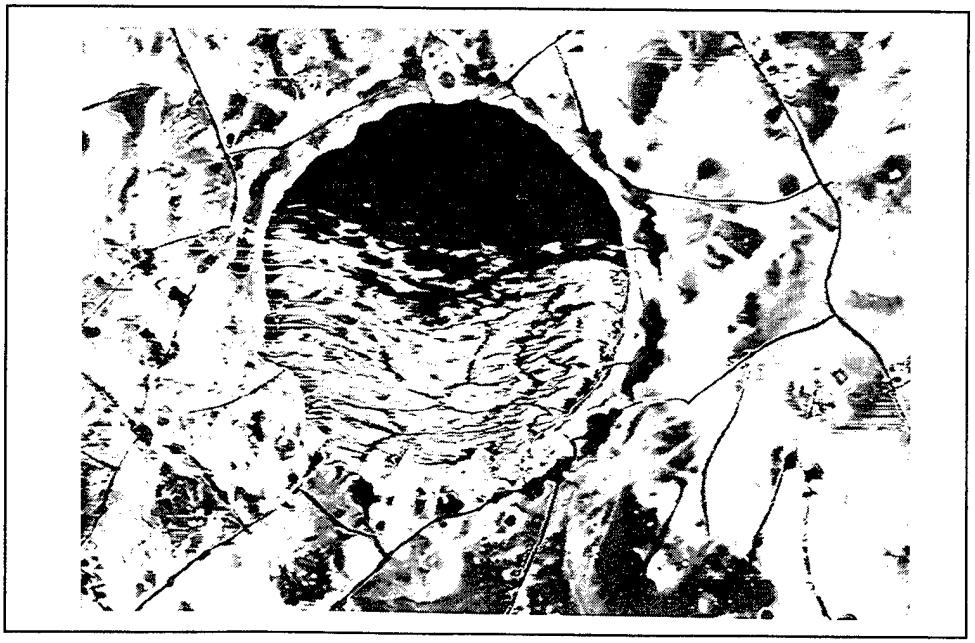

Figure 98: SEM photo of A-md25, 12 o'clock, 120 cycles, mag. 133X.

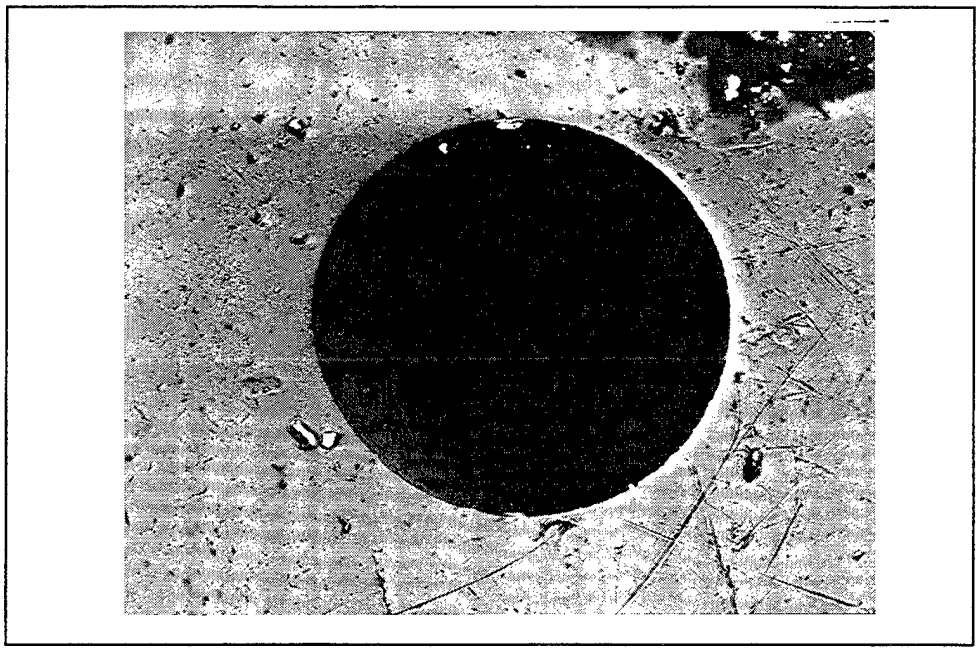

Figure 99: SEM photo of B10, 6 o'clock, 120 cycles, mag. 133X.

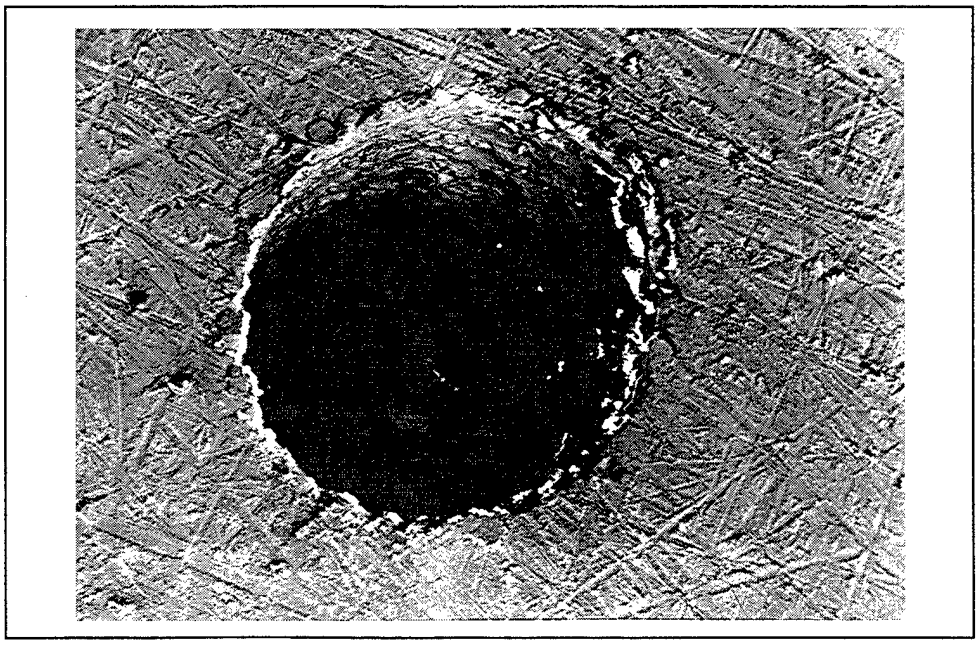

Figure 100: SEM photo of A-md25, 6 o'clock, 120 cycles, mag. 133X.

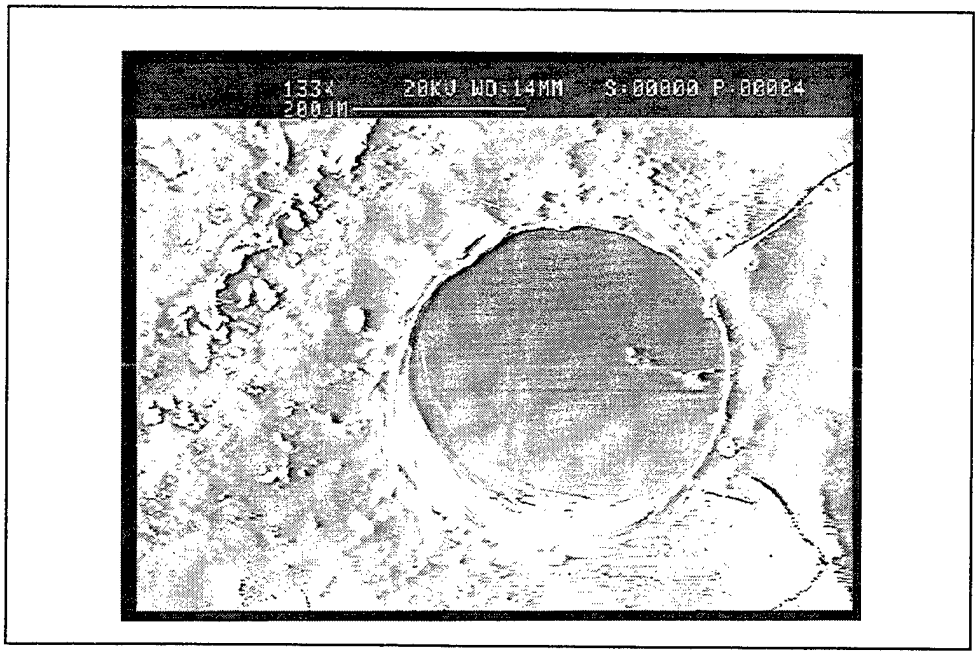

Figure 101: SEM photo of B10, 12 o'clock, 150 cycles, mag. 133X.

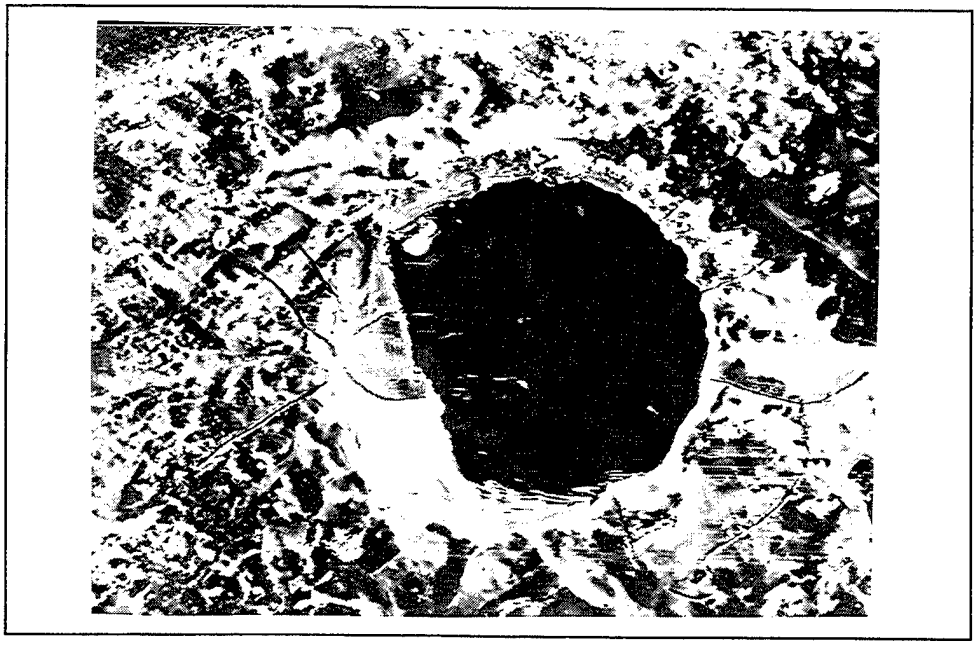

Figure 102: SEM photo of A-md25, 2 o'clock, 150 cycles, mag. 133X.

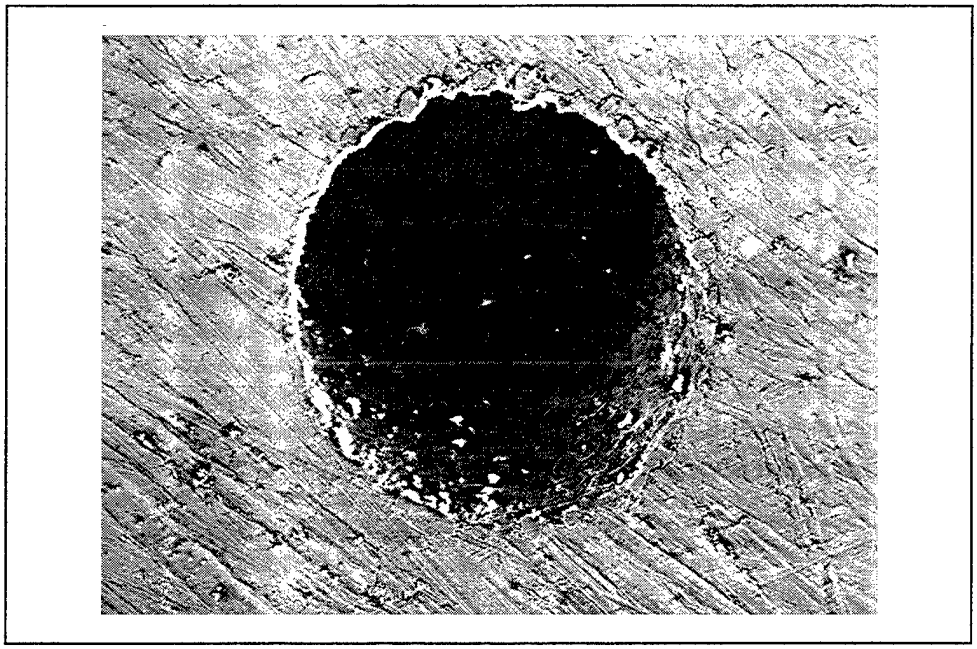

Figure 103: SEM photo of A-md25, 6 o'clock, 150 cycles, mag. 133X.

Figures 95 through 103 show another B plate versus a production A plate coated with amorphous diamond. Preferential coking is evident in both cases with the B plate showing minimal coking throughout. The amorphous diamond coating appears to enhance the coking resistivity characteristics of the production A plate as it is not severely coked as expected.

The following figures show another production plate with no coating versus a production plate with a silicon coating. Figures 104 through 111 indicate that the silicon coating also enhances the coking resistivity. There is still quite a bit if coking near the 12 o'clock position but the silicon coated plate appears to resist more the farther from the top position.

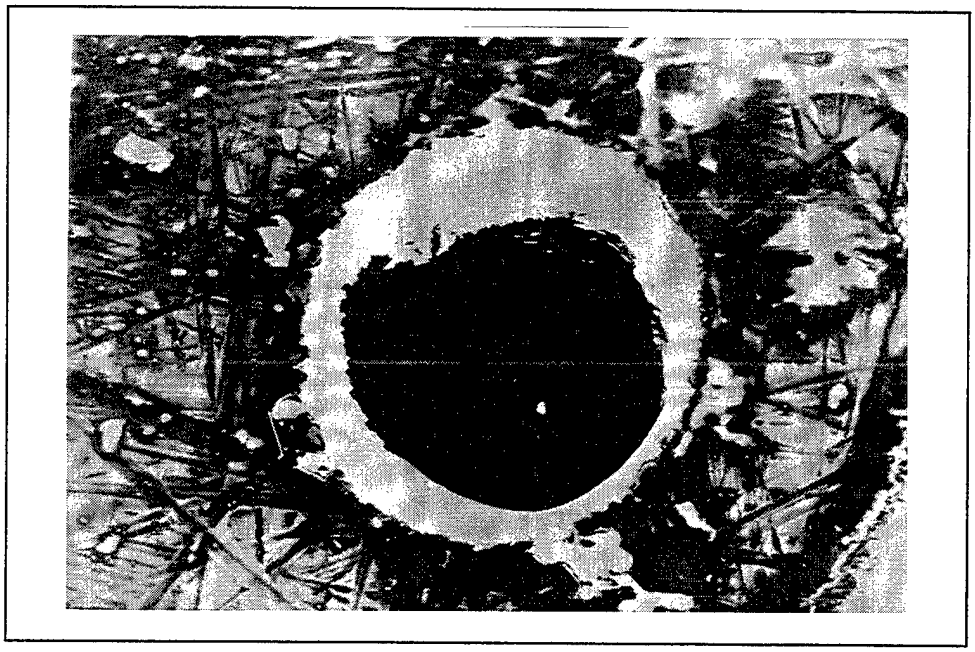

Figure 104: SEM photo of A28, 12 o'clock, 60 cycles, mag. 128X.

Figure 105: SEM photo of A-sil23, 12 o'clock, 60 cycles, mag. 121X.

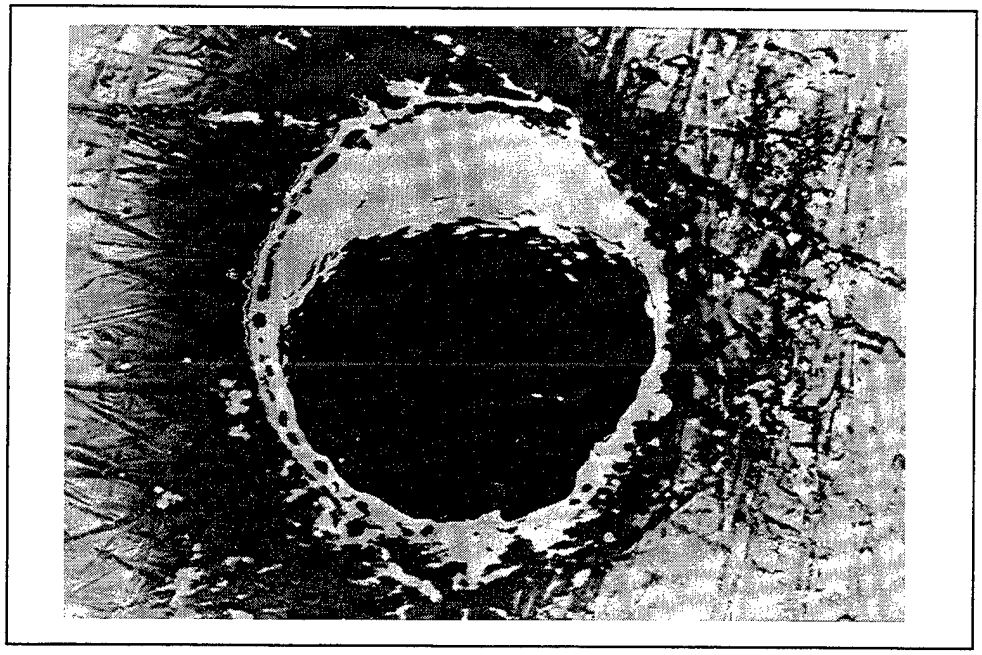

Figure 106: SEM photo of A28, 5 o'clock, 60 cycles, mag. 124X.

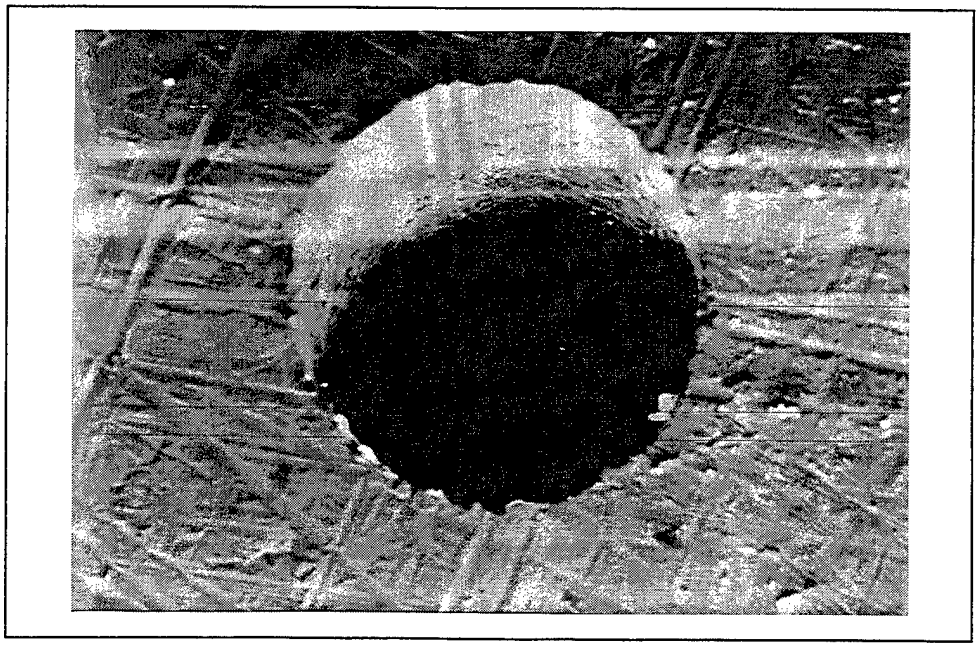

Figure 107: SEM photo of A-sil23, 6 o'clock, 60 cycles, mag. 121X.

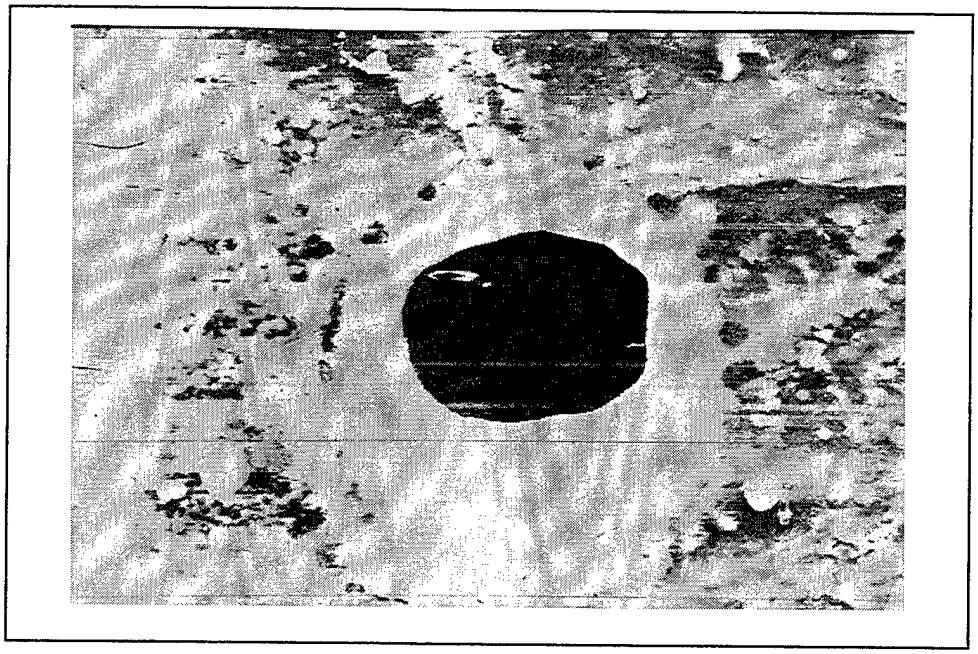

Figure 108: SEM photo of A28, 12 o'clock, 150 cycles, mag. 128X.

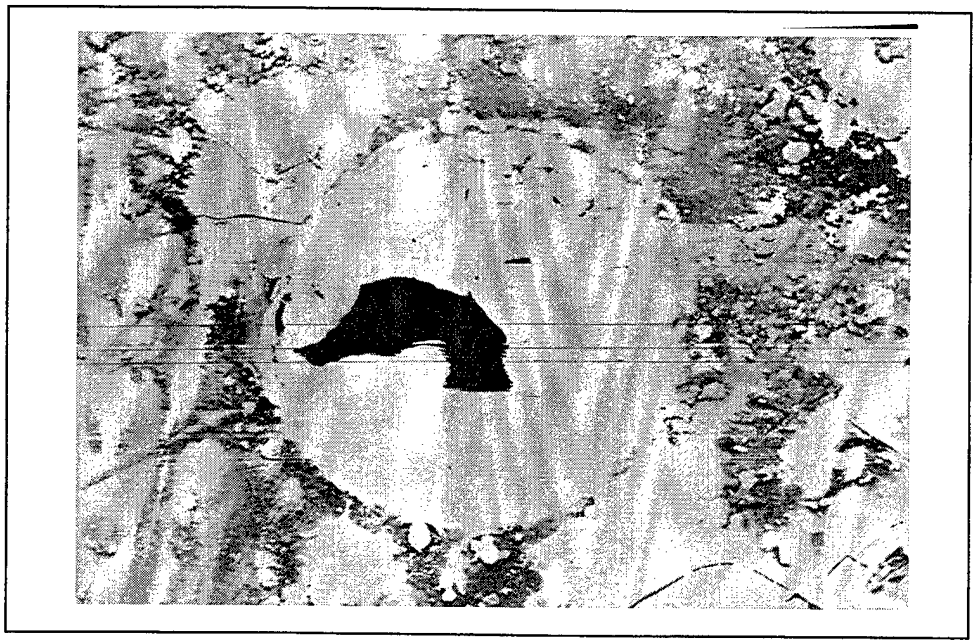

Figure 109: SEM photo of A-sil23, 12 o'clock, 150 cycles, mag. 128X.

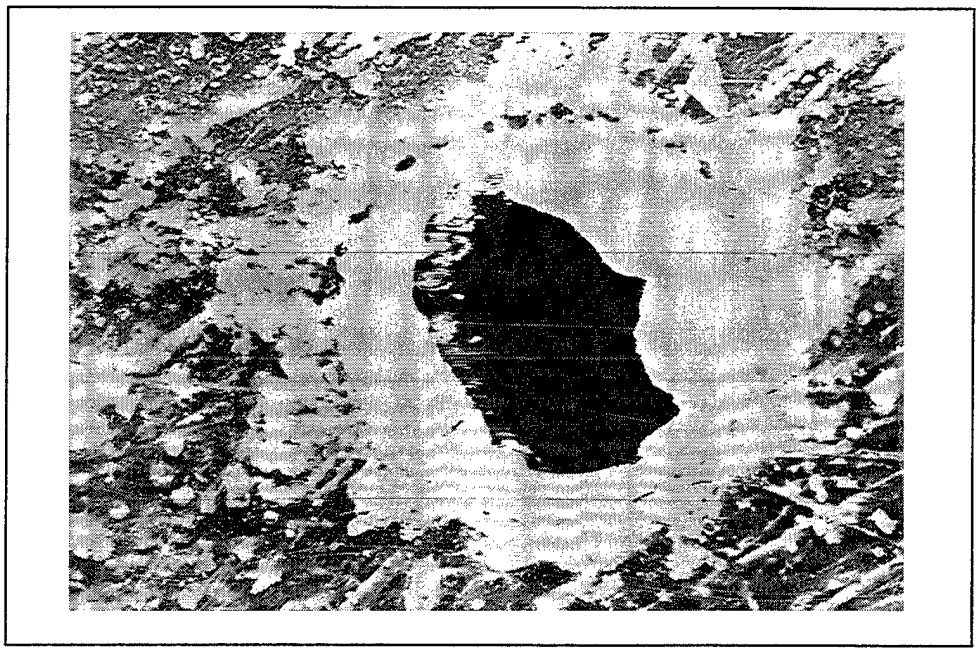

Figure 110: SEM photo of A28, 4 o'clock, 150 cycles, mag. 128X.

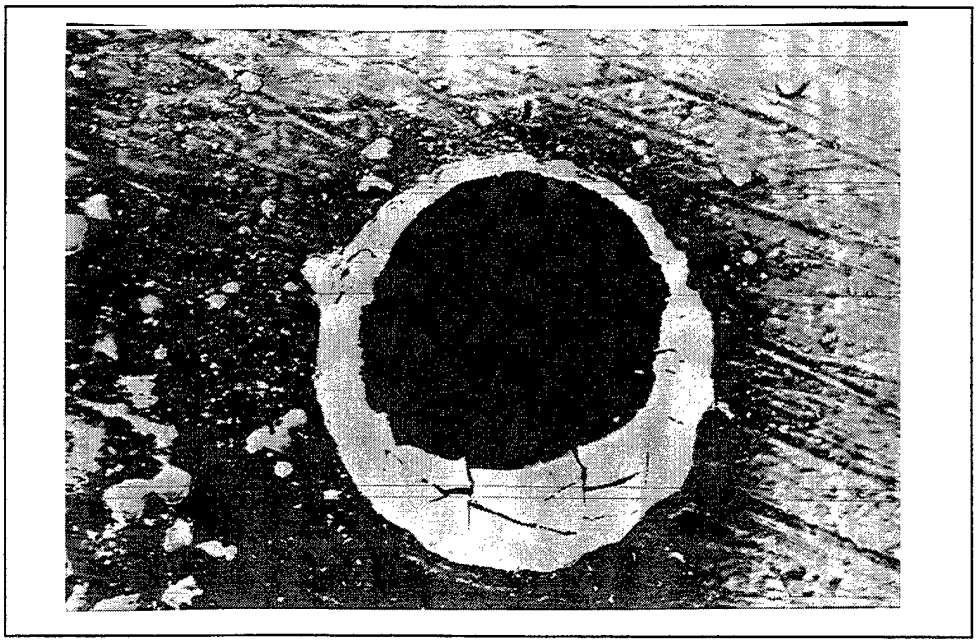

Figure 111: SEM photo of A-sil23, 4 o'clock, 150 cycles, mag. 128X.

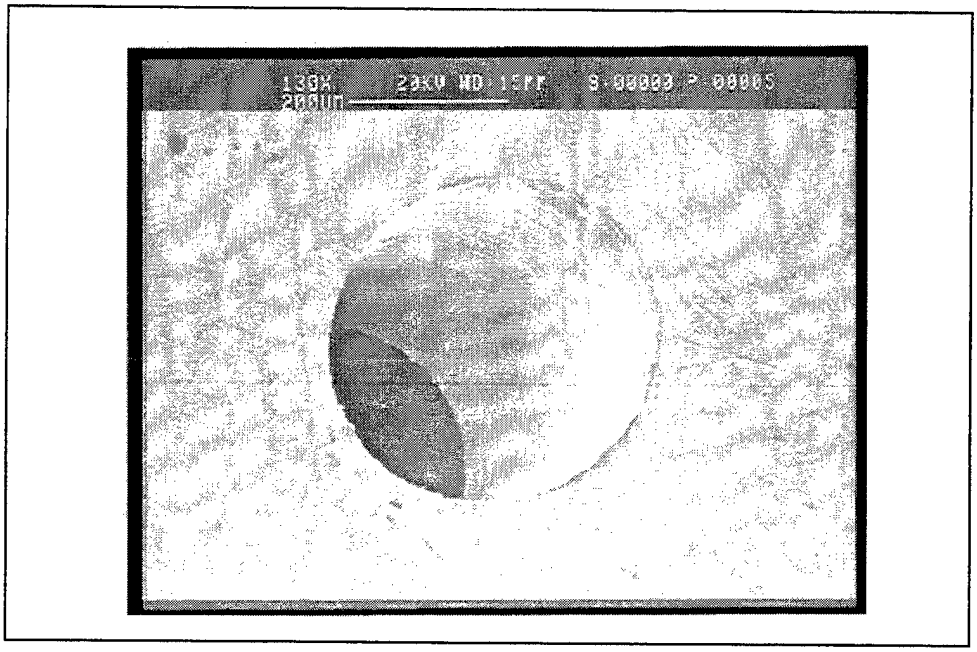

Figure 112: SEM photo of B12, 12 o'clock, zero cycles, mag. 130X.

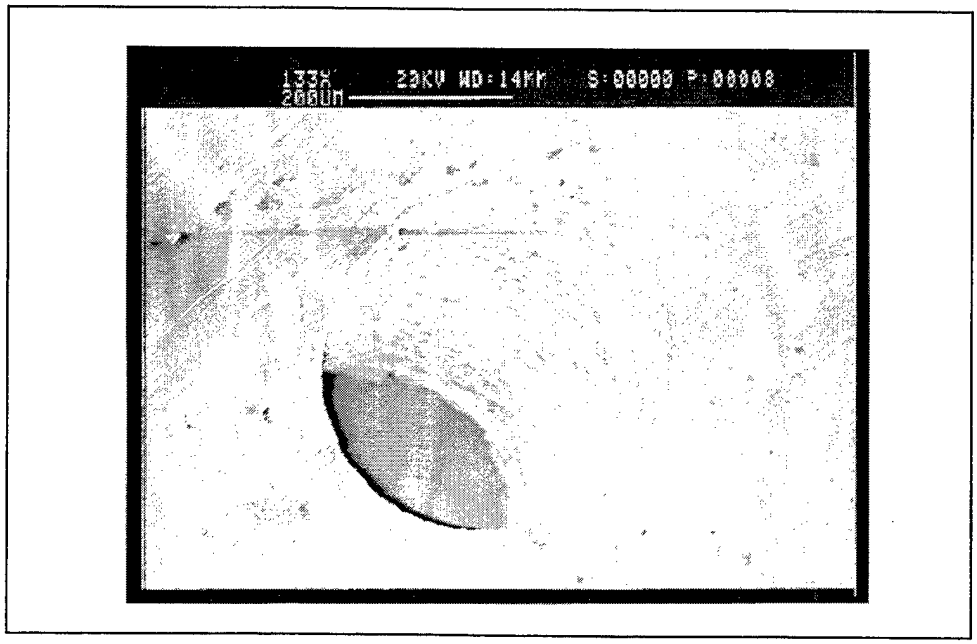

Figure 113: SEM photo of A-sil24, 12 o'clock, zero cycles, mag. 133X.

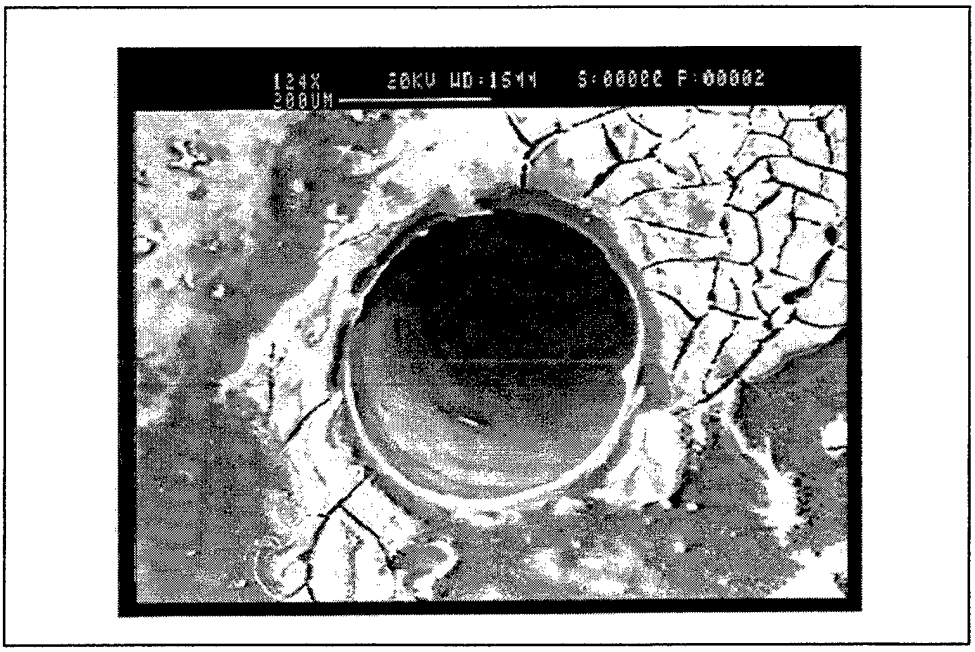

Figure 114: SEM photo of B12, 12 o'clock, 90 cycles, mag. 124X.

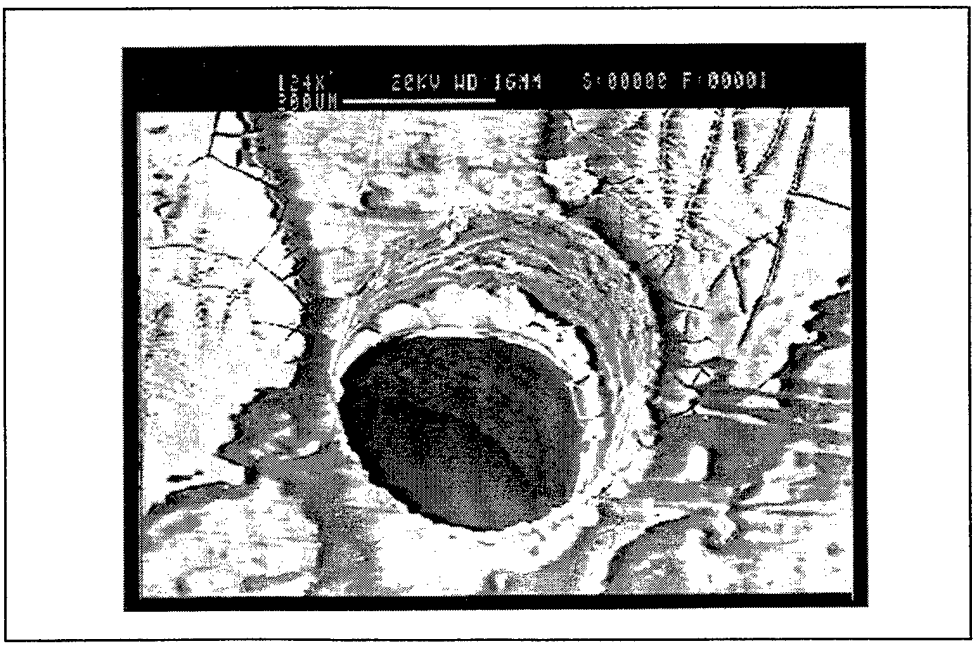

Figure 115: SEM photo of A-sil24, 12 o'clock, 90 cycles, mag. 124X.

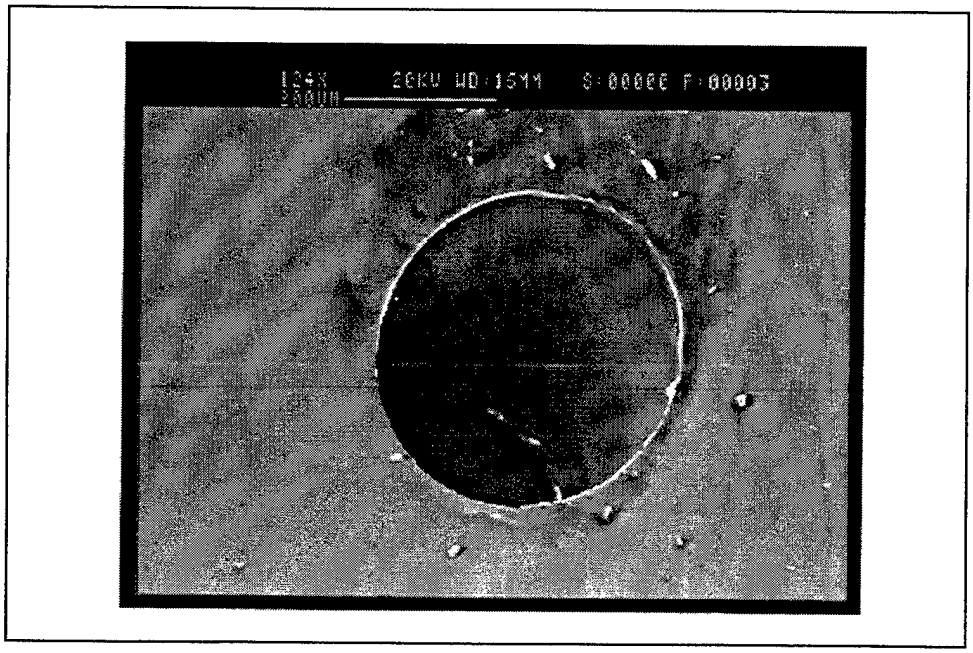

Figure 116: SEM photo of B12, 6 o'clock, 90 cycles, mag. 124X.

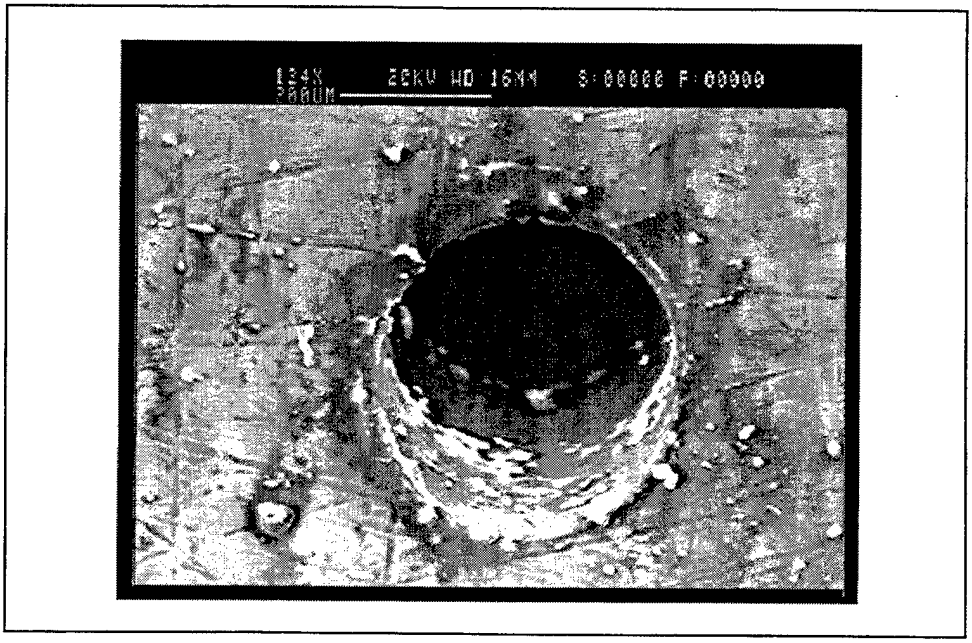

Figure 117: SEM photo of A-sil24, 6 o'clock, 90 cycles, mag. 124X.

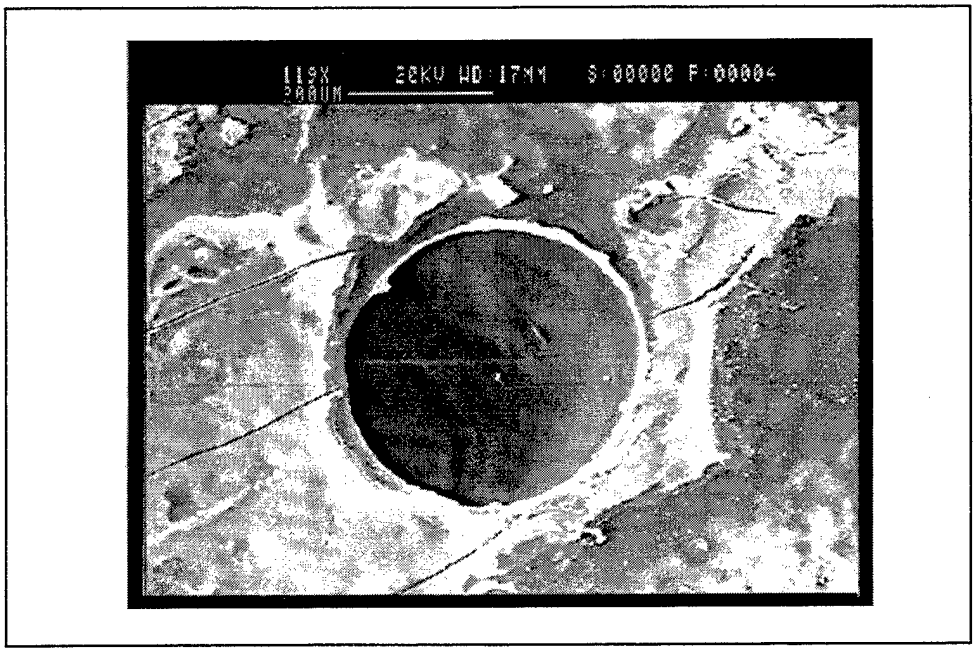

Figure 118: SEM photo of B12, 12 o'clock, 150 cycles, mag. 119X.

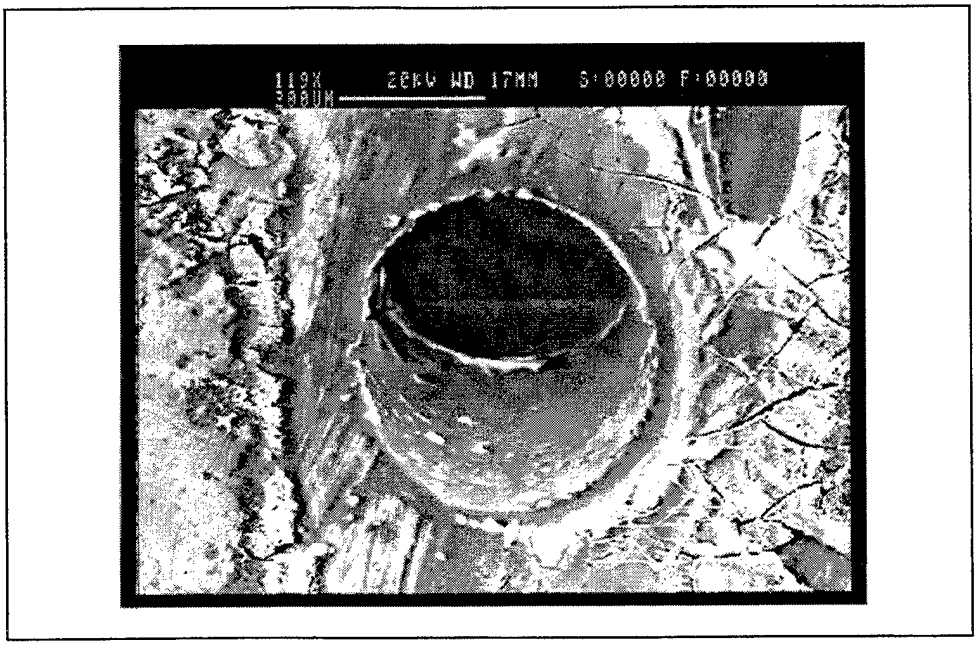

Figure 119: SEM photo of A-sil24, 12 o'clock, 150 cycles, mag. 119X.

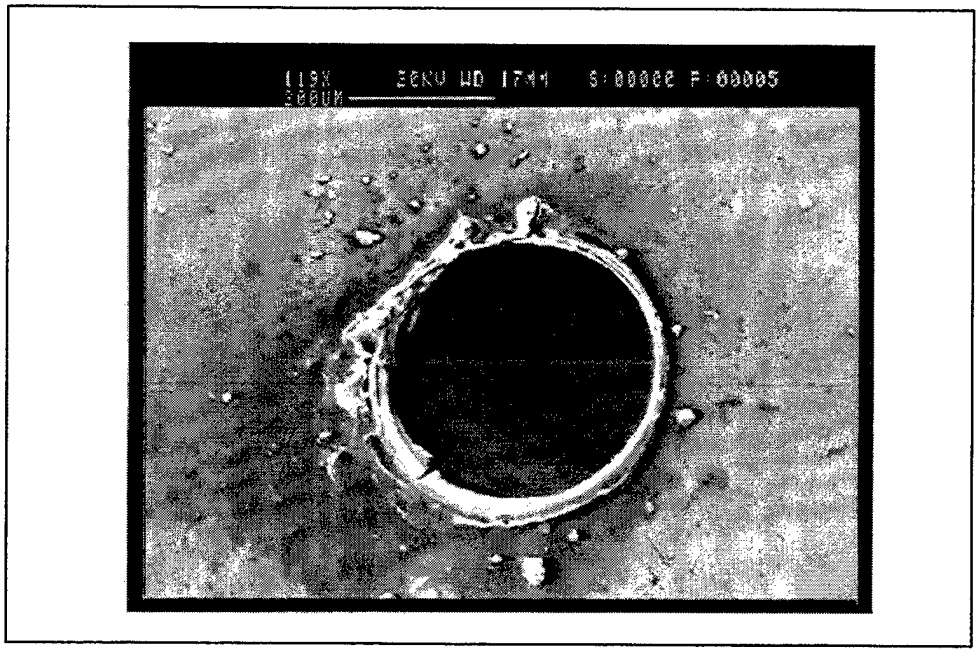

Figure 120: SEM photo of B12, 6 o'clock, 150 cycles, mag. 119X.

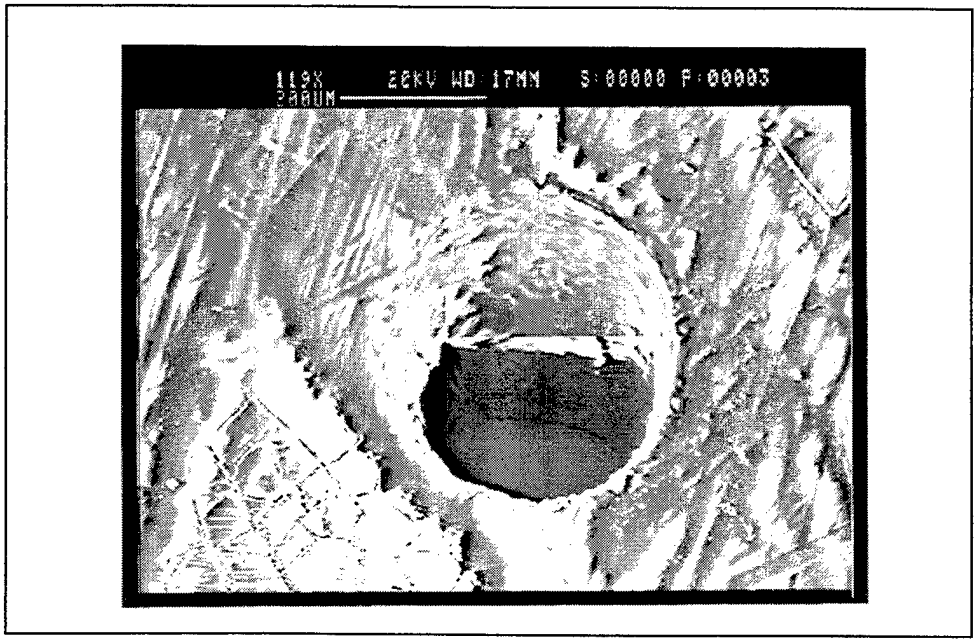

Figure 121: SEM photo of A-sil24, 6 o'clock, 150 cycles, mag. 119X.

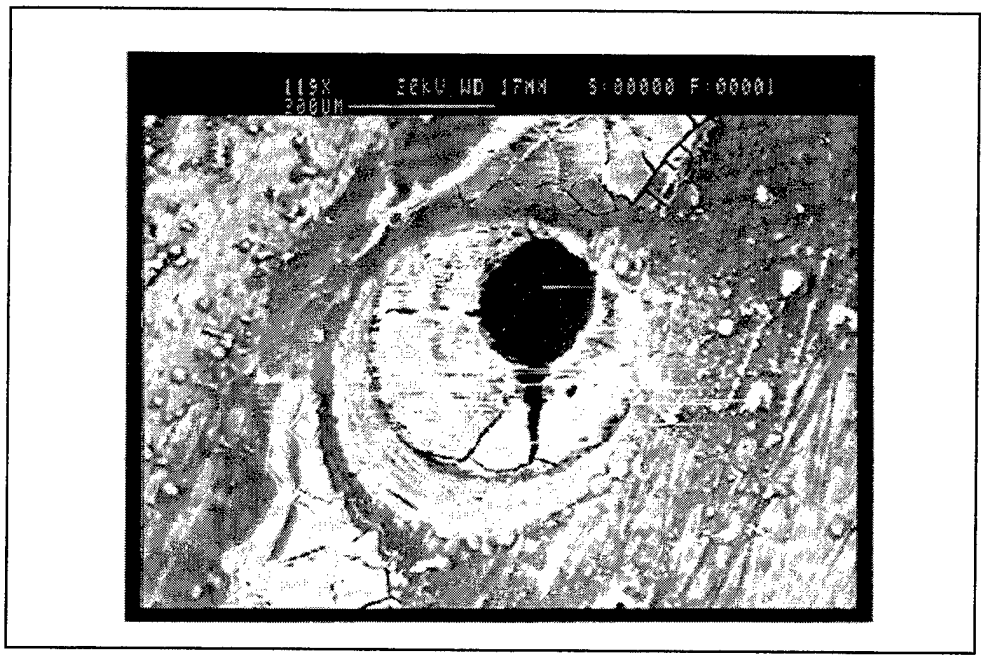

Figure 122: SEM photo of A-sil24, 1 o'clock, 150 cycles, mag. 119X.

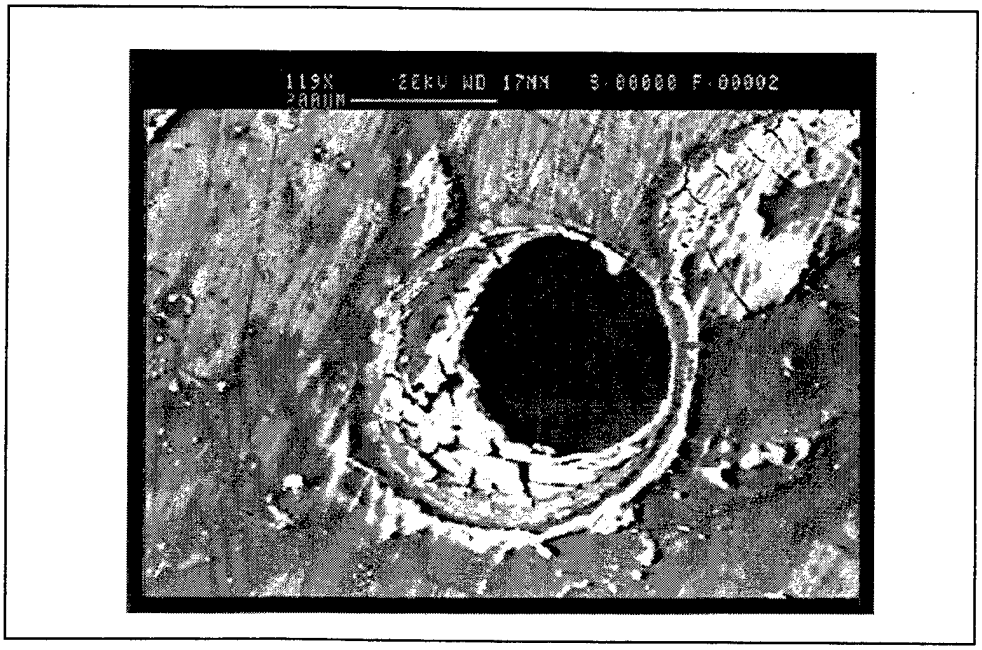

Figure 123: SEM photo of A-sil24, 2 o'clock, 150 cycles, mag. 119X.

Figures 112 through 123 are excellent examples of potential candidates for swirlplate investigation. The B plate showed very little coking throughout the run while the production swirlplate coated with silicon did a superb job resisting the adherence of coke. There is evidence of preferential coking once again on the A plate but overall there appears to be a drastic reduction.

The final set of SEM photos depicts two B type plates. All eight photos show evidence of superior coking resistance. They appear to support the previous results that the B type swirlplates have the most potential.

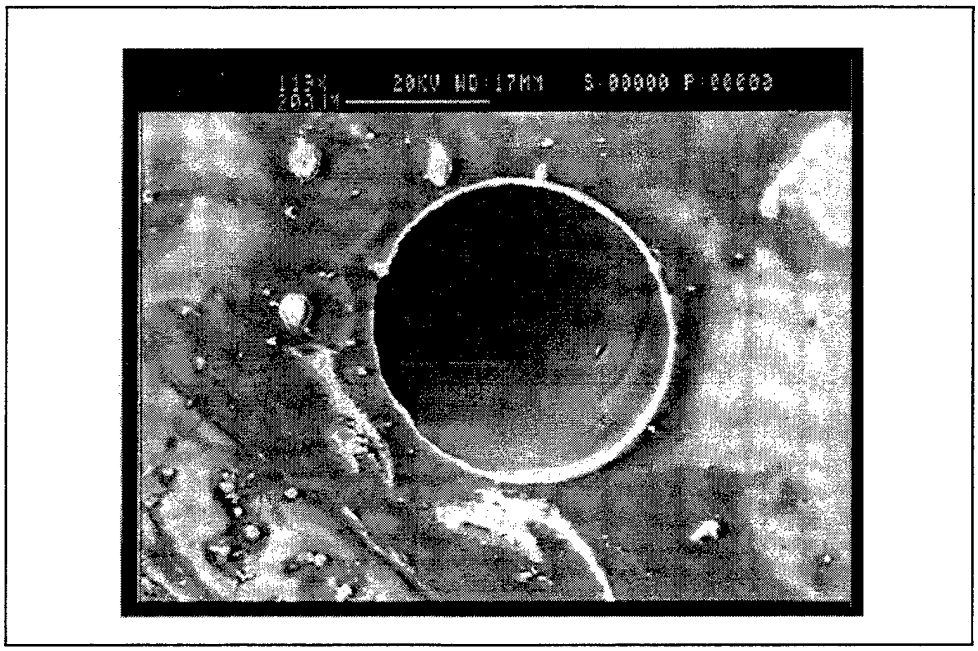

Figure 124: SEM photo of B13, 12 o'clock, 60 cycles, mag. 119X.

Figure 125: SEM photo of B14, 12 o'clock, 60 cycles, mag. 119X.

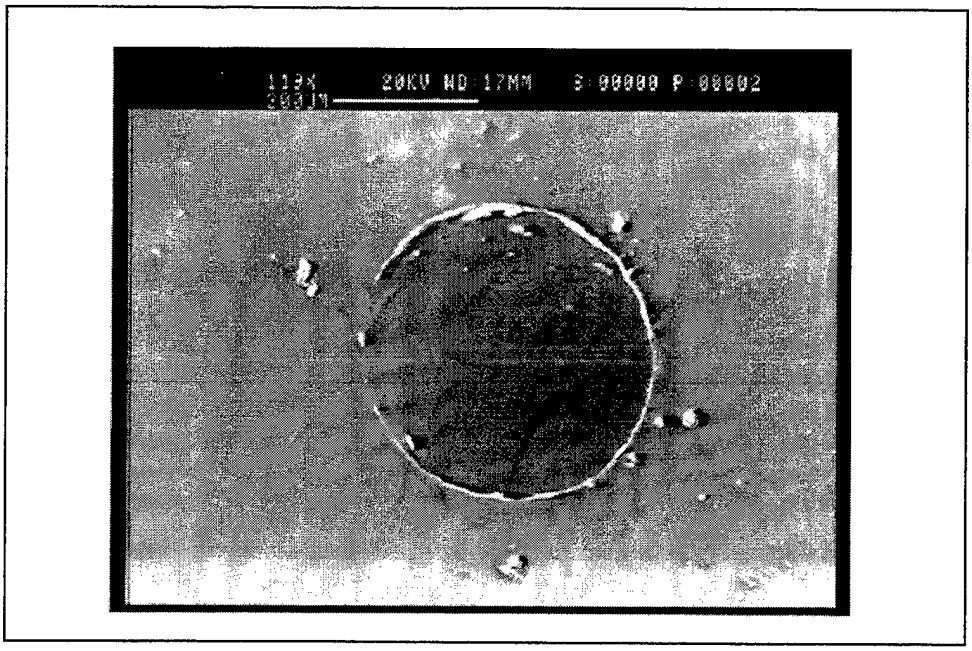

Figure 126: SEM photo of B13, 6 o'clock, 60 cycles, mag. 119X.

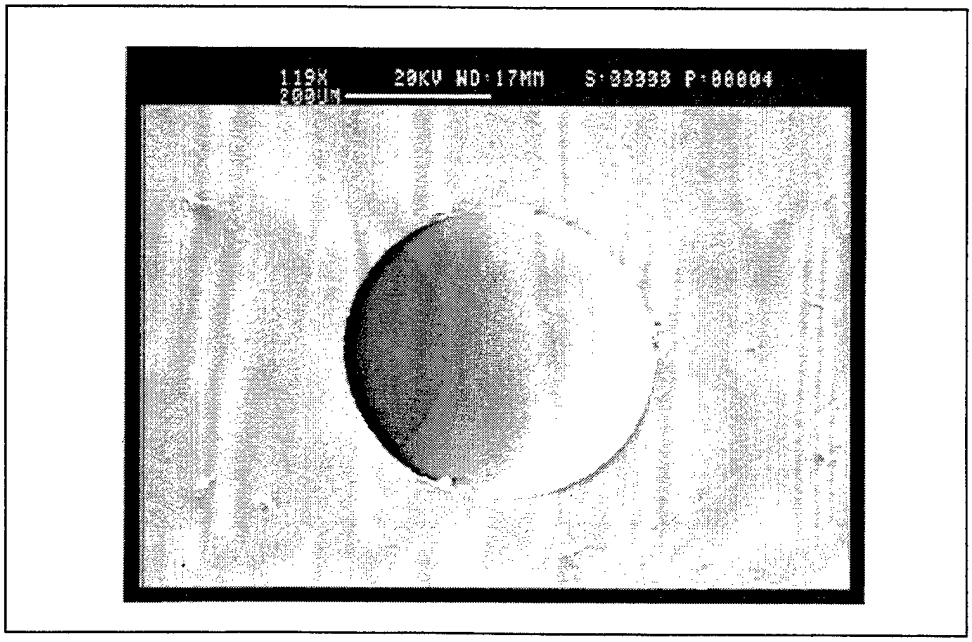

Figure 127: SEM photo of B14, 6 o'clock, 60 cycles, mag. 119X.

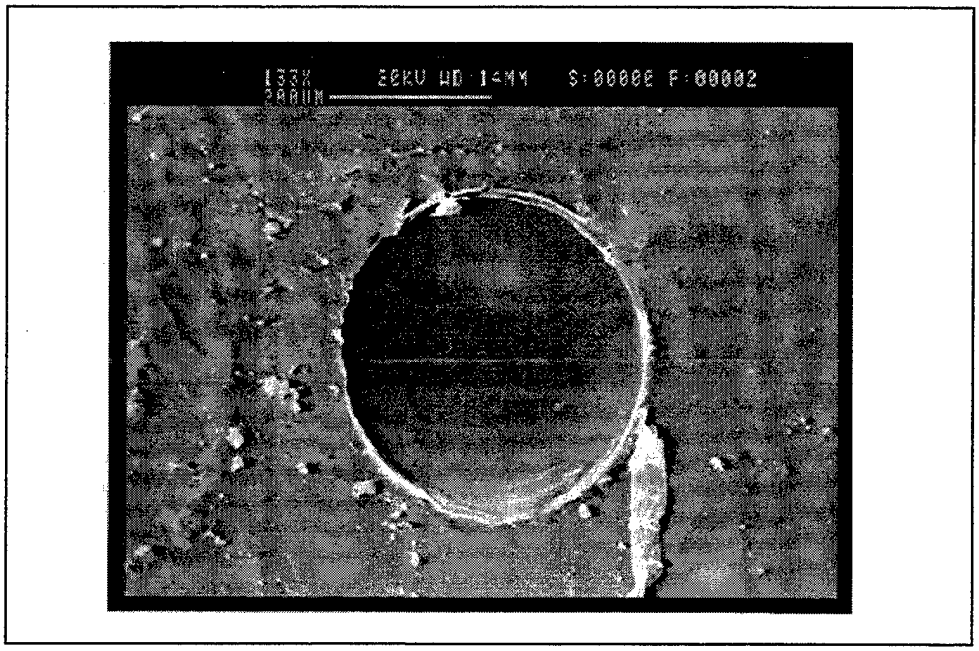

Figure 128: SEM photo of B13, 12 o'clock, 150 cycles, mag. 133X.

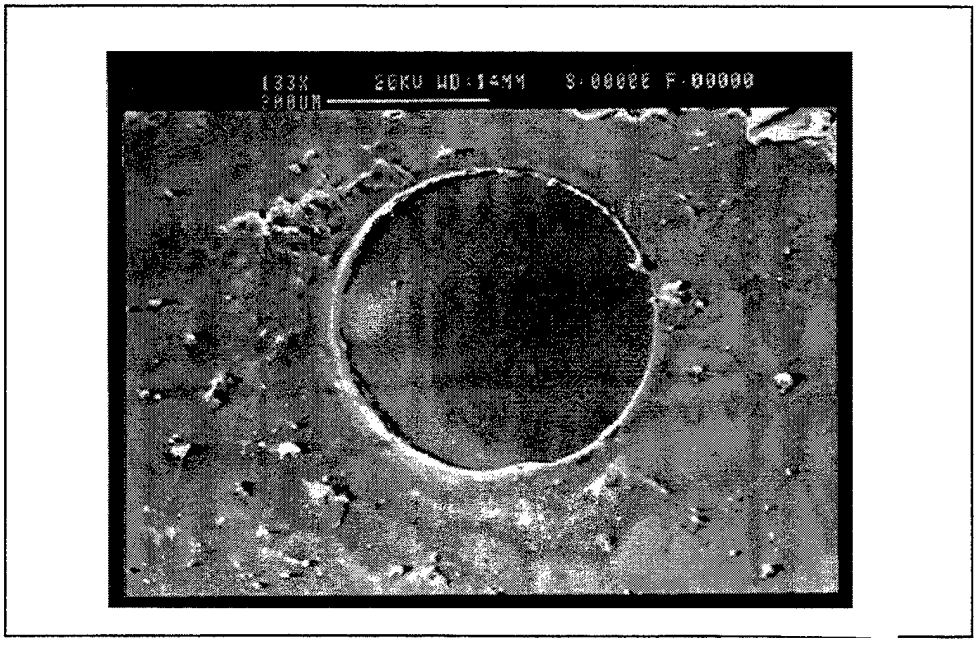

Figure 129: SEM photo of B14, 12 o'clock, 150 cycles, mag. 133X.

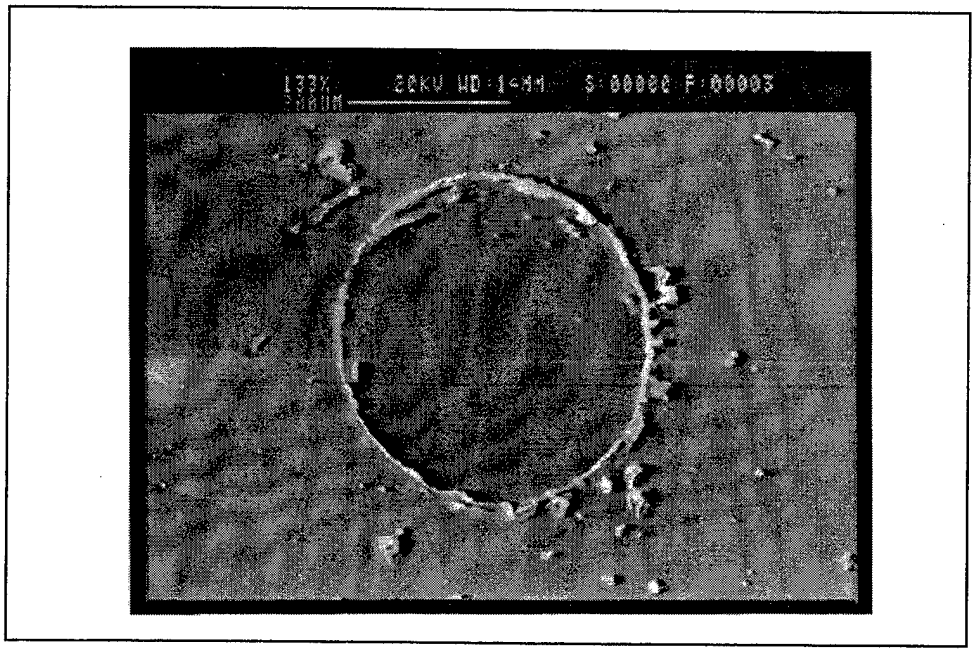

Figure 130: SEM photo of B13, 6 o'clock, 150 cycles, mag. 133X.

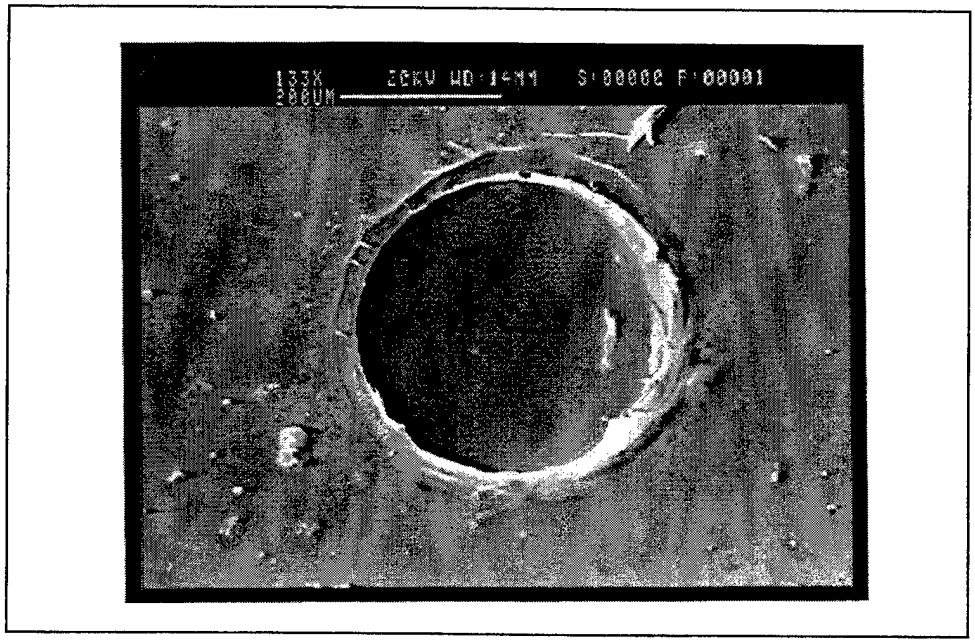

Figure 131: SEM photo of B14, 6 o'clock, 150 cycles, mag. 133X.

E. HOLE CLOSURE AND FLOW MEASUREMENTS

Weight measurements, optical and SEM pictures provide insight into the amount of coking present and where it is located. However, it is the coking that restricts flow that is our only concern. The flow measurements indicate the reduction in flow and are measured against the baseline flow value of the swirl plate. After each run, flow measurements were collected to evaluate how much of the coking was actually restricting flow. The data points were then plotted versus the pressure drop and a linear first order interpolation was performed to determine if the data did in fact follow a linear relationship, thus verifying that the assumption of isentropic flow chosen by Vassiloyanakopolous [Ref. 13] and used in this research was valid.

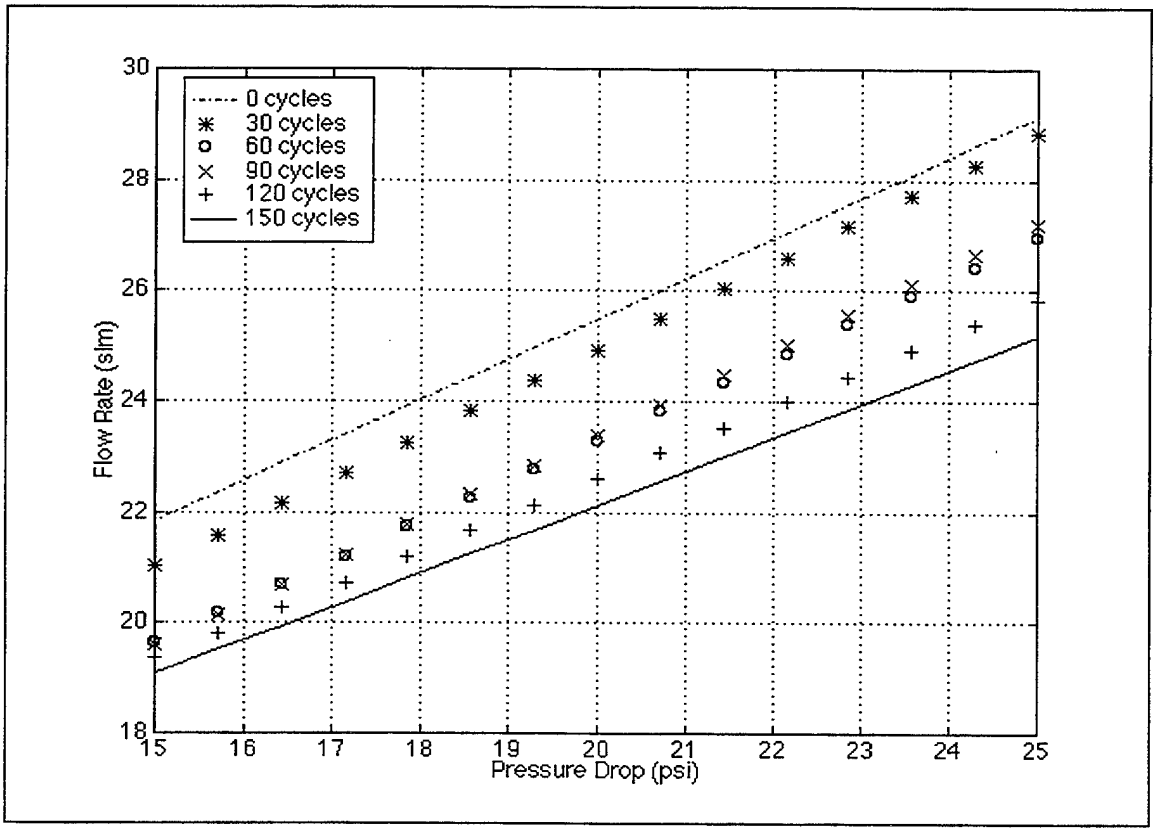

Figure 132: Linear flow relationship for B17 swirl plate.

The results shown in Figure 132 are similar to each of the other swirl plates and will be the only linear flow relationship plot presented. The tables of flow measurements for each swirl plate are presented below and plots of the percentage hole closure follow the tables.

1. A01 and A'01

Cycles	0	30	60	90	120	150
Pressure-15psi	21.6	20.9	21.2	21.1	20.0	20.3
Pressure-20psi	25.7	25.1	25.1	25.0	25.0	26.0
Pressure-25psi	28.3	28.2	28.0	27.8	28.0	28.0

Table 19: Flow Rate in Standard Liters per Minute for A01.

Cycles	0	30	60	90	120	150
Pressure-15psi	21.6	20.9	21.2	21.1	20.0	20.3
Pressure-20psi	25.7	25.1	25.1	25.0	25.0	26.0
Pressure-25psi	28.3	28.2	28.0	27.8	28.0	28.0

Table 20: Flow Rate in Standard Liters per Minute for A'01.

Figure 133 shows that there was little accumulation of coking in the holes of either A01 of A'01. This result does not support the previous work by Vassiloyanakopolous [Ref. 13] and Dr. Crooks [Ref. 1] nor is it consistent with the A28 plate tested in this research.

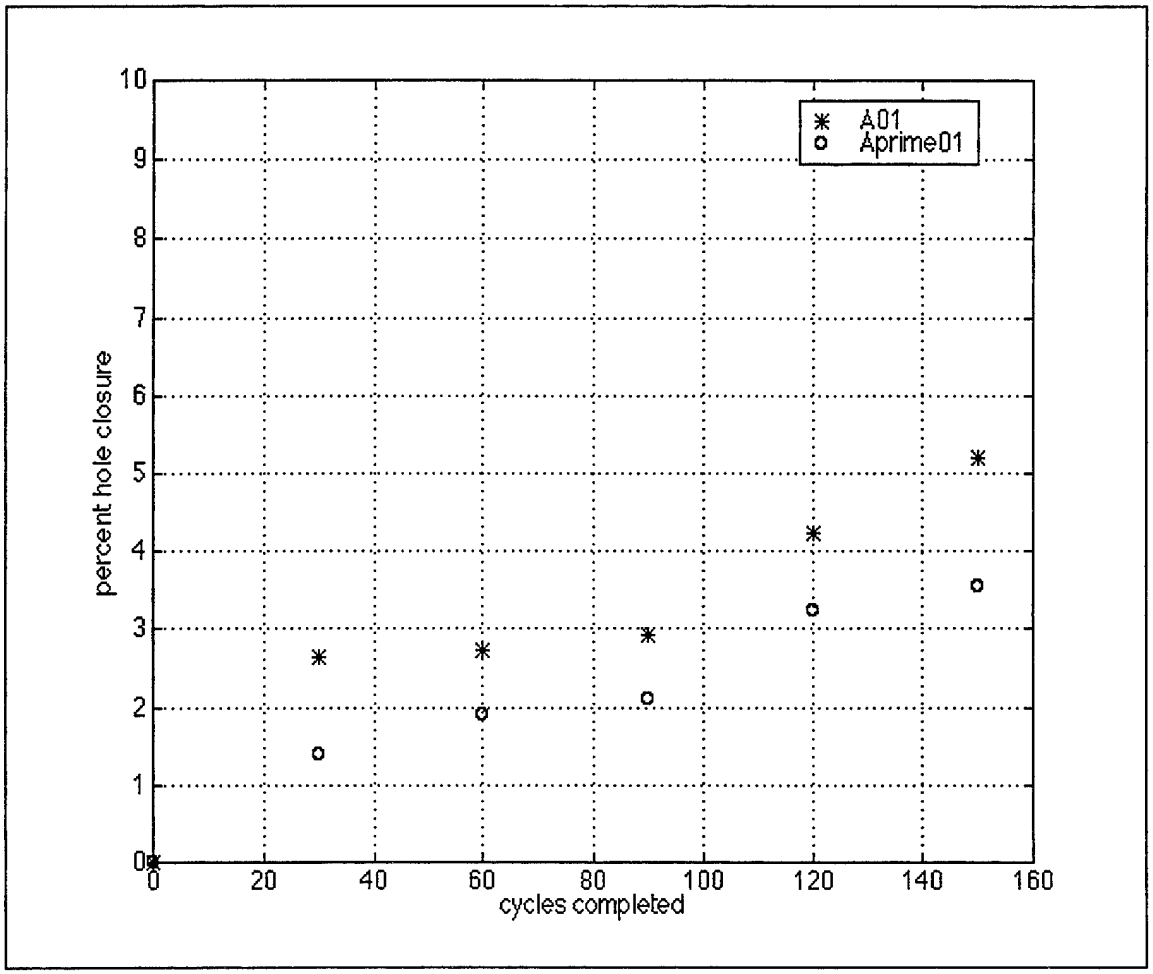

Figure 133: Average Percent Hole Closure of A01 and A'01 versus Cycles Completed.

2. B17 and B-md20.

Cycles	0	30	60	90	120	150
Pressure-15psi	21.5	20.9	19.9	19.8	18.9	18.9
Pressure-20psi	26.2	25.2	22.8	23.0	23.5	22.5
Pressure-25psi	28.8	28.7	27.2	27.4	25.4	25.0

Table 21: Flow Rate in Standard Liters per Minute for B17.

Cycles	0	30	60	90	120	150
Pressure-15psi	18.8	17.6	18.0	17.9	17.6	16.6
Pressure-20psi	23.8	23.2	23.7	23.0	22.8	21.3
Pressure-25psi	27.0	26.2	26.6	26.8	25.2	24.0

Table 22: Flow Rate in Standard Liters per Minute for B-md20.

Figure 134 shows that the amorphous diamond coating did assist in the resistivity to coking. However, both plots are higher than the previous runs with B plates as well as the subsequent runs made. The important aspect of this plot is that the coating increases the resistivity.

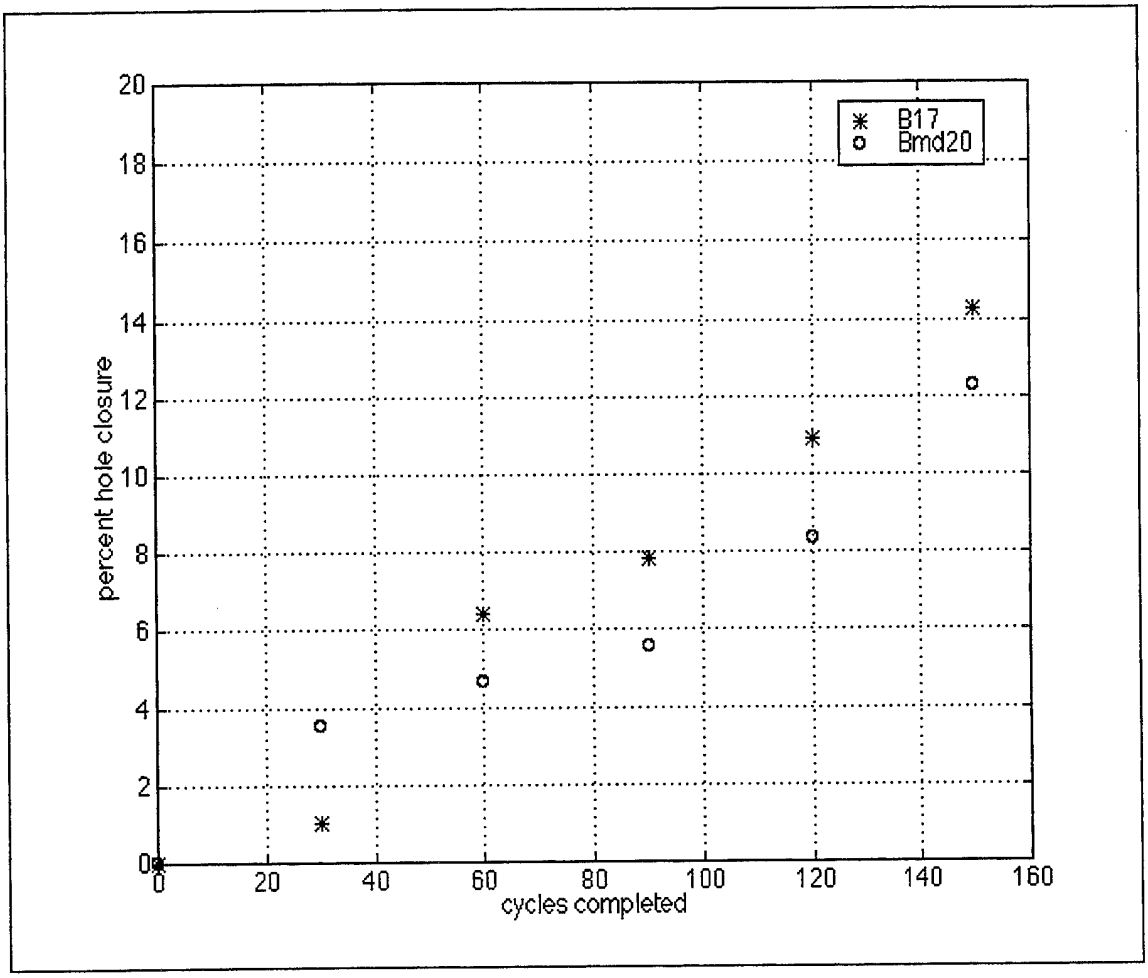

Figure 134: Average Percent Hole Closure of B17 and B-md20 versus Cycles Completed.

3. A-md25 and B19.

Cycles	0	30	60	90	120	150
Pressure-15psi	20.5	20.0	19.6	19.6	19.6	18.7
Pressure-20psi	24.3	23.9	23.9	23.3	23.0	22.7
Pressure-25psi	28.2	27.4	27.6	28.0	27.6	26.4

Table 23: Flow Rate in Standard Liters per Minute for A-md25.

Cycles	0	30	60	90	120	150
Pressure-15psi	20.6	20.6	19.7	19.7	19.8	19.7
Pressure-20psi	24.5	24.0	24.0	24.0	23.1	23.6
Pressure-25psi	28.0	27.6	27.7	27.5	27.4	27.0

Table 24: Flow Rate in Standard Liters per Minute for B10.

Figure 135 shows the B type plate is highly resistive while the A type plate coated with amorphous diamond works very efficiently until it reaches 150 cycles. At this point the amorphous coating appears to offer no protection as the percent hole closure doubles from the previous mark.

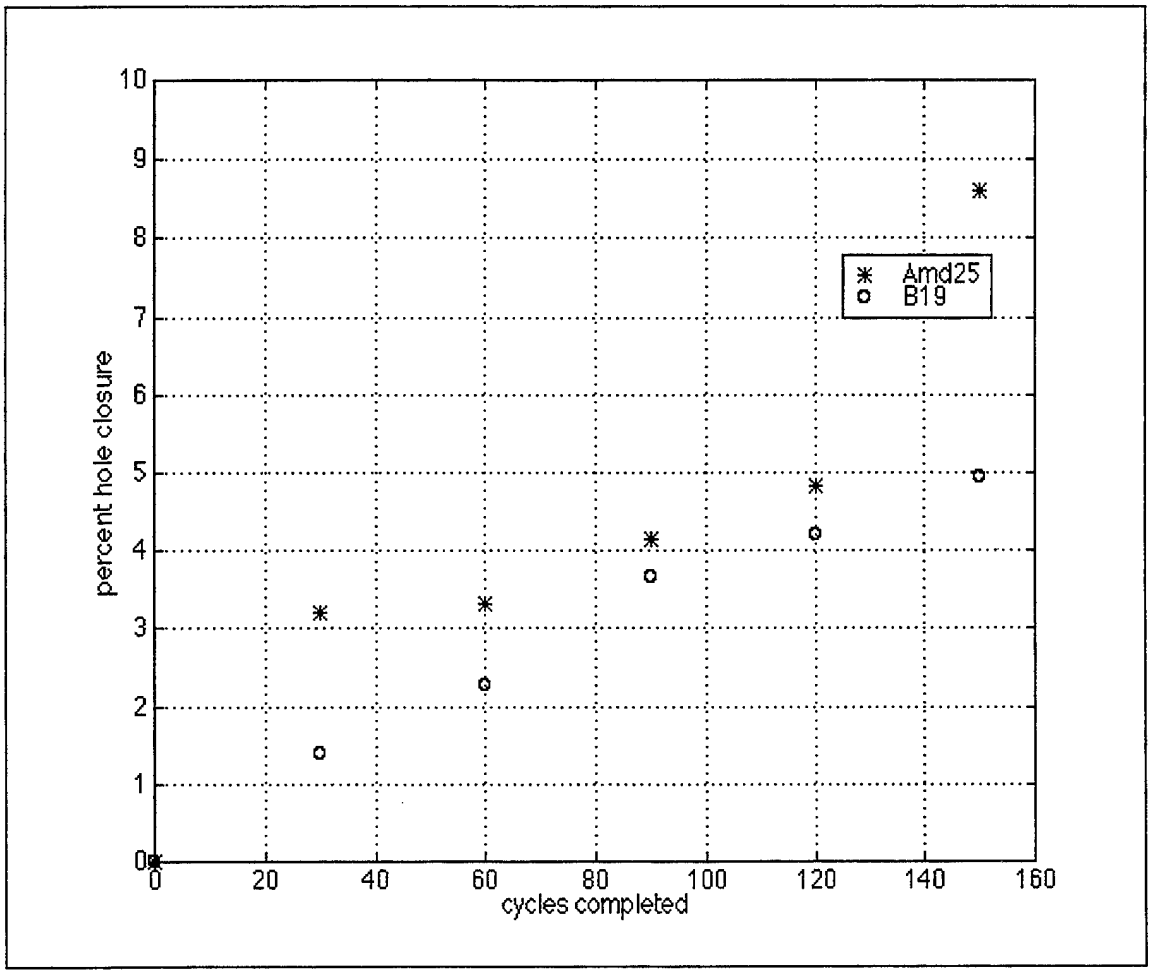

Figure 135: Average Percent Hole Closure of A-md25 and B10 versus Cycles Completed.

4. 28 and A-sil23.

Cycles	0	30	60	90	120	150
Pressure-15psi	21.6	21.1	20.3	18.9	18.7	18.0
Pressure-20psi	25.8	25.3	24.0	23.7	22.8	23.2
Pressure-25psi	29.0	28.8	28.1	27.3	26.0	25.7

Table 25: Flow Rate in Standard Liters per Minute for A28.

Cycles	0	30	60	90	120	150
Pressure-15psi	20.8	20.0	19.7	18.6	17.8	17.6
Pressure-20psi	25.3	24.2	23.5	23.6	21.8	21.0
Pressure-25psi	29.5	28.4	27.3	26.8	25.4	25.0

Table 26: Flow Rate in Standard Liters per Minute for A-sil23.

Figure 136 indicates that the silicon coating had a positive effect on the production type plate. It resisted the coking within the holes throughout the entire range of the run.

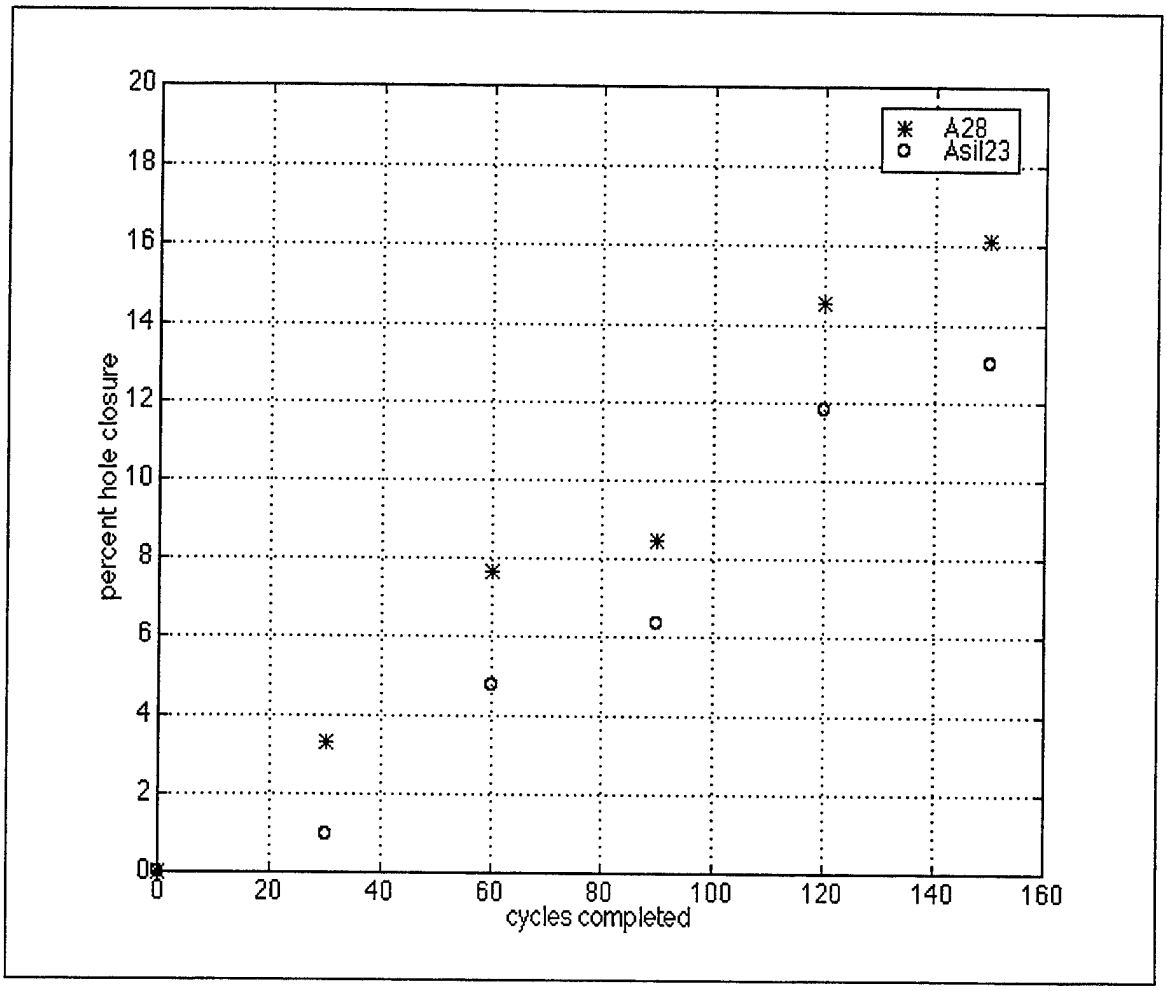

Figure 136: Average Percent Hole Closure of A28 and A-sil23 versus Cycles Completed.

5. A-sil24 and B12.

Cycles	0	30	60	90	120	150
Pressure-15psi	20.9	20.8	21.1	19.2	19.5	19.6
Pressure-20psi	24.5	24.0	23.9	24.0	23.7	23.3
Pressure-25psi	29.0	29.3	29.0	27.2	27.0	26.8

Table 27: Flow Rate in Standard Liters per Minute for A-sil24.

Cycles	0	30	60	90	120	150
Pressure-15psi	20.0	19.5	19.2	18.7	18.7	19.0
Pressure-20psi	25.2	25.0	25.0	24.0	23.8	24.0
Pressure-25psi	28.2	27.4	27.5	26.7	26.6	27.0

Table 28: Flow Rate in Standard Liters per Minute for B12.

Figure 137 shows that the silicon coating does have a positive effect. In this run, the coating appears to have reduced the levels of coking to the range of the B type plates, half the closure percent of the previous silicon treated plate. There does appear to be some sort of possible breakdown late in the cycles.

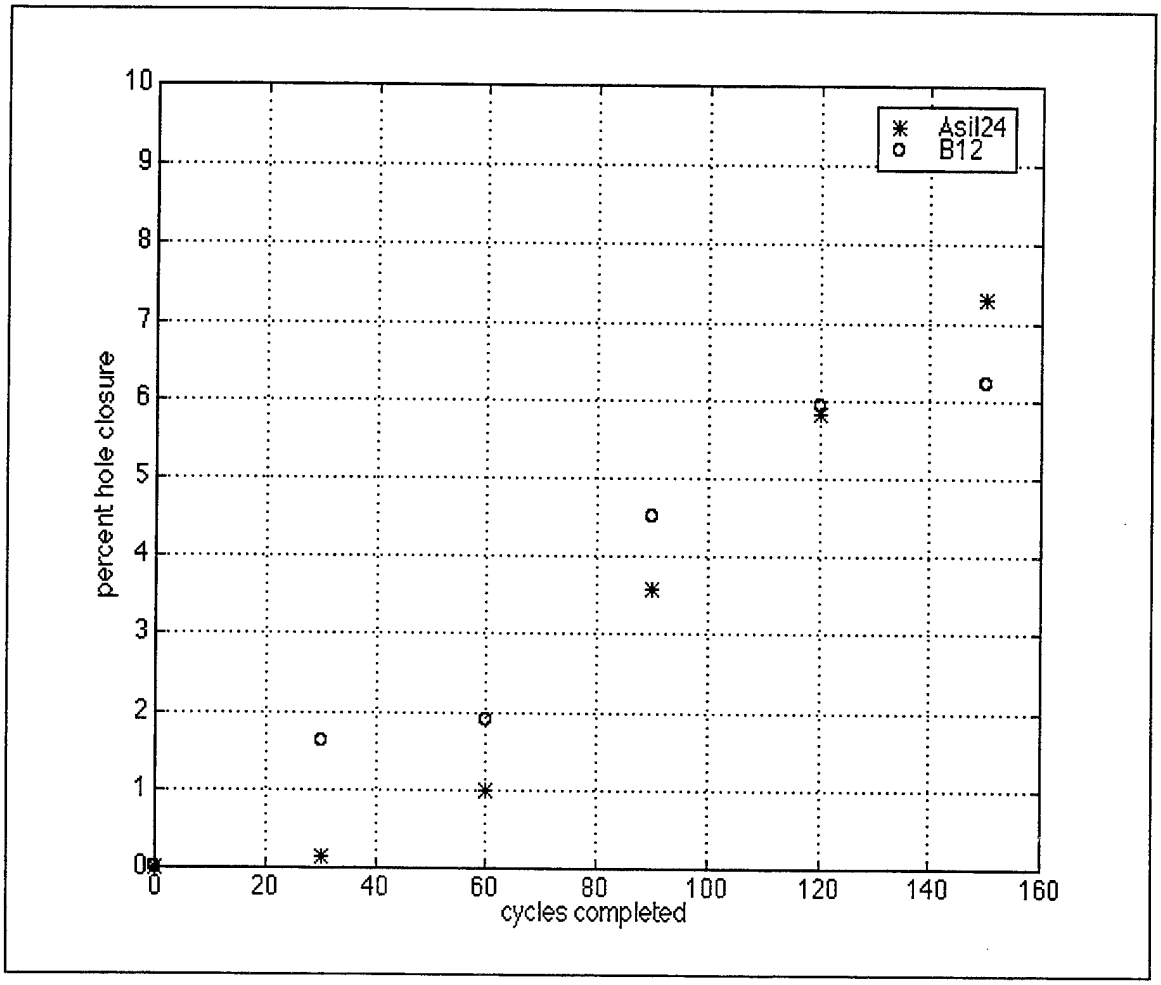

Figure 137: Average Percent Hole Closure of A-sil24 and B12 versus Cycles Completed.

6. B13 and B14.

Cycles	0	30	60	90	120	150
Pressure-15psi	21.0	20.9	20.7	20.5	20.1	20.4
Pressure-20psi	27.0	25.8	26.2	25.8	25.6	25.8
Pressure-25psi	29.4	28.5	28.6	27.9	27.7	27.8

Table 29: Flow Rate in Standard Liters per Minute for B13.

Cycles	0	30	60	90	120	150
Pressure-15psi	20.5	20.6	20.3	20.1	20.0	19.3
Pressure-20psi	26.2	26.0	26.0	25.8	25.6	25.4
Pressure-25psi	28.5	28.7	28.7	27.7	27.5	27.4

Table 30: Flow Rate in Standard Liters per Minute for B14.

Figure 138 again shows the superb results obtained when using the B type swirlplates. Both plates tracked nearly identically through the entire run.

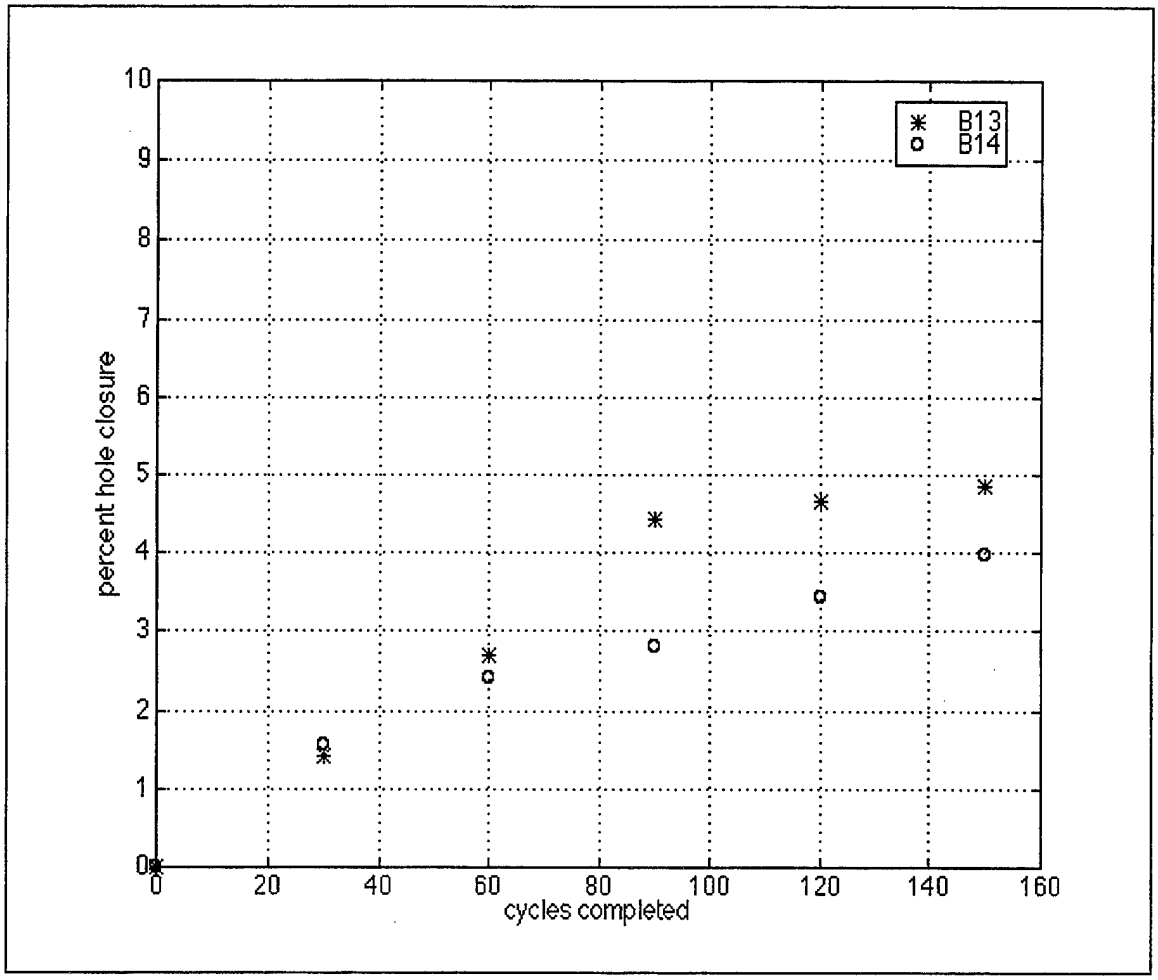

Figure 138: Average Percent Hole Closure of B13 and B14 versus Cycles Completed.

IV. CONCLUSIONS AND RECOMMENDATIONS

A. CONCLUSIONS

1. A type swirlplates.

The results of Allison's investigation into the failure of the current swirlplates [Ref. 2] are verified in the current work. Production type swirlplates offer little resistivity to coking.

2. A' type swirlplates.

The production type swirlplates with the surface polished to 30 microns appear to offer only a minimal gain in coking resistivity as compared to the original production swirlplates. Polishing the surface reduces the surface area available for coking but does not address the main issue of hole closure. The surface polish would only be pertinent if there existed proof that the surface of the plate was the initial coking site. If this were the case then polishing the surface would possibly reduce coking in the hole by prolonging the coke initiation. As it stands now, the polishing of the surface provides a very small gain in coking resistance.

3. Amorphous Diamond Coating.

Both plates tested with amorphous diamond coating provided inconsistent results throughout the entire cycle. The coating appeared to offer increased resistance in the initial cycles but gradually deteriorated after approximately the 80th cycle. It is possible

that since the amorphous diamond coating is only diamond like, and is essentially a carbon layer, the coating is breaking down and becoming coke itself.

4. Silicon Coating.

The silicon coated plates appeared to offer a greater resistivity to coking than the production plates throughout the entire range of cycles. They did not offer a significant reduction in coking but were consistently lower than the production plates.

5. Dupont Plates.

The Dupont plates indicated a percentage hole closure percent and the weight gain that were lower than any other type of swirlplate tested. The difference between the Dupont plates and the Allison surface finished plates is solely with the hole drilling technique. Dupont's method provided for a smoother bore which reduced the surface area available for coking and thus produced the best results.

The coking mechanism appears to result from the interaction of the local temperature and the fuel present and is possibly accelerated by the interaction of the oxygen and the metal ions of the surface plate. Smoothing the surfaces of the plates and holes provided for increased resistivity every time, albeit small in some instances. The concept of smoothing implies that the coke has less surface area in which to attached itself. The possibility also exists that oxygen and sulfer in the fuel are reacting with the metal ions of the swirlplate and forming microcavities that provide additional surface area for coking adherence. Therefore, surface and hole polishing may eliminate the amount of surface area present for coke adherence but not the process of microcavity formation.

Smooth coatings that cover all the surfaces of the swirlplate not only provide for reduced surface area but also eliminate metal ion interaction with the oxygen, thereby reducing potential microcavity formation and thus coke adherence.

B. RECOMMENDATIONS

1. While the results of this research have indicated that surface finishes have a dramatic effect on the resistivity of coking, the number of finishes and coatings tested were very limited. Additional coatings and hole surface finishes should be investigated to find the best coking resistivity.

2. Additional testing of the Dupont coating as well as the silicon coating could increase the statistical reliability of the results presented in this research. Further testing of the amorphous diamond coating could provide information into the possible failure of the coating at high cycles.

3. Conducting experiments into the catalysts involved or the surface tension effects relating to coking could provide valuable insight into the mechanisms of coking and thus the best possible swirlplates to avoid coking.

LIST OF REFERENCES

1. Prof. Roy Crooks archive. T56-S-427 Engine Fuel Modification.

2. Allison Service Information Letter. Gas Turbine Division, July 29, 1991.

3. NAVAIR SYSCOM, AIR-5116C, E-2C CLASS DESK, RM 1214, CDR Newman, 4 November 1991.

4. Marteney, P. J., Spadaccini, L. J., *Thermal Decomposition of Aircraft Fuel*, Journal of Engineering for Gas Turbines and Power. Vol. 108, October 1986.

5. Marteney, P. J., *Thermal Stability of JP-5 in Long Duration Tests*, American Chemical Society. September 10-15, 1989.

6. Reid, William T., *External Corrosion and Deposits*, Fuel and Energy Science Series. American Elsevier Publishing Company, Inc., 1971.

7. Hazlett, R.N., et al, *Reactions of Related n-Dodecane Liquid Flowing over Heated Metal Tubes*, Ind. And Eng. Chem., Prod. Res. Dev., Vol. 16, No.2, 1977.

8. Treager, Irwin E., *Aircraft Gas Turbine Engine Technology*, Second Edition, McGraw-Hill Inc., 1979.

9. Burman, Paul G., DeLuca, Frank, *Fuel Injection and Controls for Internal Combustion Engines-Fuel Systems for Gas Turbines and Jet Engines*, , Ch. 16, Simmons-Boardman Publishing Corporation, 1962.

10. General Information Sheet for GE Coke Barrier Coating. Information Package.

11. Technical Repair Standard for AG9130 Ship Service Gas Turbine Generator.

12. Purge System, Low Pressure Fuel Nozzle Purge System/Program Preliminary Design Review, June 1994.

13. Vassiloyanakopoulos, Vassilios P., *Design and Method for the Evaluation of the Coking Resistance of Swirlplates of E-2C Aircraft Fuel Nozzles*, March 1996.

14. Dupont Lanxide Composites Inc. Information Package, January 5, 1993.

15. Hart, P. J., *Summary of Heat Transfer Work on A427 Fuel Nozzles*, Allison Co., July 30, 1991.

16. FAX Veda Inc. NPS Fuel Nozzle Coking Research Project, July 1995.

17. Streeter, Victor L., Wylie, Benjamin E., *Fluid Mechanics*, Eighth Edition, 1985.

18. LABTECH NOTEBOOK *Reference Manual*, November 1992.

INITIAL DISTRIBUTION LIST

	No. of copies
1. Defense Technical Information Center 8725 John J. Kingman Rd. STE 0944 Alexandria, Virginia 22304-6145	2
2. Dudley Knox Library Naval Postgraduate School 411 Dyer RD. Monterey, California 93943-5101	2
3. Department Chairman, Code ME/Mc Department of Mechanical Engineering Naval Postgraduate School Monterey, California 93943-5000	1
4. Professor Jeff Perkins, Code ME/Ps Department of Mechanical Engineering Naval Postgraduate School Monterey, California 93943-5000	3
5. LT Stephen Williamson, USN 1105 Cherrytree Lane Chesapeake, Virginia 23320	3
6. Curricular Officer, Code 34 Department of Mechanical Engineering Naval Postgraduate School Monterey, California 93943-5100	1
7. Rich Hashimoto, Code ME/Ha Department of Mechanical Engineering Naval Postgraduate School Monterey, California 93943-5000	1
8. CDR Jim Clifton NAVAIR Code 411 1421 Jefferson Davis Hwy. Arlingotn, Virginia 22243-5169	1

9. Mr. Earl Eck 1
NAVAIR Code 411
1421 Jefferson Davis Hwy.
Arlingotn, Virginia 22243-5169

10. Mr. Doug Meanvis 1
NAVAIR Code:AIR 4-4
<Mgr. Fuels and Lubricants>
Propulsion and Power Division
1421 Jefferson Davis Hwy.
Arlingotn, Virginia 22243-5169

11. Mr. Wayne Osgood 1
VEDA Inc. 1800 North Beaurequet St.
Alexandria, Virginia 22311-1708

12. Mr. Michael Williamson 1
6510 Allview Drive
Columbia, Maryland 21046

13. Mr. Gary Benoit 1
General Delivery
Belle River, Ontario Canada NOR 1A0